Epigenetic and chromatin inheritance of euchromatic and heterochromatic sequences

Dissertation

zur
Erlangung der naturwissenschaftlichen Doktorwürde
(Dr. sc. nat.)

vorgelegt der
Mathematischen-naturwissenschaftlichen Fakultät

der
Universität Zürich

von
Eva Vollenweider

aus

Zürich ZH

Promotionskomitee

PD Dr. Raffaella Santoro (Leitung der Dissertation)
Prof. Dr. Dr. Michael O. Hottiger (Vorsitz der Dissertation)
Prof. Dr. Claus Azzalin
Dr. Maria-Elena Torres Padilla
Prof. Dr. Konrad Basler

Zürich, 2015

Summary

To maintain cell identity and function, a dividing cell must replicate not only its genome but also the epigenome. Epigenetic modifications at histones and DNA must surmount the challenge of DNA replication, in which chromatin is disassembled ahead of the replication fork and then reassembled onto two daughter genomes after DNA synthesis. Restoration of epigenetic modifications is a critical step since it can affect the maintenance of information conveyed at the epigenomic level and in turn impact gene expression and genome stability. However, it remains largely unknown how chromatin and epigenetic states are restored to parental states.

Current models of epigenetic inheritance are based on the notion that the newly synthesized DNA is rapidly methylated and assembled into chromatin shortly after replication. These models are mostly based on studies performed genome wide without taking in account that distinct chromatin states display different replication timings and have specific factors involved in their reestablishment.

The aims of this work were to determine the temporal dynamics of chromatin restoration after replication and to define whether euchromatin and heterochromatin use the same modalities to duplicate their chromatin and epigenetic signature.
In contrast to previously postulated models for chromatin assembly, the data of this thesis show that nucleosome assembly at heterochromatic repeats is a slow process that lasts until G2/M. This is a specific feature of heterochromatin since nucleosome assembly after replication of euchromatic sequences is a rapid process, as described for bulk chromatin in early works. Furthermore, establishment of DNA methylation, a typical mark of constitutive heterochromatin, is not completed as soon as DNA is duplicated but it requires several hours after replication.

It has previously been shown that Poly(ADP-ribose)-polymerase-1 (PARP1) transiently associates with nascent heterochromatic DNA. The results presented here reveal that ADP-ribosylation is required for the slow deposition of nucleosomes and for the establishment of DNA methylation. Pharmacological inhibition of PARP1-mediated ADP-ribosylation induces a rapid assembly of nucleosomes at nascent heterochromatin and impairs DNA methylation without altering the association of the DNA methylation machinery.

Together, the results indicate that ADP-ribosylation mediates a delayed post-replicative nucleosome assembly at heterochromatin that facilitates methylation at DNA, unraveling a post-replicative temporal coordination between nucleosome deposition and DNA methylation. Hypomethylation at heterochromatic DNA repeats is a hall-mark of cancer cells. The described post-replicative temporal coordination between nucleosome deposition and DNA methylation might represent an important process to consider in future studies aimed to understand alterations in epigenome and genome integrity during tumor progression.

Zusammenfassung

Um die Identität und Funktion zu wahren, muss eine sich teilende Zelle nicht nur ihr Genom sondern auch ihr Epigenom duplizieren. Während der Replikation wird die Chromatinstruktur vor der Replikationsgabel vorübergehend aufgelöst. Epigenetische Modifikationen an Histonen und DNA müssen nach der DNA Synthese wieder etabliert werden, damit die epigenetische Information, welche die genetische Expression und Genomstabilität kontrolliert, erhalten bleibt. Wie die Chromatinstrukturen und die epigenetische Signaturen nach der Replikation erhalten werden, ist noch nicht bekannt.

Derzeitige Modelle gehen davon aus, dass die neu synthetisierte DNA direkt nach der Replikation methyliert und wieder in Chromatin verpackt wird. Diese Modelle basieren auf Studien, welche das ganze Genom untersucht haben. Solche Daten lassen jedoch ausser Acht, dass Euchromatin (offen und ohne DNA Methylierung) und Heterochromatin (hochkondensiert und reich an DNA Methylierungen) zu verschiedenen Zeiten der S-Phase repliziert werden und dass unterschiedliche Faktoren zu deren Aufrechterhaltung benötigt werden.

Das Ziel dieser Arbeit war es, die temporale Dynamik der Chromatin-wiederherstellung nach der Replikation zu bestimmen. Zusätzlich sollte definiert werden, ob Euchromatin und Heterochromatin identische Mechanismen nutzen um ihr Chromatin zu duplizieren.

Die Ergebnisse zeigen, dass Nukleosomen nur langsam in Heterochromatin repetitiver Sequenzen inkorporiert werden. Dieser Prozess dauert mehrere Stunden bis in die G2/M Phase und ist spezifisch für Heterochromatin, da euchromatische Sequenzen gleich nach der DNA Synthese auf Nukleosomen aufgewickelt werden. Überdies demonstrieren die Daten, dass auch die DNA Methylierung nicht direkt nach der Replikation wiederhergestellt wird, sondern dafür mehrerer Stunden benötigt.

Seit kurzem ist bekannt, dass Poly(ADP-ribose)-polymerase-1 (PARP1) vorübergehend an neu synthetisierte, heterochromatische DNA bindet. Die Ergebnisse dieser Arbeit zeigen nun, dass die ADP-ribosylierung für eine langsame Inkorporierung der Nukleosomen und die Wiederherstellung der DNA Methylierung unabdingbar ist. Wird die PARP1-abhängige ADP-ribosylerung pharmakologisch

blockiert, werden Nukleosomen, wie bei euchromatischen Sequenzen, sofort nach der Replikation in das neue Heterochromatin eingebaut. Zusätzlich verhindert die Inhibierung der PARP1-Aktivität die Erhaltung der DNA Methylierung, jedoch ohne dabei die Rekrutierung der verantwortlichen Faktoren zu beeinflussen.

Zusammengefasst zeigen die Daten, dass ADP-ribosylierung eine verlangsamte post-replikative Nukleosominkorporation vermittelt, welche die DNA Methylierung vereinfacht. Somit beschreibt diese Arbeit eine temporale Koordination zwischen der Inkorporation von Nukleosomen und der DNA Methylierung. Hypomethylierung von heterochromatischen, repetitiven DNA Sequenzen ist ein Kennzeichen von Krebszellen. Die beschriebene post-replikative temporale Koordination zwischen Nukleosominkorporation und DNA Methylierung könnte einen wichtigen Prozess repräsentieren, welchen man für zukünftigen Studien von Veränderungen des Epigenoms und der Genomintegrität während der Tumorentwicklung in Betracht ziehen sollte.

Abbreviations

5mC	5-methylcytosine
Acetyl-CoA	acetyl coenzyme A
ATP	adenosine triphosphate
ARTD	diphtheria toxin-like ADP-ribosyltransferase
bp	base pair
BrdU	Bromodeoxyuridine
CGI	CpG island
ChIP	Chromatin Immunoprecipitation
DNA	deoxynucleic acid
DNMT	DNA methyltransferase
DTT	dithiothreitol
FACS	flurescence-activated cell sorting
HA	hemagglutinin
HAT	histone acetyl transferase
HDAC	histone deacetylase
HMT	histone methyltransferase
KCl	potassium chloride
L, Lys	lysine
MeCP2	methyl CpG binding protein
mRNA	messanger ribonucleic acid
NaCl	sodium chloride
NAD	nictoinamide adenine dinucleotide
NCC	nascent chromatin capture
NoRC	nucleolar remodeling complex
NORs	nucleolar organizing regions
NP-40	nonident P-40
nt	nucleotide
PAR	poly(ADP)ribose
PARG	poly(ADP)gylcohydrolase
PARP	poly(ADP-ribose)polymerase
PARylation	poly(ADP-ribosyl)ation
PCNA	Proliferating cell nuclear antigen

Pol I	RNA polymerase I
pre-rRNA	precursor ribosomal RNA
pRNA	promoter RNA
PTM	post-translational modification
qPCR	quantitative polymerase chain reaction
R, Arg	arginine
rDNA	ribosomal DNA
RNA	ribonucleic acid
rRNA	ribosomal RNA
RT-PCR	reverse transcription polymerase chain reaction
SDS	sodium dodecyl sulfate
SDS-PAGE	sodium dodecyl sulfate polyacrylamide gel electrophoresis
SILAC	stable isotope labeling by amino acids in cell culture
SNF2h	sucrose non-fermenting protein 2 homologue
SETDB1	SET domain, bifurcated 1
SRA	SET and RING finger associated
SUV39H2	Suppressor of variegation 3-9 homolog 2
TIP5	TTF1-interacting protein 5
TSS	transcription start site
TTF-1	transcription termination factor
UBF	upstream binding factor
UHRF	ubiquitin-like with PHD and ring finger domains

Table of Contents

Summary **2**

Zusammenfassung **4**

Abbreviations **6**

Table of Contents **8**

1 Introduction **10**

1.1 Chromatin **10**

1.1.1 Euchromatin and heterochromatin 10

1.1.2 Histone modifications 12

1.1.3 PARP1 in the chromatin context 13

1.1.4 DNA methylation 15

1.2 Epigenetic inheritance **17**

1.2.1 Chromatin replication 18

1.2.1 Histone segregation and the inheritance of histone modification 19

1.2.2 DNA methylation maintenance 22

1.3 Inheritance of rDNA chromatin **24**

1.3.1 Epigenetic feature of rDNA 24

1.3.2 TIP5 and PARP1 in the inheritance of rDNA heterochromatin 26

1.3.3 rDNA heterochromatin and the formation of nuclear heterochromatin 27

Aims **28**

3 Results **29**

3.1 Published and submitted results **29**

3.1.1 Assembly of heterochromatin after replication is a slow process required for DNA methylation 29

3.1.2 lncRNA maturation to initiate heterochromatin formation in the nucleolus is required for exit from pluripotency in ESCs 29

3.1.3 Pramel7 is implicated in naïve pluripotency through proteasomal-epigenetic combined pathways 30

3.2 Unpublished Results **127**

3.2.1 PARP1 and UHRF1 bound DNA is heterochromatic and enriched in

unmodified Histone 3 127

4 Discussion 131

4.1 Establishment of heterochromatic states does not occur immediately after the passage of the replication fork 132

4.2 PARP1-activity creates a indispensable window of opportunity for DNMT1 to methylate nascent DNA 133

4.3 Genomic and epigenomic instability in cancer 136

Bibliography 137

Curriculum Vitae 150

Acknowledgements 152

1 Introduction

1.1 Chromatin

A human haploid genome consists of approximately 3.2 billion nucleotide bases, which make up about two meters in length. Each eukaryotic cell contains a complete genome and has to compact the DNA approximately 100 000 times in order to fit it into the nucleus. The long DNA molecules in any eukaryotic cell are packed and organized into a DNA-protein complex called chromatin (**Figure 1**). Chromatin controls all nuclear processes like DNA repair, recombination, replication and transcription. In eukaryotes, a so called nucleosome consists of 147 base pairs of DNA wrapped around a histone octamer assembled from 2 copies of the core histones H2A, H2B, H3 and H4 (Kornberg, 1974). Nucleosomes are connected by linker DNA of variable lengths which is bound by the linker histone H1 (Thoma et al., 1979). However, nucleosomes can be further diversified through the incorporation of histone variants, differing in their amino acid sequences from the canonical histones. These histone variants can have a great impact on chromatin structure and function through alterations the nucleosome architecture (Bernstein and Hake, 2006; Sarma and Reinberg, 2005).

1.1.1 Euchromatin and heterochromatin

The foundation to categorize the eukaryotic genome into two major functional states was already laid in 1928 by differential chromosomal staining. Basic dyes let to the observation of distinct chromatin regions with some being brightly stained whereas others remained barely visible. These two distinct regions were termed heterochromatin and euchromatin. Euchromatin corresponds to a rather open and transcriptionally active conformation and is usually replicated early in S phase. Heterochromatin designates a condensed and transcriptionally inert conformation that is generally replicated late in S phase. The main function of heterochromatin is shielding the underlying DNA sequences from proteins or factors trying to access the DNA for a number of processes like transcription or repair (Dillon and Festenstein, 2002). Heterochromatin can be further divided into two categories: facultative and

constitutive heterochromatin. Facultative heterochromatin can be found on multiple chromosomal regions and its genes have mostly been silenced upon developmental cues (Saksouk et al., 2015). A typical histone mark for facultative heterochromatin is H3K27me3 (Cao et al., 2002). On the other hand, constitutive heterochromatin is usually enriched in H4K20me3, H3K64me2/3, H3K9me3 and poor in acetylation (Daujat et al., 2009; Schotta et al., 2004). Furthermore, constitutive heterochromatin is though to be gene poor and occur at the same chromosomal regions in every cell type. It is found at pericentromeric regions (satellites), telomeres, ribosomal regions, as well as at different loci along the chromosomes (transposable elements).

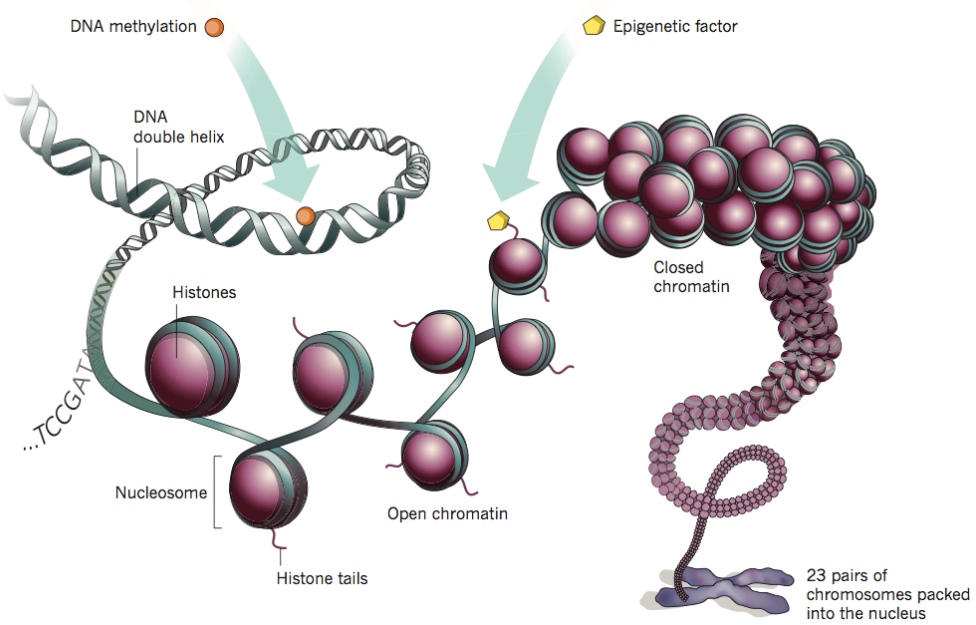

Figure 1. Structure of chromatin DNA molecule wrapped around nucleosomes gives rise to a higher order structure allowing for compaction into the characteristic chromatin fibre and chromosomes. DNA methylation influences which genes are expressed, and other epigenetic factors (e.g. histone modifications) determine the compaction status of chromatin. Hence, both epigenetic marks control the transcriptional and compaction state of DNA without changing the underlying DNA sequence. (Marx, 2012)

Heterochromatin prevents recombination of these repetitive elements and transposition of transposable elements, rendering it paramount for genome stability (Carone and Lawrence, 2013; Guetg et al., 2010; Peng and Karpen, 2007). Moreover, heterochromatin integrity at centromeres has been shown to be indispensible for correct chromatid segregation during mitosis (Bernard et al., 2001). Interestingly, constitutive heterochromatic regions clusters together and are enriched at the nuclear

periphery and around the nucleolus (Meister and Taddei, 2013).

1.1.2 Histone modifications

Histones are globular proteins apart from their N-terminal tails, which protrude from the globular domain. The N-terminal tails of core histones can be a target of posttranslational modifications such as acetylation, methylation, and ADP-ribosylation (Kouzarides, 2007). Even though they are not very well understood, also PTMs of the globular core have been described and assigned crucial function in chromatin regulation (Cosgrove and Wolberger, 2005). Most histone modifications are reversible and represent a highly dynamic and versatile mechanism to control gene expression patterns and cell specification (Jenuwein and Allis, 2001). Histone modifications not only regulate higher-order chromatin structure and transcriptional states, but also recruit proteins and complexes, which have specific binding motifs for modified histone tails. These proteins can be scaffold proteins or have enzymatic activities such as remodelling enzymes to reposition nucleosomes. Histone modifications can occur in variable combination and characterize specific chromatin domains. This combinatory occurrence of histone modifications led to the concept of the histone code (Strahl and Allis, 2000). The histone code extends the information given by the genetic code and allows a highly dynamic regulation of transcriptional programs, replication, repair and recombination.

Methylation of histone residues can mediate both active and repressive signals through recruitment of the according downstream effector proteins. Histone methylation occurs mainly on the side chains of lysis (K) and arginines (R) in the N-terminal tails of histones H3 and H4 as well as in the globular domains of histones. The enzymes responsible for histone methylation are called histone methyltransferases (HTMs). They catalyse the transfer of a methyl group from S-adenosylmethionine to a lysine or arginine residue. All known histone methyltransferases contain a conserved methyltransferase domain called SET (Su(var)3-9, Enhancer-of-zeste, Tritorax) (Lachner et al., 2003). Lysine methylation can occur in three different states: mono-, di-, and trimethyl. These states are catalysed by different HMTs and have different effects on chromatin structure and transcription. For histone 3 lysine 9 (H3K9), G9a and GLP are mono- and di-methylases. SUV39H1/2 then di- and tri-methylate the methylated substrate. The trimethylated state of H3K9 (H3K9me3) mediates

heterochromatin condensation, gene silencing and the recruitment of Heterochromatin-protein 1 (HP1) (Bannister et al., 2001; Lachner et al., 2001). Similarly, methylation of H3K27 and H4K20 are associated with repressed chromatin states, whereas methylations on H3K4, H3K36 and H3K29 are associates with expressed genes (Martin and Zhang, 2005; Volkel and Angrand, 2007).

Histone acetylation is a dynamic chromatin mark, with important roles in gene regulation, DNA damage repair, and DNA replication. The balance between histone acetylation and deacetylation is kept through the action of two counteracting enzymes called histone acetyltransferases (HATs) and histone deacetyltransferases (HDACs). HATs catalyze the transfer of an acetyl group from acetyl-CoA to lysine residues, whereas HDACs remove the acetyl group from the lysine (Yang, 2004). Acetylation of histones are generally associated with transcriptionally active and chromatin regions with a low degree of condensation. Newly synthesized histones carry the very specific and evolutionary conserved combination of K5 and K12 acetylation on histone H4, which gets swiftly removed after incorporation into chromatin (Sobel et al., 1995).

A less thoroughly described and understood histone modification is histone ribosylation. The transfer of a single ADP-ribose moiety from NAD^+ to an acceptor site causes the release of nicotinamide. ADP-ribose residues can be found as mono-ADP-ribosylation, long linear or branched chains of poly-(ADP-ribose) (PAR) of different length and complexity (D'Amours et al., 1999; Kawaichi et al., 1980). PAR polymerses (PARPs) can covalently attach PARs on acceptor proteins like histones (Hassa and Hottiger, 2008)

1.1.3 PARP1 in the chromatin context

PARPs are involved in many physiological and pathophysiological processed, including inter- and intracellular signaling, transcription, DNA repair, cell cycle regulation, mitosis as well as necrosis and apoptosis (Hassa et al., 2006). Poly(ADP)-ribose polymerase 1 (PARP1, also known as ARTD1 (Hottiger et al., 2010)) is the most abundant (1-2 million proteins per cell) nuclear chromatin associated protein (Kawaichi et al., 1980). PARP1 can synthesize PAR polymers up to 200 ADP-ribose units *in vitro* (Alvarez-Gonzalez and Jacobson, 1987) (**Figure 2**).

PARP1 can be divided into three basic functionally distinct domains: the N-

terminal DNA binding domain, the central auto-modification domain and the C-terminal catalytic domain (Ruf et al., 1996). Since its discovery, most investigatory efforts have been conducted towards its role DNA damage detection and repair responses (D'Amours et al., 1999). In the past decades the research field increasingly focused on understanding the role of PARP1 in other contexts like gene expression regulation or chromatin modulation. However, the role of PARP1 in chromatin regulation is poorly understood (Krishnakumar and Kraus, 2010).

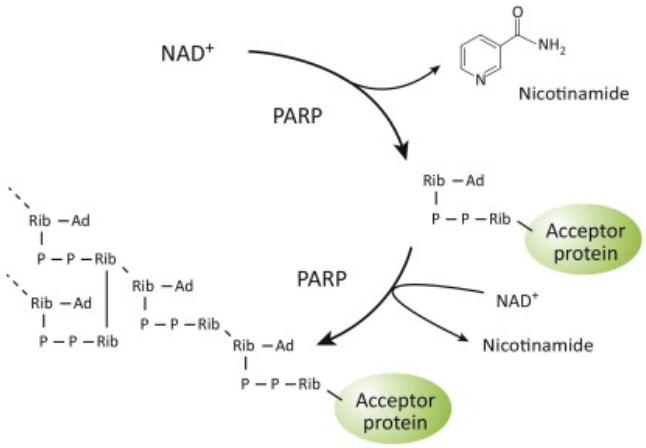

Figure 2. PARP proteins catalyze ADP-ribosylation using NAD$^+$ as a substrate. (Imai and Guarente, 2014)

Much evidence exists to support a paradoxical dual contribution of PARP1 in transcription and chromatin regulation. One of the earliest functional effects described for PARP1 is the disruption of chromatin structures upon PARylation of histones and the destabilization of nucleosomes (Tulin and Spradling, 2003). Interestingly, histones have also been shown to bind to PAR in a non-covalent manner. 40 ADP-ribose residues covalently attached to PARP1 apparently suffice to fully disrupt a chromatosome (Althaus, 1992; Realini and Althaus, 1992). The affinity of histones for poly(ADP-ribose), especially on automodified PARP1, led to the proposal of a 'histone shuttle' mechanism for chromatin relaxation/recondensation involving poly(ADP-ribose) (Realini and Althaus, 1992). According to this scenario, poly(ADP-ribose) synthesized on PARP1 could locally dissociate histones from chromatin. Poly(ADP-ribose) would serve as a scaffold onto which histones could be sequestered in order to facilitate processes like DNA repair. Subsequent cleavage of poly(ADP-

ribose) by PARG would then allow histone-DNA complexes to reform. Data to support this model are offered by early work from the Althaus and Poirer's groups (Aubin et al., 1983; Poirier et al., 1982; Realini and Althaus, 1992). The possibility that automodified PARP1 can act as a scaffold for the transient and local sequestration of histones within relaxed chromatin domains, and by extension for the recruitment of enzymes and co-factors, is attractive, not only in the context of repair, but also for replication and transcription (Rouleau et al., 2004).

Although PARP1 associates with the promoters of almost all actively transcribed genes, it only regulates a subset of the bound genes and has both positive and negative effects of transcription (Krishnakumar et al., 2008). PARP1-mediated PARylation has the ability to induce chromatin decondensation and enhance transcription (Kim et al., 2004). On the other hand, PARP1 binds to and regulates repressive heterochromatic structures such as telomeres (Beneke et al., 2008), centromeres (Kanai et al., 2003), ribosomal RNA repeats and human alpha satellites (Guetg et al., 2012) and is important for their maintenance and function. PARP1 has also been implicated in various ways in DNA methylation. Whereas it has been suggested that PARP1-mediated PARylation inhibits DNA methyltransferase 1 (DNMT1) (Reale et al., 2005; Zampieri et al., 2012), recent evidence shows that PARylation of Ubiquitin-like, containing PHD and RING finger domains, 1 (UHRF1) inhibits UHRF1 mediated ubiquitination of DNMT1, therefore stabilizing DNMT1 protein levels (De Vos et al., 2014). An additional level of complexity to this very diverse protein was added with the discovery of PARP1 as a histone chaperone, able to sequester histones (both *in vivo* and in cells) and to assemble nucleosomes *in vitro* when automodified (Muthurajan et al., 2014; Realini and Althaus, 1992). From all the before mentioned studies emerges a picture showing PARP1 as a versatile regulator of both eu- and heterochromatic regions. However the mechanistic details into each specific processes and their interplay *in vivo* remain unknown.

1.1.4 DNA methylation

DNA methylation is a highly conserved epigenetic modification of DNA playing a pivotal role in gene expression regulation. In higher eukaryotes, cytosines in CpG-dinucleotides are frequently modified to 5-methylcytosines (5mC) (Bestor, 2000). Approximately 80% of all CpG-dinucleotied are methylated in the genome of

vertebrates and highly methylated sequences are found in satellite DNAs, repetitive elements, gene bodies and non-repetitive intergenic DNA (Li and Zhang, 2014). Generally, DNA methylation in GC-rich gene promoters is associated with gene repression, whereas active genes usually correlate with low DNA methylation levels at TSS and high levels in the gene body (Laurent et al., 2010). The remaining unmethylated CpGs are often located in clusters called CpG islands (CGIs). In the human genome 30% of the CGIs are located at transcription start sites (TSS) of so called housekeeping gens, allowing their constitutive expression (Han et al., 2008).

Genome-wide methylation patterns are established during embryogenesis and are propagated during cell divisions. During the development, CpG methylation regulates developmental stage and tissue specific gene expression (Baranzini et al., 2010). Although the precise mechanisms by which DNA methylation affects chromatin states and architecture remain unknown, it is accepted that DNA methylation has a direct role in generating a closed chromatin structure (Keshet et al., 1986).

The three DNA methyltransferase (DNMT) family members DNMT1, DNMT3A and DNMT3B harmonize in the establishment and maintenance of DNA methylation patterns in mammals. DNMT3a and DNMT3b are known as *de novo* DNA methyltransferases, which are able to act on hemi-methylated as well as unmethylated CpG dinucleotides. In fact, DNMT3a shows a three times higher activity on unmethylated versus hemi-methylated DNA (Yokochi and Robertson, 2002). Inactivation of genes encoding DNMT3a and DNMT3b blocks *de novo* methylation in embryonic stem cells (ESC) and mouse embryos. DNMT3a and DNMT3b are required for normal mammalian development but have no influence on the maintenance of imprinted methylation patterns (Okano et al., 1999).

Established DNA methylation patterns are stably inherited by the action of DNMT1. Reduction of DNMT1 in somatic cells leads to hypomethylation, genomic instability and cancer (Brown and Robertson, 2007). DNA methylation maintenance is discussed further in chapter 1.2.3 DNA methylation maintenance.

Even though the exact mechanisms are not yet satisfactorily elucidated, there is overwhelming evidence speaking for a complex interplay between DNA methylation and histone modifications. Typical regions marked with DNA methylation and H3K9me2/3 are silenced and consist of constitutive heterochromatin like ribosomal RNA and centric- and pericentric repeats. A special relationship has been described in

numerous publications between these heterochromatic marks. DNMT1 is targeted to nascent DNA by UHRF1 (Sharif et al., 2007). UHRF1 has a unique hemi-methylated DNA binding activity as well as a Tudor domain binding specifically to H3K9m2/3. It has been shown very recently that UHRF1 with a mutated binding domain for hemi-methylated DNA can still partially recruit DNMT1 to pericentric heterochromatin by its Tudor domain alone and *vise versa* (Liu et al., 2013). These data provide a mechanistic connection between DNA methylation maintenance and the H3K9me2/3 mark. Furthermore, UHRF1 directly binds the H3K9 specific methyltransferase G9a, thus ensuring a tight interplay between histone mark reader and writer (Kim et al., 2009). Another link between DNA methylation and H3K9me is provided by data showing that the DNA methylation reader methyl CpG binding protein (MeCP2) associates with the HMT SUV39H1/2 (Fuks et al., 2003). Fittingly, both proteins are concentrated at pericentromeric regions of heterochromain in immunostainings. Not only have functional links between DNA methylation and H3K9 methylation been described for the DNA methylation maintenance, but also for the *de novo* methylation. DNMT3a and DNMT3b are recruited to major satellites to H3K9 marks *via* HP1, and interact directly with SUV39H1 and SETDB1 (SET domain, bifurcated 1, an other enzyme methylating H3K9) (Fuks et al., 2003; Lehnertz et al., 2003; Muramatsu et al., 2013). The list of evidence does not end here and there are still innumerable open questions. However, the before mentioned studies clearly show a tight and crucial interplay between DNA methylation and H3K9 methylation in embryonic development and epigenetic maintenance of heterochromatin.

1.2 Epigenetic inheritance

During development of multicellular organisms, different cell types establish distinct gene expression profiles. Every cell of a particular organism comprises the identical genomic sequence and these transcriptional states are regulated through epigenetics. This comprises the stable and heritable information that is not encoded in the DNA. Every time a cell divides, its DNA as well as the epigenetic features must be duplicated to conserve the cellular identity. Epigenetic information provides a form of memory not only for transcriptional programs but also architectural features

of constitutive heterochromatin needed for genome stability and chromatid segregation (see 1.1.1 euchromatin and heterochromatin). During DNA replication, both heterochromatin and euchromatin are disrupted ahead of the replication fork and are then reassembled into their original epigenetic states. How chromatin domains are restored on new DNA and transmitted through mitotic cell division remains a fundamental question in biology, with implications for development and complex diseases like cancer. Replication timing is generally recognized as an important control point for epigenetic inheritance (Hand, 1978). Active, euchromatic genes tend to be replicated in early S phase, whereas silent heterochromatic DNA regions are replicated in late S phase. The "window of opportunity" is an interesting model to explain this phenomenon (Goren and Cedar, 2003). It suggests that euchromatin replicated in early S phase is exposed to a nuclear environment favouring the formation of active transcription complexes. On the other hand, late replicating genes comprising heterochromatin are exposed to factors generating repressive structures.

1.2.1 Chromatin replication

Histones are displaced ahead of the replication fork to make the DNA accessible for the replication machinery and chromatin has to be reassembled after the passage of the replication fork. Nucleosome assembly is a two-step process where histones H3 and H4 are deposited onto DNA first, followed by two H2A-H2B heterodimers. Subsequently, 147 bps of DNA are wrapped around the yielded octamer core. Histones are highly charged proteins and are incorporated at their designated place onto DNA through the help of histone chaperones (Smith and Stillman, 1989). Experiments in the 1970s and 1980s have shown that nucleosomes reassembles immediately behind the replication fork and that nascent chromatin loses its susceptibility to DNase I and MNase 10-15 min after replication (Hildebrand and Walters, 1976; Seale, 1975; Sogo et al., 1986). A large number of efforts that have been made to clarify the exact timing of chromatin maturation were performed *in vitro*. However, these results fail to take the complexity of different replication timings and epigenetic states into consideration. Moreover, different factors interfering or assisting with chromatin assembly are neglected in *in vitro* assembly studies.

A central role in chromatin restoration *in vivo* plays Proliferating-Cell-Nuclear-

Antigen (PCNA), since it has been shown to interact with various important chromatin factors including chromatin assembly factor 1 (CAF-1, the best characterized histone chaperone), DNMT1, HDACs, HMTs and chromatin remodelers (Alabert and Groth, 2012). Still it remains largely unknown when and how most chromatin components and modifiers are recruited.

1.2.1 Histone segregation and the inheritance of histone modification

When chromatin is reassembled, newly synthesized histones are incorporated alongside parental histones. New histones are generally thought to not carry the post-translational modifications known to be involved in transmitting epigenetic information (Sobel et al., 1995). How new and old histones or histone dimers are distributed and reassembled after replication is still under debate. There is experimental evidence in the context of histone segregation supporting three distinct models (**Figure 3**).

First, chromatin could be formed from a pool of new and old histones and distributed in a random fashion. This way, epigenetic marks would only be propagated if enrichment in several adjacent nucleosomes can be detected, whereas highly diluted marks would be lost. A second possibility is the semi-conservative manner *via* equal distribution of either H3-H4 dimers or tetramers on the nascent chromatin. In this manner, the old histones would represent a sort of template and post-translational modifications can be copied onto new dimers or tetramers from the adjacent histones/nucleosomes (Margueron and Reinberg, 2010). In 2013, Tran et al. could show that histones distribute asymmetrically in asymmetric divisions of *Drosophila* germ line stem cells. The differentiating daughter cell was enriched in newly synthesized histones, whereas the daughter cell maintaining the stem cell fate retained the parental histones (Tran et al., 2013). The distribution of old and new histones on the daughter strands could therefore be differential state-, species- and tissue-specific.

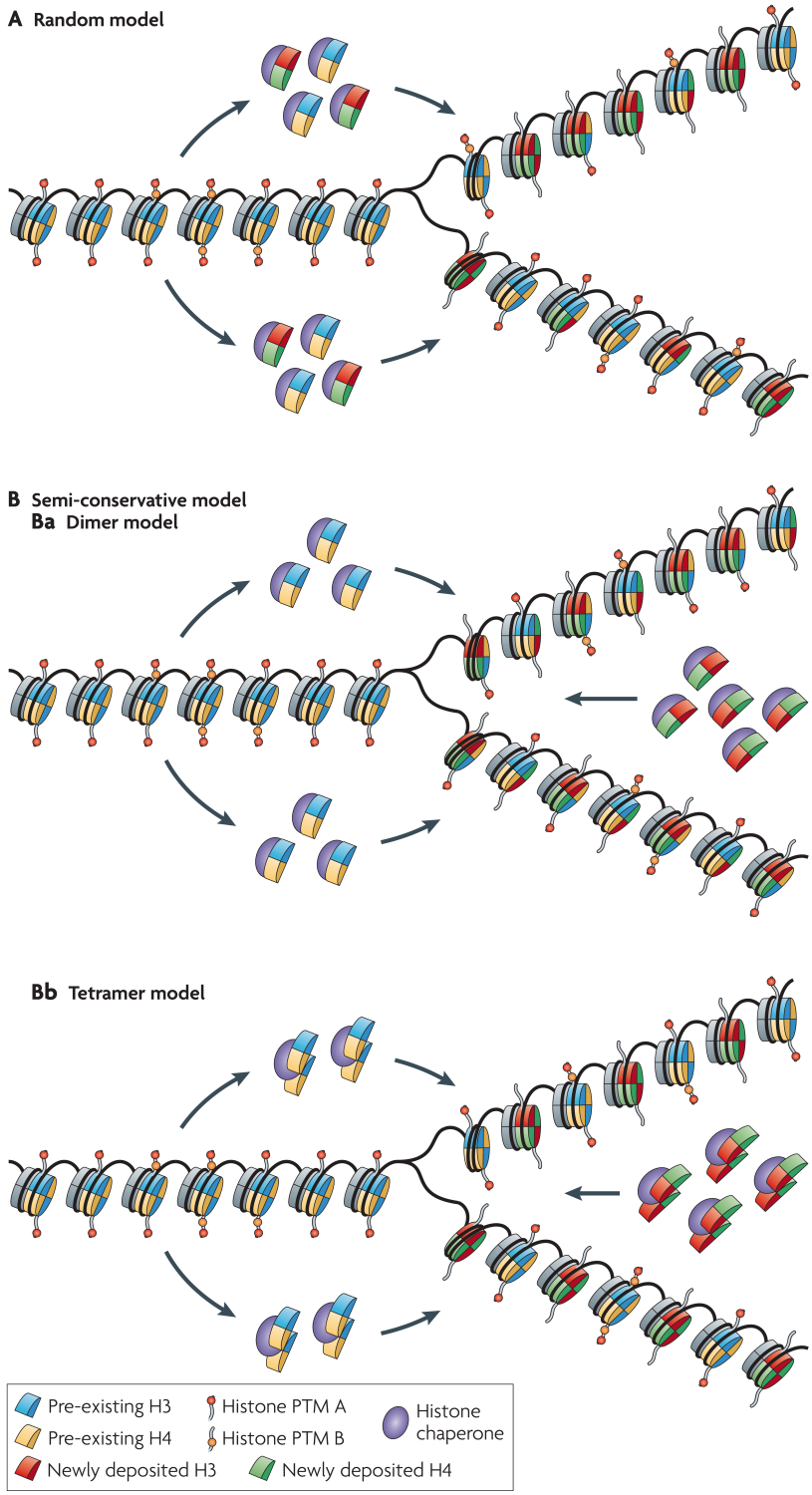

Figure 3. Two models of histone deposition during replication. A. Histones segregate randomly between the leading and lagging DNA strands. B. The semi-conservative model of histone segregation. Ba Scheme showing H3-H4 segregating as dimers onto the nascent DNA. Newly synthesized H3-H4 complete the tetramer. Bb This scheme shows the model were H3-H4 tetramers are inherited during the cell cycle. (Margueron and Reinberg, 2010)

Whichever way new and old histones are distributed, the assembly of new nucleosomes or nucleosome arrays inevitably causes a dilution of posttranslational epigenetic marks. To ensure the stability of chromatin structures and a faithful propagation of epigenetic states, cells need to reestablish the post-translational modifications. It is widely accepted, that histone marks are transferred with old histones into newly synthesized DNA (Alabert et al., 2015; Alabert et al., 2014; Margueron and Reinberg, 2010) . New histones however, have to be modified to stably maintain epigenetic signatures after replication. Until recently, it was believed that new histones are modified immediately after the passage of the replication fork. Similarly to current models about nucleosome assembly, this data was based on the findings that HMTs interact with PCNA. In recent years however, contradictory evidence has been found, showing that new histones are not always modified immediately after replication. Three different models have been described. A first model suggests that some modifications show the highest enrichment before replication, which gets diluted after segregation to the new daughter strands. In this way marks do not have to be added after replication, but are diluted to the right concentration after the passage of the replication fork (Lanzuolo et al., 2012). The second, and most thoroughly investigated model suggests a slow restoration of histone modifications, which can last until G1 of the next cell cycle (Scharf et al., 2009; Xu et al., 2012; Zee et al., 2012). Data from a recent publication combining nascent chromatin capture (NCC) and triple-SILAC (stable isotope labeling with amino acids in cell culture) supports the model that most histone modifications are gradually restored after dilution (Pesavento et al., 2008; Scharf et al., 2009; Sweet et al., 2010). However, this work additionally found evidence that H3K9me3 and H3K27me2 marks are not simply inherited by a 2:1 dilution of marks and a gradual re-establishment by modification of the new histones (Alabert et al., 2015). Their data support a previously postulated model, that old and new histones are continuously modified through every cell cycle, while keeping the total number of modified lysines constant (Lanzuolo et al., 2012; Xu et al., 2012). Parental histones accumulate modifications with age and this “over-modification” is compensated by the new histones carrying fewer modifications. How histone modifications are maintained exactly is hence still under debate and conflicting evidence suggests that this complex question may have multiple valid answers.

1.2.2 DNA methylation maintenance

DNA methylation is the only epigenetic mark, which is not removed by the replication fork. The DNA template during replication keeps its methylation mark throughout the cell cycle, however, newly synthesized strands incorporate only unmethylated cytosins. By virtue of the fact that CpG dinucleotides are symmetrically methylated, the parental strand functions as a template for the complementary daughter strand. DNMT1 is known as the maintenance enzyme for CpG methylation (**Figure 4**). Its specific role in DNA methylation maintenance at replication forks was long based on the fact that DNMT1 has been shown to have a 7.2 fold higher preference for hemi-methylated DNA over unmethylated DNA, and on its interaction with PCNA (Chuang et al., 1997; Hermann et al., 2004). However, DNMT1 also exhibits *de novo* methylation activity and it has recently been shown that its ability to bind PCNA is neither absolutely required nor sufficient for DNA methylation maintenance (Pradhan et al., 1999; Schermelleh et al., 2007; Spada et al., 2007). Recent evidence now suggests that UHRF1 represents the crucial mechanistic link between hemi-methylated DNA and DNMT1. Depletion of UHRF1 in mice results in methylation defects resembling the ones observed in loss of DNMT1 (Sharif et al., 2007). UHRF1 (also known as ICBP90 in human and NP95 in mouse) contains a SET and ring-associated domain (SRA) that recognizes preferentially hemi-methylated DNA. Additionally, UHRF1 has an H3K9me2/3-specific-binding activity and has been shown to associate with pericentric heterochromatin (Karagianni et al., 2008). These unique features suggest that UHRF1 has a dominant role in recruiting DNMT1 to nascent, hemi-methylated DNA associated with heterochromatic sequences. However, recruiting DNMT1 is not the only role reported for UHRF1. UHRF1 is also endowed with E3 ubiquitin ligase activity. It has been reported that UHRF1 is responsible to maintain a balance of DNMT1 levels by ubiquitinating DNMT1 and thereby compromising its stability (Qin et al., 2011). Additional evidence suggests, that this process is highly dynamic and can be fine tuned by a number of proteins, including PARP1. PARP1 has been shown to inhibit DNMT1 activity, whilst others report that PARP1 enzymatic activity suppresses the ability of UHRF1 to ubiquitinate DNMT1, thereby stabilizing DNMT1 (De Vos et al., 2014; Reale et al., 2005; Zampieri et al., 2009).

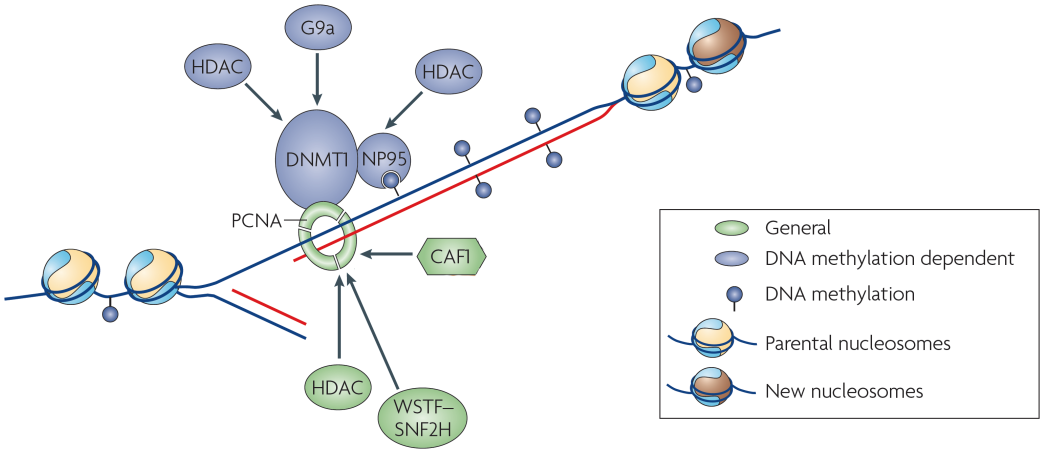

Figure 4. Chromatin maintenance during replication. Parental and new nucleosomes are assembled behind the replication fork. PCNA recruits general chromatin factors like CAF1, HDACs and chromatin remodelers (William syndrome transcription factor WSTF-SNF2H). Depending on the methylation state of the replicated DNA, NP95 (UHRF1) and PCNA recruit DNMT1. Certain histone modifying enzymes like HDACs and G9a are indirectly recruited to methylated DNA through the DNA methylation maintenance machinery. (modified from (Probst et al., 2009)

The before mentioned PCNA independence of DNMT1 implies that DNMT1 activity may not be restricted to the replication fork. Indeed it has been shown that the interaction of DNMT1 with the replication machinery *in vivo* is highly dynamic and that DNMT1 binding to hemi-methylated sites does not prevent the progression of DNA replication. Additionally, it is doubtful if DNA methylation can come close to the DNA replication rate, as cytosine incorporation is 1000-10000 times faster than cytosine methylation (Schermelleh et al., 2007). These recent findings combined, suggest that DNMT1 does not depend on direct replication fork coupling. However, the question arises whether DNMT1 activity is highest at the replication foci due to easy accessibility of the DNA after replication. Several studies have tried to addressed this issue. The first *in vitro* study showed a reduced activity of DNMT1 in a chromatin environment in a highly DNA sequence dependent manner. CpG sites on the surface of 5S rRNA genes or the H19 promoter were completely methylated, whereas nucleosomes containing the Air promoter lost 90% of their DNA methylation (Okuwaki and Verreault, 2004). The same year another group showed that sea urchin 5S rDNA sequences wrapped around a nucleosome decreased DNMT activity 8 fold compared to naked DNA (Robertson et al., 2004). A definite answer on the effect of DNMT1 activity in a chromatin context has not yet been found. However, published data suggest a dynamic interplay of a wide variety of chromatin-

associated factors (i.e. PCNA, UHRF1, PARP1), specific DNA sequences and chromatin environment for DNMT1 activity and stability.

1.3 Inheritance of rDNA chromatin

Ribosomal RNA genes (rDNA) localize within nucleoli and are transcribed by RNA Polymerase I (Pol I). The resulting 47S transcripts are the rRNA precursors, which are subsequently processed into 28S, 18S and 5.8S and packaged with ribosomal proteins to form the large and small subunits of ribosomes (Santoro, 2005). rRNA gene transcription can make up between 30 and 60% of a eukaryotic cell's whole transcription effort to meet the high demand of ribosomes. In human diploid cells there are 400 copies of rRNA genes distributed on the short arms of acrocentric chromosome 13, 14, 15, 21 and 22 (Henderson et al., 1972). These regions are called nucleolar organizing regions (NORs) and fuse together to form the nucleoli. It has been proposed that the position of NORs helps to isolate rDNA units from other, Pol II or Pol III transcribed genes. Further isolation from other is granted through the adjacent centric- and pericentric constitutive heterochromatic consisting of repeats like macro- and alpha-satellites (in mouse major- and minor satellites) (McStay and Grummt, 2008; Saksouk et al., 2015).

1.3.1 Epigenetic feature of rDNA

Despite the high levels of rRNA synthesis, not all rRNA genes are actively transcribed. In each cell, a fraction of rRNA genes is competent for transcription and organized in euchromatic structures while the other portion is transcriptionally silent and heterochromatic (Santoro, 2011). Early studies have shown that Pol I is not loaded on all rRNA genes, indicating that they are not all actively transcribed (McKnight and Miller, 1976). Similarly, psoralen crosslinking, which only crosslinks naked DNA not associated with a histone octamer, produced crosslinked and uncrosslinked rRNA genes (Sogo et al., 1984). The relative amount of these two fractions stays the same in resting as well as growing cells. Therefore, the two chromatin states are stably inherited through the cell cycle and are maintained independently of rRNA transcription rate (Conconi et al., 1989). Transcriptional

silencing of rRNA genes was shown to occur through CpG methylation (Santoro and Grummt, 2001). In mouse cells, methylation of CpG at -133 impairs the association of the transcription factor UBF with rRNA sequences assembled into chromatin. Relying on these observations, an assay developed by Santoro et al. in 2002 based on chromatin immuno-precipitation (ChIP) coupled to CpG methylation measurement (ChIP-chop) enabled to distinguish protein factors, including posttranslational modifications of histones, bound to active (non-CpG methylated) or silent (CpG methylated) repeats (Santoro et al., 2002). This methodology allowed determining that rRNA genes competent for transcription (active rRNA genes), are free of CpG methylation, carry transcriptionally permissive histone modifications on their nucleosomes in the promoter regions (i.e. H4ac, H3K4me3) and associate with RNA Polymerase I (Pol I) and the upstream binding factor (UBF).

On the other hand, silent CpG-methylated rRNA genes carry typical heterochromatic and repressive histone modifications (i.e. H4K20me3, H3K9me3) and do not associate with Pol I and UBF (Santoro et al., 2002) (**Figure 5**). An important factor that specifically associates with silent rRNA genes is the NoRC complex (Nucleolar remodeling complex), comprising TIP5 (TTF1-interacting protein 5) and the ATPase SNF2h. NoRC is key for heterochromatin maintenance at the rRNA genes. TIP5 creates a platform to recruit a number of crucial epigenetic factors for heterochromatin silencing like DNMT1, HDACs and HMTs (Santoro and Grummt, 2005; Santoro et al., 2002; Zhou et al., 2002). Recently, PARP1 has been identified as a new player essential for rDNA heterochromatic maintenance (Guetg et al., 2012).

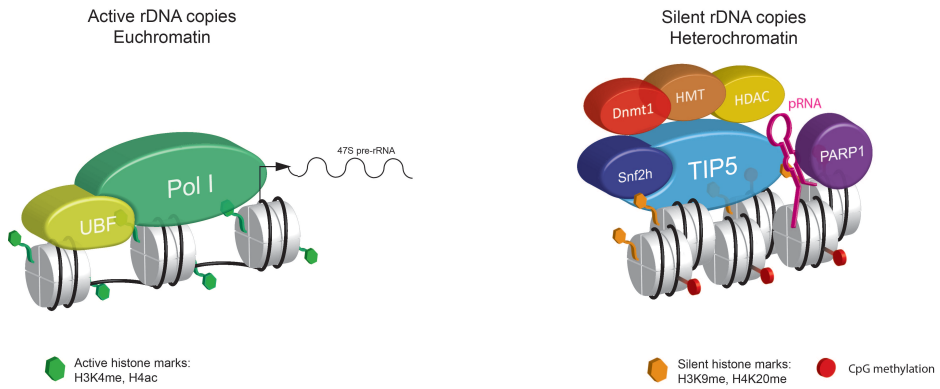

Figure 5. Model showing the chromatin composition of active and silent rRNA genes. Active rRNA genes are associated with UBF, Pol I and histones containing active modifications such as histone acetylation and methylation at H3K4. The silent rRNA genes are associated with the nucleolar remodeling complex NoRC. TIP5 through its association with the lncRNA, pRNA, and epigenetic enzymes (DNMT, HMT, HDAC and PARP1) is required to establish epigenetic silencing at rRNA genes. (red: DNA methylation; orange: histone repressive marks, i.e. H3K9methylation)

1.3.2 TIP5 and PARP1 in the inheritance of rDNA heterochromatin

Due to their distinct chromatin signatures, active and silent rDNA copies have distinct windows of replication. Active, and therefore euchromatic rDNA, replicates during early S phase, whereas heterochromatic rDNA replicates during mid/late S phase (Li et al., 2005; Santoro et al., 2010). As mentioned above, NoRC is crucial to maintain heterochromatic states during cell divisions and it has been shown that its function requires a non-coding RNA (pRNA, promoter RNA) (Mayer et al., 2006). This long non-coding RNA is a processed intergenic RNA transcript of 200-250nt in size with a complementary sequence to the rDNA promoter. Binding of TIP5 to pRNA is essential for TIP5 nucleolar localization, binding to rDNA and establishment of silent rDNA chromatin (Mayer et al., 2008; Mayer et al., 2006; Savic et al., 2014). Recently, PARP1 has been identified as a further key player in rDNA silencing, specifically associating with silent rRNA genes (Guetg et al., 2012). The association of PARP1 with TIP5 is mediated by pRNA and the recruitment to rRNA genes is cell cycle dependent, occurring immediately after replicaton of silent rDNA (**Figure 6**). Once bound, PARP1 specifically parylates components of rDNA heterochromatin (i.e. PARP1 as automodification, TIP5, histones) (Guetg et al., 2012). PARP1 and ADP ribosylation of nascent rDNA is transient and significantly decrease two hours after replication.

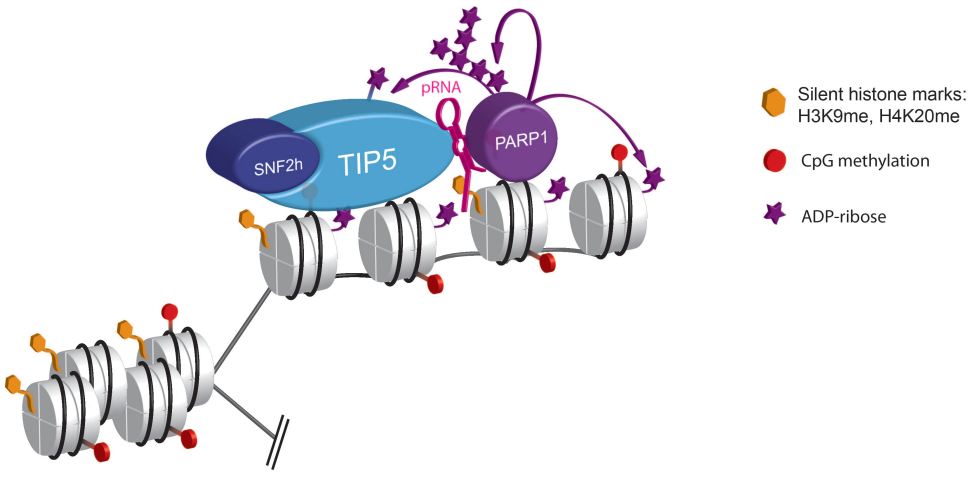

Figure 6. Inheritance of silent rDNA chromatin mediated by TIP5, pRNA and PARP1. After the passage of the replication fork in mid S phase, TIP5-pRNA-PARP1 complex binds to rRNA genes. PARP1 transiently parylates itself, TIP5 and histones.

PARP1 activity is crucial for heterochromatin maintenance at rDNA. CpG methylation as well as silent histone modifications (i.e. H3K9me3) decrease upon PARP1 knockdown or overexpression of an enzymatic mutant PARP1 (lacking ability to generate PAR polymers). The observation that PARP1 only transiently parylates nascent heterochromatic rDNA implies a functional relevance of PARP1 activity during heterochromatin formation after replication. How PARP1 dependent parylation influences heterochromatin formation will be addressed in this PhD thesis.

1.3.3 rDNA heterochromatin and the formation of nuclear heterochromatin

Similarly to constitutive heterochromatic domains, rDNA heterochromatin replicates during mid/late S phase. Remarkably, constitutive heterochromatic structures also physically associate with nucleoli, surrounding them in interphase cells (Guetg et al., 2010; Pluta et al., 1995). In mice, these sequences mainly represent repetitive satellites sequences like the pericentric and centric repeats (corresponding to alpha satellites in humans). Moreover, the inactive X-chromosome contacts the nucleolus during mid/late S phase and this interaction is required for silent chromatin maintenance of its facultative heterochromatin (Zhang et al., 2007). Recent findings further linked rDNA heterochromatin to the formation of centric- pericentric heterochromatin. Depletion of TIP5 and PARP1 not only decrease silent histone modifications (i.e. H3K9me3, H3K9me2) at rDNA, but also on major and minor satellites (mouse) and alpha satellites (human) (Guetg et al., 2010; Guetg et al., 2012). Consequently, cells lacking TIP5 suffer severe genome instability. Similarly, lack of PARP1 is associated with chromosomal instability, characterized by increases chromosome fusion and aneuploidy (d'Adda di Fagagna et al., 1999). Consistent with a role of PARP1 in the formation of constitutive heterochromatin PARP1 was identified as interacting partner of SMARCAD1, a protein that is recruited to sites of DNA replication and ensures correct reestablishment of pericentric heterochromatin (Rowbotham et al., 2011). PARP1 is also bound to telomeres and has been implicated in the formation of facultative heterochromatin at the inactive X chromosome (Beneke et al., 2008; Nusinow et al., 2007).

Aims

Analysis of the temporal dynamics of post-replicative chromatin restoration at euchromatin and heterochromatin and the role of PARP1

To maintain cell identity and function, a dividing cell must replicate not only its genome but also the epigenome. Epigenetic modifications at histones and DNA must surmount the challenge of DNA replication, in which chromatin is disassembled ahead of the replication fork and then reassembled onto two daughter genomes after DNA synthesis. Restoration of epigenetic modifications is a critical step since it can affect the maintenance of information conveyed at the epigenomic level and in turn impact gene expression and genome stability. However, it remains largely unknown how chromatin and epigenetic states are restored to parental states. Moreover, whether the distinctive features of euchromatin and heterochromatin require different modalities for the restoration of the parental chromatin state remains yet to be elucidated.

In this work, we aimed to analyse the temporal dynamics of post-replicative chromatin restoration at euchromatin and heterochromatin.
The specific aims were:

1. To establish an assay to monitor the maturation of chromatin and epigenetic modifications after replication
2. To determine the temporal dynamics of chromatin restoration after replication
3. To define whether euchromatin and heterochromatin use the same modalities to duplicate their chromatin and epigenetic signature.

3 Results

3.1 Published and submitted results

3.1.1 Assembly of heterochromatin after replication is a slow process required for DNA methylation

Authors:	Eva Vollenweider, Anita Steiner & Raffaella Santoro
Journal:	Submitted for publication
Link:	Not yet available
Contribution:	Experimental design, performance and analysis of all main and supplementary figures. R.S. supervised the project and wrote the manuscript together with E.V.

3.1.2 lncRNA maturation to initiate heterochromatin formation in the nucleolus is required for exit from pluripotency in ESCs

Authors:	Natasa Savic, Dominik Bär, Sergio Leone, Sandra C. Frommel, Fabienne A. Weber, Eva Vollenweider, Elena Ferrari, Urs Ziegler, Andres Kaech, Olga Shakhova, Paolo Cinelli & Raffaella Santoro
Journal:	Cell Stem Cell
Link:	http://www.cell.com/cell-stem-cell/abstract/S1934-5909(14)00456-1
Contribution:	Experimental contribution to Figure 5B and Supplementary Figure 3B.

3.1.3 Pramel7 is implicated in naïve pluripotency through proteasomal-epigenetic combined pathways

Authors:	Urs Graf, Elisa Casanova, Eva Vollenweider, Sarah Wyck, Fabienne A. Weber, Sameera S. Patel, Jiwen Li, Jafar Sharif[6], Guido A. Wanner, Haruhiko Koseki, Jiemin Wong, Raffaella Santoro and Paolo Cinelli
Journal:	Under review for publication in Molecular Cell
Link:	Not yet available
Contribution	Experimental contribution to Figure 1c and 1d

Assembly of heterochromatin after replication is a slow process required for DNA methylation

Eva Vollenweider[1,2], Anita Steiner[1] and Raffaella Santoro[1*]

[1]Institute of Veterinary Biochemistry and Molecular Biology, University of Zurich; [2]Molecular Life Science Program, Life Science Zurich Graduate School, University of Zurich, Switzerland

*Correspondence: raffaella.santoro@vetbio.uzh.ch

Abstract

A dividing cell must not only accurately duplicate its genome, but also its organization into chromatin. This process includes the post-replicative restoration of epigenetic modifications at DNA and histones that specify distinct chromatin states such as euchromatin and heterochromatin. Current models of epigenetic inheritance are based on the notion that the newly synthesized DNA is rapidly methylated and assembled into chromatin shortly after replication. By profiling the temporal dynamics of post-replicative establishment of euchromatin and heterochromatin, we found that the assembly of nucleosomes and DNA methylation at nascent constitutive heterochromatin is a slow process that lasts until G2/M. PARP1 transiently associates with nascent heterochromatic DNA, a time that coincides with the restrained assembly of nucleosomes. Inhibition of PARP1-mediated ADP-ribosylation caused a rapid assembly of nucleosomes at nascent heterochromatin as observed at euchromatin and impairs DNA methylation without altering the association of the DNA methylation machinery. The results indicate that a delayed post-replicative nucleosome assembly at heterochromatin facilitates methylation at DNA, unravelling a post-replicative temporal coordination between nucleosome deposition and DNA methylation.

In eukaryotic organisms, the replication of the genome and epigenome are critical to maintain cell identity and function. The restoration of epigenetic modifications at histones and DNA onto the two daughter genomes is a critical step since it can affect the maintenance of information conveyed at epigenetic level and in turn impact gene expression and genome stability (*1*). Histones and their modifications must surmount the challenge of DNA replication, in which chromatin is disassembled ahead of the replication fork and reassembled onto two daughter genomes after DNA synthesis (*2*). Moreover, due to the semi-conservative nature of DNA replication, methylation at cytosines has to be re-established (*3*). Studies on chromatin restoration after replication have mainly focused on the constitutive heterochromatin, which is enriched in repetitive sequences, highly condensed, and replicating in late S-phase (*4*). In the post-replicative re-establishment of heterochromatin, the proliferating cell nuclear antigen (PCNA) seems to play a central role by coordinating replication of DNA with the restoration of the epigenome through its ability to recruit the maintenance DNA methyltransferase DNMT1, several chromatin remodelers, histone modifying enzymes and histone chaperons (*5*). Still, it remains largely unknown how most regulators are recruited and when heterochromatin is completely restored to parental states. Furthermore, it is still unknown how chromatin structures other than constitutive heterochromatin are re-established after replication. Euchromatin is fundamentally different from constitutive heterochromatin due to a less condensation, gene-rich content, high transcription levels, enrichment in active histone modifications and replication in early S-phase (*6*). Whether the distinctive features of euchromatin and heterochromatin require different modalities for the restoration of the parental chromatin state remains yet to be elucidated.

In this work, we analysed and compared the temporal dynamics of post-replicative chromatin restoration at euchromatin and heterochromatin. We established an assay based on BrdU labelling of nascent euchromatic or heterochromatic DNA in synchronized cells and tracking the maturation of the formed chromatin at later time points. We circumvent the use of DNA polymerases inhibitors for cell cycle synchronization (known to induce cellular stress) by using T24 bladder tumour cells. T24 cell cycle synchronization is based upon a contact inhibition for 3 days, followed by seeding at a lower cell density to let cells re-enter into cell cycle (*7, 8*) (**Fig. 1A**).

T24 cell-cycle synchronization and progression is highly efficient and reproducible and was confirmed by flow cytometry (FACS) for every experiment (**Fig. 1B**). After 14 hours, cells reach G1/S (here referred to as t = 0h) and synchronously progress through S, G2 and M phases. The majority of DNA synthesis is completed 8 hours after entry into S phase as indicated by measurements of BrdU incorporation (**Fig. 1C**). The significant increase of mitotic histone H3S10 phosphorylation ($H3S10_{ph}$) locates G2/M phase boundary at h 10 (**Fig. 1D**).

To compare the maturation of euchromatin and heterochromatin after replication, we excluded a bias based on DNA sequences by measuring chromatin maturation at ribosomal RNA (rRNA) genes, which represent a paradigm of both euchromatin and heterochromatin. In each cell, rRNA genes are present in 400 copies of identical sequences. A fraction of genes is organized in euchromatic structures and replicate in early S-phase while the other portion is heterochromatic and replicates in mid/late S-phase (**Fig. S1A**) (*8, 9*).

First, we monitored the temporal dynamics of heterochromatin restoration after replication by analysing nascent heterochromatic rRNA genes and alpha satellites. We synchronized T24 cells and labelled DNA replicating during h 6 after entry into S phase with a 1 h BrdU pulse, a time that coincides with the replication of heterochromatic rRNA repeats and a portion of alpha satellites (**Fig. 2A, Fig. S1A,B**). After removal of BrdU, cells were chased with thymidin and progressed into late S, G2 and M phases. BrdU labelling was limited to sequences replicating during h 6. As shown in **Figure 2B**, DNA from equal amounts of cells collected at the indicated time points (h 6-10) displayed BrdU enrichment at rRNA repeats as well as alpha satellites at h 6 and no further increase in the following time points. Equivalent BrdU-IP efficiencies were ensured by amplification of β-lactamase sequences from BrdU-labelled pBluescript plasmid DNA (BrdU-pBS), which was added to all samples prior IP. Efficiency of cell cycle synchronization, specificity of BrdU-labelling and BrdU-IP were further supported by the lack of BrdU at *GAPDH*, which replicates in early S-phase (**Fig. S1B**).

We initially measured the assembly of nucleosomes at heterochromatic rRNA genes and alpha satellites after the passage of the replication fork. The current model proposes that histones are placed on new DNA as soon as the replication is completed (*10*). This model is based on

pioneering work using nucleases to probe chromatin assembly after replication, which defined a time window of approximately 15-20 min for new DNA to be packaged into a structure with nucleosomal periodicity and nuclease resistance similar to bulk chromatin (*11, 12*). However, these studies were performed on total replicating DNA and, consequently, were not informative on the kinetics of nucleosome assembly at different chromatin domains. We performed BrdU-IP on DNA purified from mononucleosomes obtained by Micrococcal nuclease (MNase) digestion of chromatin from h 6 BrdU-labelled cells collected every hour until G2/M (**Fig. 2C, Fig. S1D**). Surprisingly, we observed an increase of nucleosome occupancy lasting until G2/M, suggesting that assembly of nucleosomes into newly replicated heterochromatic rRNA repeats and alpha satellites is not completed immediately after replication. A similar result was obtained with heterochromatic rRNA genes and major satellites in mouse NIH3T3 cells, indicating that the slow incorporation of nucleosomes on nascent heterochromatin is a conserved process (**Fig. 2D, Fig. S1E**). Consistent with these results, sequential anti-histone H3 ChIP followed by BrdU-IP revealed that the assembly of histone H3 into h 6 replicated heterochromatic rDNA and alpha satellites continues until 3 hours after replication (**Fig. 2E**). The slow incorporation of histone H3 could also be detected by immunoblot analysis of hourly taken chromatin-bound fractions of equal numbers of synchronized T24 cells which show a global increase of chromatin-bound histones H3 that lasts until G2 (**Fig. 1D**). Accordingly, the silent H3K9me2 mark at replicated DNA displays a similar profile of histone H3 incorporation, increasing for 3 further hours after replication of rRNA genes and 4 hours on alpha satellites (**Fig. 2F**). Although in this experimental set-up we cannot distinguish parental from new histones, the slow acquisition of H3K9 methylation is consistent with recent proteomic analyses showing that the majority of lysine modifications on new histones are acquired after the S-phase (*13-15*). Together, these results indicate that at heterochromatic regions not only the re-establishment of H3K9 dimethylation but also the assembly of nucleosomes is not taking place immediately after replication, but is a slow process.

Next, we monitored DNA methylation after replication. Since DNA replication is a semi-conservative mechanism, post-replicated DNA is hemi-methylated and its methylation pattern is restored on the newly synthesized daughter strand by DNMT1, while the parental strand serves

as template (*3*). Due to the association of DNMT1 with PCNA and with sites of DNA replication, it is generally assumed that DNA replication and methylation are kinetically and mechanistically coordinated (*16, 17*). Consequently, DNA methylation is considered to be restored immediately after the passage of the replication fork. To determine the restoration timing of DNA methylation at heterochromatic repeats (*18*), we established an assay based on sequential IP on h 6 BrdU-labelled cells (**Fig. 2G**). We first immuno-precipitated methylated ss-DNA (MeDIP) followed by BrdU-IP to quantify and monitor methylation of rRNA sequences replicated during h 6. As shown in **Figure 2H**, DNA methylation increases throughout the 3 hours post-replication and shows a profile that recalls the slow assembly of nucleosomes. These results strongly suggest that DNA methylation is not kinetically coordinated with the replication machinery and that methylating a cytosine might take far longer than to incorporate it. The uncoupling of DNA methylation and DNA replication is also consistent with previous studies showing a PCNA-independent localization of DNMT1 at constitutive heterochromatin in late S and G2-phases (*19*). These results are further supported by the 3-4 orders of magnitude difference in the estimated kinetics of DNA replication in vivo (0.035s per nucleotide) and DNA methylation by Dnmt1 *in vitro* (70-450s per methyl group transfer) (*20, 21*). Our results reflect this different kinetics and indicated that the re-establishment of DNA methylation at heterochromatin is not completed immediately after replication but is a slow process.

To determine whether the slow nucleosome assembly after replication is a specific feature of heterochromatin, we analysed euchromatic rRNA genes replicating during early S-phase. To this purpose, we labelled with BrdU euchromatic sequences replicating in the second hour of S phase (h 2, **Fig. 3A**). BrdU labelling was limited to sequences replicating in this time window, indicated by BrdU-IP showing no further increase in BrdU incorporation at rRNA repeats as well as the early-replicating *GAPDH* after h 2 of S phase (**Fig. 3B**). In contrast to heterochromatin, the amounts of BrdU-labeled mononucleosomal DNA display no further increase after h 2 (**Fig. 3C**). A similar result was obtained with histone H3 ChIP analysis followed by BrdU-IP (**Fig. 3D**). Taken together, these results indicate that, in contrast to heterochromatin, nucleosome assembly at replicated euchromatin occurs immediately after replication.

We then asked whether the slow assembly of nucleosomes at nascent heterochromatin is required for a faithful duplication of heterochromatic marks. Previous results indicated that nascent heterochromatic rRNA repeats are associated with the poly(ADP-ribose)-polymerase-1 (PARP1) while the euchromatic rRNA genes are not (*8*). At replicated heterochromatic rRNA repeats, PARP1 synthesizes and transfers ADP-ribose (PAR) polymers on itself and other proteins such as histones. In the context of DNA repair, the automodified PARP1 has been proposed to act as a scaffold for the transient and local sequestration of histones at DNA damage sites (*22*). Although PARP1 activity is generally considered to promote decompaction of chromatin and reduction of higher-order structures (*23*), PARP1-mediated parylation is required to establish a closed and epigenetic repressed chromatin at rRNA genes, including CpG methylation (*8*). Importantly, PARP1 binding and parylation of heterochromatic rRNA sequences after replication is a transient event (*8*); the association of PARP1 with rRNA repeats and alpha satellites timely coincides with the restrained assembly of nucleosomes at replicated heterochromatin (**Fig. 4A**). These results prompted us to investigate if the slow nucleosome assembly on nascent heterochromatin is mediated by PARP1 and whether this process is implicated in the maintenance of DNA methylation. Since depletion of PARP1 by siRNA inevitably alters cell cycle progression (data not shown), we decided to use the fast-response pharmacological inhibition of PARP1 activity by exposing the cells from h 5 on to the PARP1 inhibitor ABT-888 (PARPi, **Fig. S2A,B).** This treatment did not perturb replication of heterochromatic DNA and S phase progression (**Fig. S2C,D**). Analysis of nucleosome deposition of h 6 replicated DNA under inhibition of PARP1 activity showed a completed assembly shortly after replication (**Fig. 4B, Fig. S2E**) and exhibits a kinetics comparable to the chromatinization of euchromatic DNA (**Fig. 3C**). A similar fast assembly was also obtained for the incorporation of histone H3 and H3K9me2 at nascent DNA on cells treated with PARPi (**Fig. 4C,D**). PARP1 activity only affects the post-replicative kinetics of nucleosome deposition during S and G2 phases, as the total amounts of the assembled nucleosomes and the levels of H3K9 methylation with or without PARPi show no significant difference at G2/M. Together these results indicate that

PARP1 activity is required for the slow deposition of nucleosomes at heterochromatic DNA after replication.

The catalytic efficiency of DNMT1 was shown to be significantly compromised on nucleosome substrate when compared to naked DNA (*24, 25*), a result that is consistent with the low DNA methylation content measured on nucleosomes in vivo (*26*). The inaccessibility of nucleosomal DNA for methylation was also proposed for the *de novo* methylation directed by Dnmt3a and Dnm3b, which is occluded from nucleosomal DNA (*27*). We reasoned that an efficient post-replicative DNA methylation observed on rRNA heterochromatin might greatly depend on the amounts of nucleosomes assembled on replicated DNA. Therefore, we asked whether the accelerated loading of nucleosomes caused by inhibition of PARP1 activity might affect DNA methylation at heterochromatic rRNA genes after replication. As shown in **Figure 4E**, inhibition of PARP1 strongly reduces the incorporation of methyl groups on nascent rRNA genes (**Fig. 4F, Fig. S2F**). Inactivation of PARP1 activity did not affect two crucial factors for the transmission of DNA methylation, DNMT1 and UHRF1 (*28*). PARP1 inhibition does not alter DNMT1 expression, the interaction of DNMT1 with the heterochromatic repeats and the global association with chromatin during S phase progression (**Fig. S3A,B**). Similarly, the association of DNMT1 with rRNA genes and alpha satellites does not depend on PARP1 itself (**Fig. S3C**). Moreover, the interaction of DNMT1 with TIP5, a factor implicated in the establishment of DNA methylation at rRNA genes (*29*), was not altered upon PARP1 inhibition (**Fig. S3D**). The previously described interaction of UHRF1 with PARP1 (*30*) does not depend on PARP1 activity (**Fig. S4A**). Similarly, binding of UHRF1 and PARP1 with rRNA repeats and alpha satellites does not require active PARP1 (**Fig. S4B**). Finally, the association of TIP5 with UHRF1 is not mediated by PARP1 (**Fig. S4C**). Together, these results indicated that PARP1 activity is required for the establishment of DNA methylation patterns after replication without affecting the association of the DNA methylation machinery.

Faithful maintenance of methylation over many cell divisions is critical for proper formation of heterochromatic structures. Even a mildly inhibitory effect on DNMT activity by nucleosomes assembled on newly synthesized DNA would result in substantial losses in DNA methylation over

the course of many cell divisions. The slow deposition of nucleosomes mediated by PARP1-ADP-ribosylation might represent an important opportunity for the heterochromatin to allow the completion of methylation at the DNA, which would be inefficiently modified if immediately assembled into condensed chromatin structures (**Fig. 4F, S5**). This temporary restrained deposition of nucleosomes is a specific feature of heterochromatin as indicated by the rapid assembly of nucleosomes observed after replication of euchromatic genes, which are generally free of DNA methylation. Hypomethylation at heterochromatic DNA repeats is a hall-mark of cancer cells (*31*). The post-replicative temporal coordination of DNA methylation and nucleosome assembly at heterochromatin might represent an important process to consider in future studies aimed to understand alterations in epigenome and genome integrity during tumour progression.

Acknowledgments

This work was supported by the Swiss National Science Foundation (310003A-135801 and 31003A-152854), UBS-Promedica Stiftung and Forschungskredit of the University of Zurich (to E.V.).

References

1. C. Rivera, Z. A. Gurard-Levin, G. Almouzni, A. Loyola, Histone lysine methylation and chromatin replication. *Biochim Biophys Acta* **1839**, 1433-1439 (2014).
2. I. Whitehouse, D. J. Smith, Chromatin dynamics at the replication fork: there's more to life than histones. *Curr Opin Genet Dev* **23**, 140-146 (2013).
3. P. A. Jones, G. Liang, Rethinking how DNA methylation patterns are maintained. *Nat Rev Genet* **10**, 805-811 (2009).
4. G. Almouzni, A. V. Probst, Heterochromatin maintenance and establishment: lessons from the mouse pericentromere. *Nucleus* **2**, 332-338 (2011).
5. C. Alabert, A. Groth, Chromatin replication and epigenome maintenance. *Nat Rev Mol Cell Biol* **13**, 153-167 (2012).
6. S. I. Grewal, S. Jia, Heterochromatin revisited. *Nat Rev Genet* **8**, 35-46 (2007).
7. Y. Jin *et al.*, Cell cycle-dependent colocalization of BARD1 and BRCA1 proteins in discrete nuclear domains. *Proc Natl Acad Sci U S A* **94**, 12075-12080 (1997).
8. C. Guetg, F. Scheifele, F. Rosenthal, M. O. Hottiger, R. Santoro, Inheritance of Silent rDNA Chromatin Is Mediated by PARP1 via Noncoding RNA. *Mol Cell* **45**, 790-800 (2012).
9. J. Li, R. Santoro, K. Koberna, I. Grummt, The chromatin remodeling complex NoRC controls replication timing of rRNA genes. *EMBO J* **24**, 120-127 (2005).
10. A. T. Annunziato, Assembling chromatin: the long and winding road. *Biochim Biophys Acta* **1819**, 196-210 (2013).
11. C. E. Hildebrand, R. A. Walters, Rapid assembly of newly synthesized DNA into chromatin subunits prior to joining to small DNA replication intermediates. *Biochem Biophys Res Commun* **73**, 157-163 (1976).
12. R. L. Seale, Assembly of DNA and protein during replication in HeLa cells. *Nature* **255**, 247-249 (1975).

13. B. M. Zee, L. M. Britton, D. Wolle, D. M. Haberman, B. A. Garcia, Origins and formation of histone methylation across the human cell cycle. *Mol Cell Biol* **32**, 2503-2514 (2012).
14. M. Xu, W. Wang, S. Chen, B. Zhu, A model for mitotic inheritance of histone lysine methylation. *EMBO Rep* **13**, 60-67 (2012).
15. C. Alabert *et al.*, Two distinct modes for propagation of histone PTMs across the cell cycle. *Genes Dev* **29**, 585-590 (2015).
16. L. S. Chuang *et al.*, Human DNA-(cytosine-5) methyltransferase-PCNA complex as a target for p21WAF1. *Science* **277**, 1996-2000 (1997).
17. H. Leonhardt, A. W. Page, H. U. Weier, T. H. Bestor, A targeting sequence directs DNA methyltransferase to sites of DNA replication in mammalian nuclei. *Cell* **71**, 865-873 (1992).
18. R. Santoro, I. Grummt, Molecular mechanisms mediating methylation-dependent silencing of ribosomal gene transcription. *Mol Cell* **8**, 719-725 (2001).
19. L. Schermelleh *et al.*, Dynamics of Dnmt1 interaction with the replication machinery and its role in postreplicative maintenance of DNA methylation. *Nucleic Acids Res* **35**, 4301-4312 (2007).
20. D. A. Jackson, A. Pombo, Replicon clusters are stable units of chromosome structure: evidence that nuclear organization contributes to the efficient activation and propagation of S phase in human cells. *J Cell Biol* **140**, 1285-1295 (1998).
21. S. Pradhan, A. Bacolla, R. D. Wells, R. J. Roberts, Recombinant human DNA (cytosine-5) methyltransferase. I. Expression, purification, and comparison of de novo and maintenance methylation. *The Journal of biological chemistry* **274**, 33002-33010 (1999).
22. M. Rouleau, R. A. Aubin, G. G. Poirier, Poly(ADP-ribosyl)ated chromatin domains: access granted. *Journal of cell science* **117**, 815-825 (2004).
23. K. W. Ryu, D. S. Kim, W. L. Kraus, New facets in the regulation of gene expression by ADP-ribosylation and poly(ADP-ribose) polymerases. *Chem Rev* **115**, 2453-2481 (2015).
24. A. K. Robertson, T. M. Geiman, U. T. Sankpal, G. L. Hager, K. D. Robertson, Effects of chromatin structure on the enzymatic and DNA binding functions of DNA methyltransferases DNMT1 and Dnmt3a in vitro. *Biochem Biophys Res Commun* **322**, 110-118 (2004).
25. M. Okuwaki, A. Verreault, Maintenance DNA methylation of nucleosome core particles. *J Biol Chem* **279**, 2904-2912 (2004).
26. M. Felle *et al.*, Nucleosomes protect DNA from DNA methylation in vivo and in vitro. *Nucleic Acids Res* **39**, 6956-6969 (2011).
27. T. Baubec *et al.*, Genomic profiling of DNA methyltransferases reveals a role for DNMT3B in genic methylation. *Nature* **520**, 243-247 (2015).
28. J. Sharif *et al.*, in *Nature*. (2007), vol. 450, pp. 908-912.
29. R. Santoro, J. Li, I. Grummt, The nucleolar remodeling complex NoRC mediates heterochromatin formation and silencing of ribosomal gene transcription. *Nat Genet* **32**, 393-396 (2002).
30. M. De Vos *et al.*, Poly(ADP-ribose) polymerase 1 (PARP1) associates with E3 ubiquitin-protein ligase UHRF1 and modulates UHRF1 biological functions. *The Journal of biological chemistry* **289**, 16223-16238 (2014).
31. M. Ehrlich, DNA hypomethylation in cancer cells. *Epigenomics* **1**, 239-259 (2009).

Figure legends

Figure 1

Cell cycle synchronization of T24 cells

(**A**) Outline of cell cycle synchronization for T24 cells.

(**B**) FACS analysis. Representative cell cycle profile of T24 cells progressing from G1/S to G2/M phases.

(**C**) Quantifications of BrdU incorporation of synchronized T24 cells that were 1h pulse-labeled at the indicated time points (Fig. S1A). Anti-BrdU immunofluorescent images were digitally recorded and quantified by counting BrdU positive cells relative to total cell number (100-200 cells).

(**D**) Western blot analysis for chromatin bound histone H3 and the mitotic marker histone H3S10p from equal amounts of T24 cells collected at the indicated time points of synchronized cells. Histone H3 signal was quantified using the Odyssey® software. Data are mean ± SEM (n = 4 independent experiments).

*P < 0.05 (unpaired, two tailed t-test)

Figure 2

Nucleosome occupancy and DNA methylation at heterochromatin are not restored immediately after replication

(A) Scheme representing the strategy to monitor chromatin maturation after replication of heterochromatic rRNA genes and alpha satellites. DNA replicating during h 6 was labelled with a 1h BrdU pulse. Arrows indicate the time of sample collection before (h 5) and after BrdU-labeling.

(**B**) BrdU-labelling is limited to rRNA genes and alpha-satellites replicating only during h 6. qPCR of anti-BrdU immuno-precipitation (BrdU-IP) of DNA from equal amounts of h 6 BrdU-labelled T24 cells collected at the indicated time points. Equal IP efficiencies are shown by amplification of β-lactamase sequences from BrdU-labelled pBluescript plasmid DNA (BrdU-pBS). Data are normalized to input and h 6 values and are mean ± SEM (error bars) (n = 3 independent experiments).

(**C** and **D**) Deposition of nucleosomes after replication of heterochromatin is a slow process. Anti-BrdU-IP of mononucleosomal DNA of T24 (C) or NIH3T3 (D) cells labelled with BrdU during h 6. rRNA genes (C,D), alpha satellites (C) and major satellites (D) were quantified by qPCR and normalized to input and h 6 values. Data are mean ± SEM (error bars) (n = 3 independent experiments).

(**E** and **F**) Deposition of histone H3 and H3K9me2 after replication of heterochromatin is a slow process. Sequential ChIP/BrdU-IP. Data are normalized to input and h 6 values and are mean ± SEM (error bars) (independent experiments: n=5 for histone H3, n=3 for H3K9me2).

(**G**) Experimental strategy to quantify CpG methylation at newly synthesized DNA strands of h 6 replicated heterochromatin.

(**H**) Sequential MeDIP/BrdU-IP analysis in T24 cells showing post-replicative methylation levels of h 6 replicated heterochromatic rRNA genes. Data are normalized to input and h 6 values and are mean ± SEM (error bars) (n = 4 independent experiments).

*P < 0.05, **P < 0.01, ***P < 0.001 ns: not significant (unpaired, two tailed t-test)

Figure 3

Nucleosomes at euchromatic genes are restored immediately after replication.

(**A**) Scheme representing the strategy to monitor chromatin maturation after replication of euchromatic rRNA and *GAPDH* genes. DNA replicating during h 2 was labelled with a 1h-pulse of BrdU. Arrows indicated the time of sample collection before (h 1) and after BrdU-labelling.

(**B**) BrdU-IP showing that BrdU-labelling is limited to h 2 replicated euchromatic genes only. BrdU-DNA levels were measured by qPCR, normalized to input and h 2 values and are mean ± SEM (error bars) (n = 3 independent experiments).

(**C**) Anti-BrdU-IP of mononucleosomal DNA of T24 cells labelled with BrdU at h 2 of S phase. h 2 replicated rRNA and *GAPDH* genes were quantified by qPCR, normalized to input and h 2 values and are mean ± SEM (error bars) (n = 2 independent experiments).

(**D**) Sequential ChIP/BrdU-IP analysis showing post-replicative occupancy of histone H3 at h 2 replicated rRNA and *GAPDH* genes. Values are normalized to input and h 2 values and are mean ± SEM (error bars) (n = 3 independent experiments).

ns: not significant (unpaired, two tailed t-test)

Figure 4

PARP1 activity slows down post-replicative nucleosome assembly and is essential for the maintenance of DNA methylation.

(**A**) Sequential PARP1-ChIP/BrdU-IP analysis showing that the association of PARP1 with rRNA genes and alpha satellites is restricted to the first 2 hours after replication.

(**B**) Anti-BrdU-IP of mononucleosomal DNA of T24 cells treated with or without PARPi. BrdU-labeled rRNA genes and alpha satellites levels were measured by qPCR, normalized to input and h 6 value of the untreated group and are mean ± SEM (error bars) (n = 3 independent experiments).

(**C** and **D**) Sequential ChIP/BrdU-IP analysis showing accelerated post-replicative occupancy of histone H3 (D) and H3K9me2 (E) at h 6 replicated DNA in cells treated with PARPi. Values normalized to input and h 6 values and are mean ± SEM (error bars) (n = 4 independent experiments).

(**E**) Sequential MeDIP/BrdU-IP analysis showing inhibition of post-replicative DNA methylation at rRNA genes in cells treated with or without PARPi. Values normalized to input and h 6 values and are mean ± SEM (error bars) (n = 2 independent experiments).

**P* < 0.05, ***P* < 0.01, ****P* < 0.001 ns: not significant (unpaired, two tailed t-test)

(F) Model showing the slow deposition of nucleosomes after replication of heterochromatic DNA. The restrained assembly of nucleosomes mediated by PARP1-ADP-ribosylation allows the completion of methylation at the DNA, which would be inefficiently modified if immediately assembled into chromatin.

Supplementary Figures

Supplementary Figure S1

(**A**) Scheme representing the strategy used to label nascent DNA to quantify BrdU incorporation (Fig. 1A) and for replication timing analysis. BrdU was added 1 hour before sample collection.

(**B**) qPCR of BrdU-IPs showing replication timing of rRNA genes, alpha satellites and *GAPDH* in T24 cells.

(**C**) qPCR of the early replicating *GAPDH* gene after BrdU-IP of DNA from T24 cells pulse-labelled with BrdU at h 6 of S phase. Lack of *GAPDH* enrichment indicates specificity of BrdU-IP and efficiency of cell cycle synchronization. Values are normalized to input and values of h 6 and are mean ± SEM (n = 3 independent experiments).

(**D**) Representative ethidium bromide-stained agarose gel showing efficiency of MNase digestion to obtain mononucleosomes (DNA length ca. 145 bp).

(**E**) FACS analysis. Representative cell cycle profile of NIH3T3 cells progressing from G1/S to G2/M phases.

Supplementary Figure S2

(**A**) 1 h treatment with 10 μM PARPi (ABT-888) is sufficient to inhibit PARP activity in T24 cells. Immunofluorescence analysis with anti-10H antibodies showing formation of PAR foci upon H_2O_2 treatment of T24 cells. Formation of PAR foci is impaired in cells pre-treated for one hour with PARPi.

(**B**) Scheme representing the strategy to monitor post-replicative heterochromatin maturation in T24 cells treated with PARP1 inhibitor (PARPi).

(**C**) Treatment with PARPi does not alter progression from S to G2/M phases. FACS profile of synchronized T24 cells with and without PARPi.

(**D**) qPCR of anti-BrdU-IP of DNA from h 6 BrdU-labeled T24 cells which were treated with PARPi. Values are normalized to input and values of h 6 and are mean ± SEM (n = 4 independent experiments).

(**E**) Efficiency of BrdU-IP of mononucleosomal DNA from h 6 BrdU-labeled T24 cells, which were treated with PARPi. Values show qPCR amplification of *β*-Lactamase sequences from BrdU-pBS which was added at each sample prior IP. Values are normalized to h 6 of control and are mean ± SEM (n = 3 independent experiments).

(**F**) Similar BrdU-IP efficiencies of MeDIP-DNA samples. qPCR amplification of *β*-Lactamase on BrdU-pBS after BrdU-IP. Values are normalized to h 6 of control and are mean ± SEM (n = 2 independent experiments).

ns: not significant (unpaired, two tailed t-test)

Supplementary Figure S3

PARP1 activity does not alter DNMT1 recruitment to heterochromatin

(**A**) Immunoblot showing soluble and chromatin-bound DNMT1 and PARP1 in untreated and PARPi treated synchronized T24 cells during late S phase. Coomassie staining of histone proteins and anti-tubulin blot serve as loading controls.

(**B**) DNMT1 binds to rRNA genes and alpha satellites independently of PARP1 activity. ChIPs showing association of DNMT1 in T24 cells treated with or without PARPi. Values are normalized to input and are mean ± SEM (n = 3 independent experiments).

(**C**) DNMT1 binds to rRNA genes and alpha satellites independently of PARP1. ChIPs showing association of DNMT1 in T24 cells upon knockdown of *PARP1* with siRNA. Values are normalized to input. Data are mean ± SEM (n = 2 independent experiments). Right panel shows *PARP1* knockdown efficiency measured by qRT-PCR. *PARP1* mRNA values are normalized to *GAPDH* mRNA levels.

(**D**) UHRF1 and TIP5 interact in a PARP activity independent manner. FLAG-immunoprecipitation of HEK293T cells co-expressing HA-FLAG-TIP5 and DNMT1-MYC. Co-precipitated proteins are visualized with HA and Myc antibodies.

Figure 1

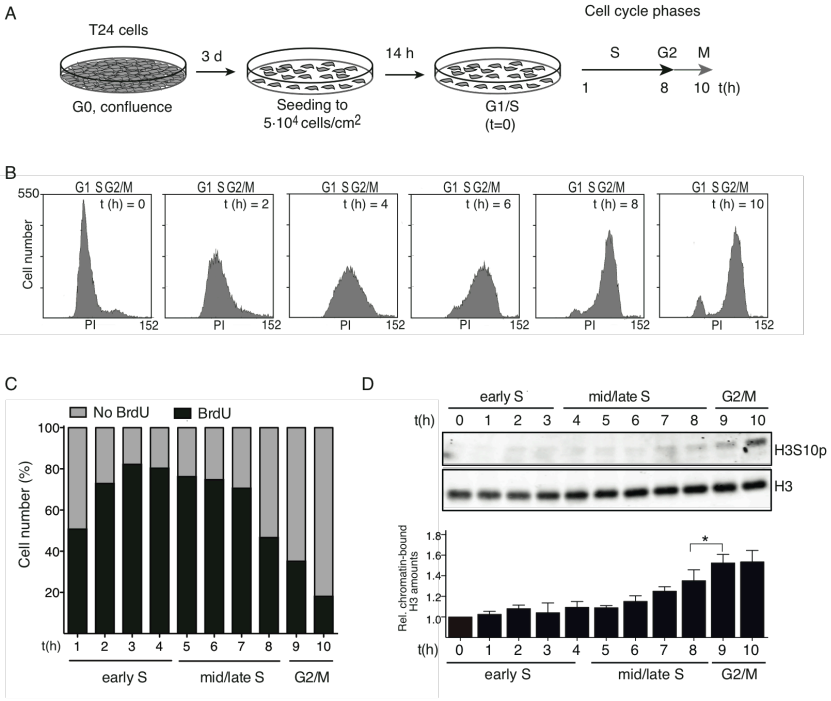
A
T24 cells
3 d
14 h
Cell cycle phases
S
G2
M
1
8
10 t(h)
G0, confluence
Seeding to
5·10⁴ cells/cm²
G1/S
(t=0)
B
G1 S G2/M
t (h) = 0
t (h) = 2
t (h) = 4
t (h) = 6
t (h) = 8
t (h) = 10
Cell number
550
PI
152
C
No BrdU
BrdU
Cell number (%)
100
80
60
40
20
t(h) 1 2 3 4 5 6 7 8 9 10
early S
mid/late S
G2/M
D
early S
mid/late S
G2/M
t(h) 0 1 2 3 4 5 6 7 8 9 10
H3S10p
H3
Rel. chromatin-bound H3 amounts
1.8
1.6
1.4
1.2
1.0
*
t(h) 0 1 2 3 4 5 6 7 8 9 10
early S
mid/late S
G2/M

Figure 2

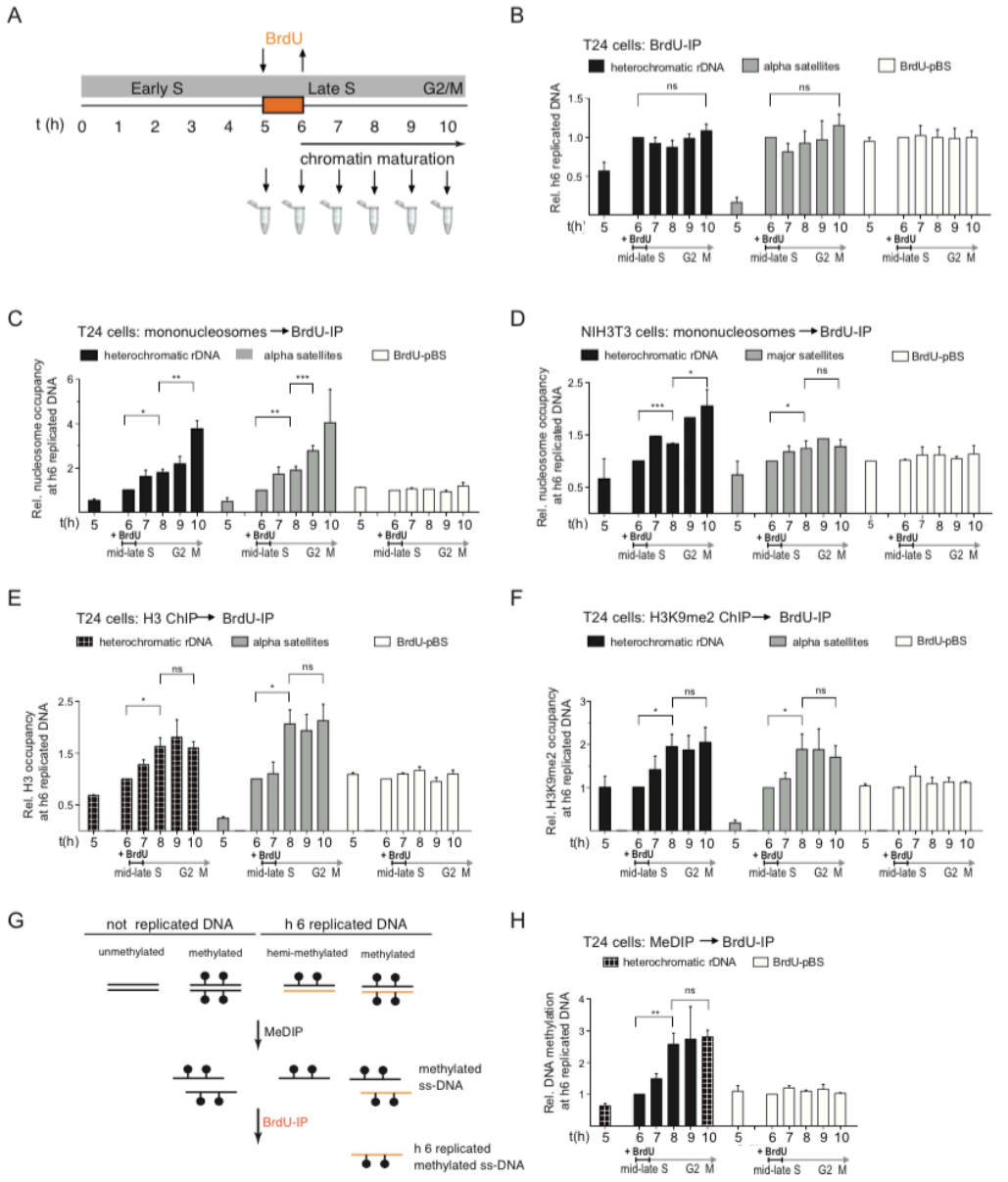
A
BrdU
Early S
Late S
G2/M
t (h) 0 1 2 3 4 5 6 7 8 9 10
chromatin maturation
B
T24 cells: BrdU-IP
heterochromatic rDNA
alpha satellites
BrdU-pBS
Rel. h6 replicated DNA
C
T24 cells: mononucleosomes → BrdU-IP
Rel. nucleosome occupancy at h6 replicated DNA
D
NIH3T3 cells: mononucleosomes → BrdU-IP
major satellites
E
T24 cells: H3 ChIP → BrdU-IP
Rel. H3 occupancy at h6 replicated DNA
F
T24 cells: H3K9me2 ChIP → BrdU-IP
Rel. H3K9me2 occupancy at h6 replicated DNA
G
not replicated DNA
h 6 replicated DNA
unmethylated
methylated
hemi-methylated
MeDIP
BrdU-IP
methylated ss-DNA
h 6 replicated methylated ss-DNA
H
T24 cells: MeDIP → BrdU-IP
Rel. DNA methylation at h6 replicated DNA
+ BrdU
mid-late S
G2
M
ns

Figure 3

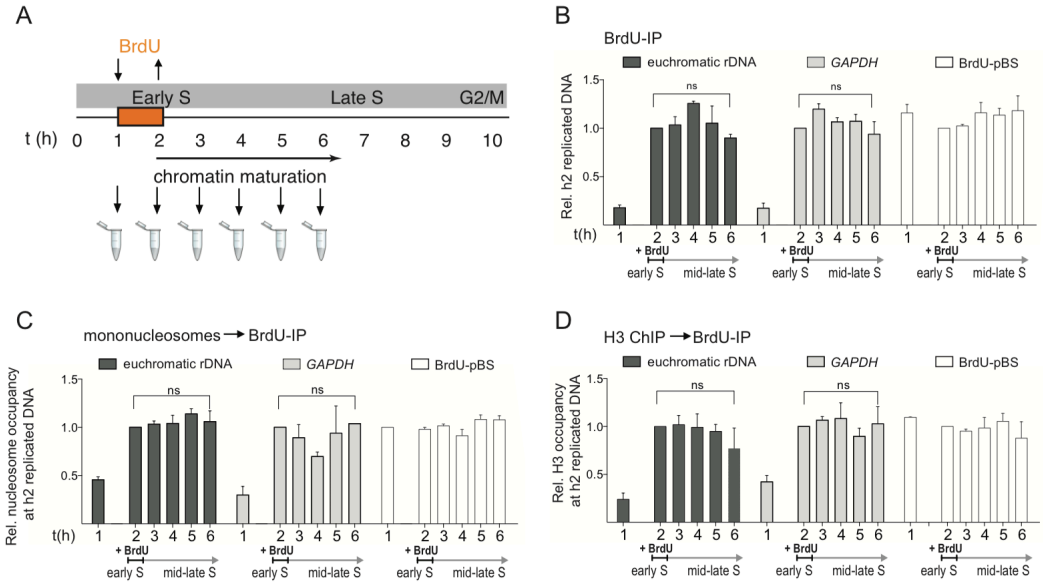
A
BrdU
Early S
Late S
G2/M
t (h) 0 1 2 3 4 5 6 7 8 9 10
chromatin maturation
B
BrdU-IP
euchromatic rDNA
GAPDH
BrdU-pBS
Rel. h2 replicated DNA
ns
t(h)
+ BrdU
early S
mid-late S
C
mononucleosomes → BrdU-IP
Rel. nucleosome occupancy at h2 replicated DNA
D
H3 ChIP → BrdU-IP
Rel. H3 occupancy at h2 replicated DNA

Figure 4

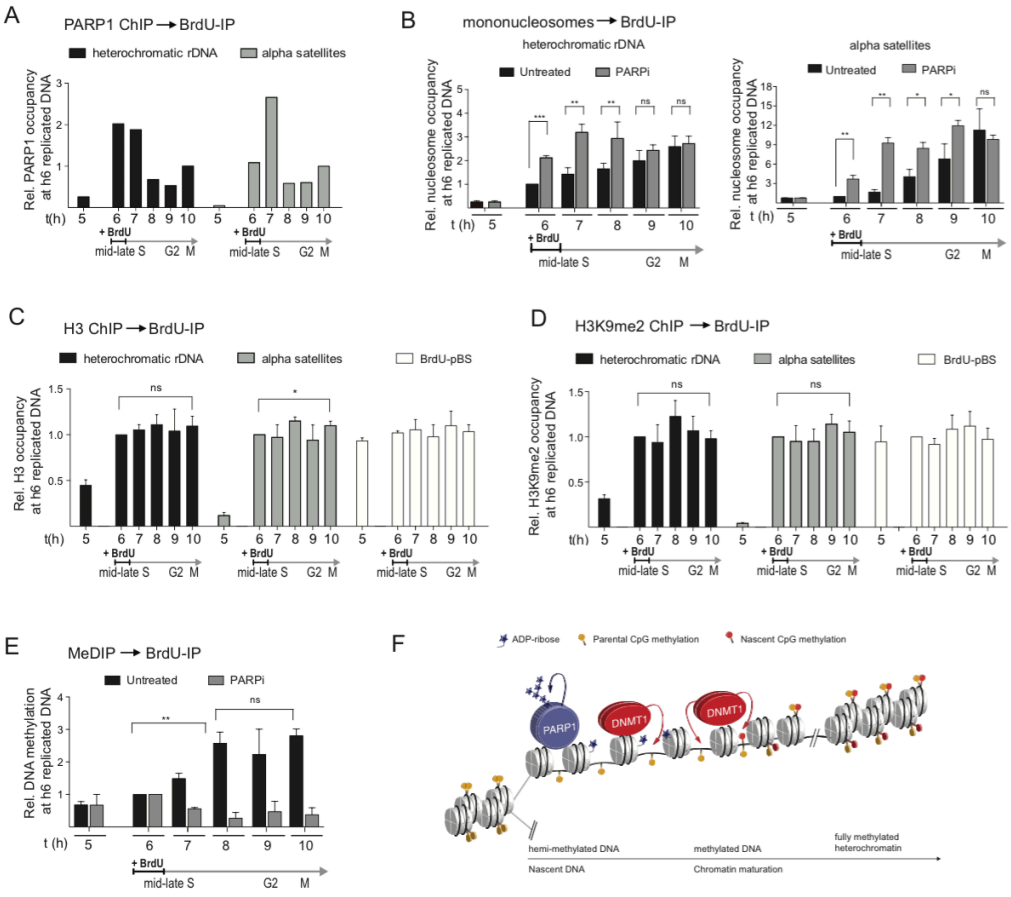
A
PARP1 ChIP → BrdU-IP
heterochromatic rDNA
alpha satellites
Rel. PARP1 occupancy at h6 replicated DNA
t(h) 5 6 7 8 9 10 5 6 7 8 9 10
+ BrdU
mid-late S G2 M
B
mononucleosomes → BrdU-IP
heterochromatic rDNA
alpha satellites
Untreated
PARPi
Rel. nucleosome occupancy at h6 replicated DNA
t (h) 5 6 7 8 9 10
+ BrdU
mid-late S G2 M
C
H3 ChIP → BrdU-IP
heterochromatic rDNA
alpha satellites
BrdU-pBS
Rel. H3 occupancy at h6 replicated DNA
ns
*
t(h) 5 6 7 8 9 10
+ BrdU
mid-late S G2 M
D
H3K9me2 ChIP → BrdU-IP
heterochromatic rDNA
alpha satellites
BrdU-pBS
Rel. H3K9me2 occupancy at h6 replicated DNA
ns
t(h) 5 6 7 8 9 10
+ BrdU
mid-late S G2 M
E
MeDIP → BrdU-IP
Untreated
PARPi
Rel. DNA methylation at h6 replicated DNA
**
ns
t (h) 5 6 7 8 9 10
+ BrdU
mid-late S G2 M
F
ADP-ribose
Parental CpG methylation
Nascent CpG methylation
PARP1
DNMT1
DNMT1
hemi-methylated DNA
methylated DNA
fully methylated heterochromatin
Nascent DNA
Chromatin maturation

Supplementary Figure S1

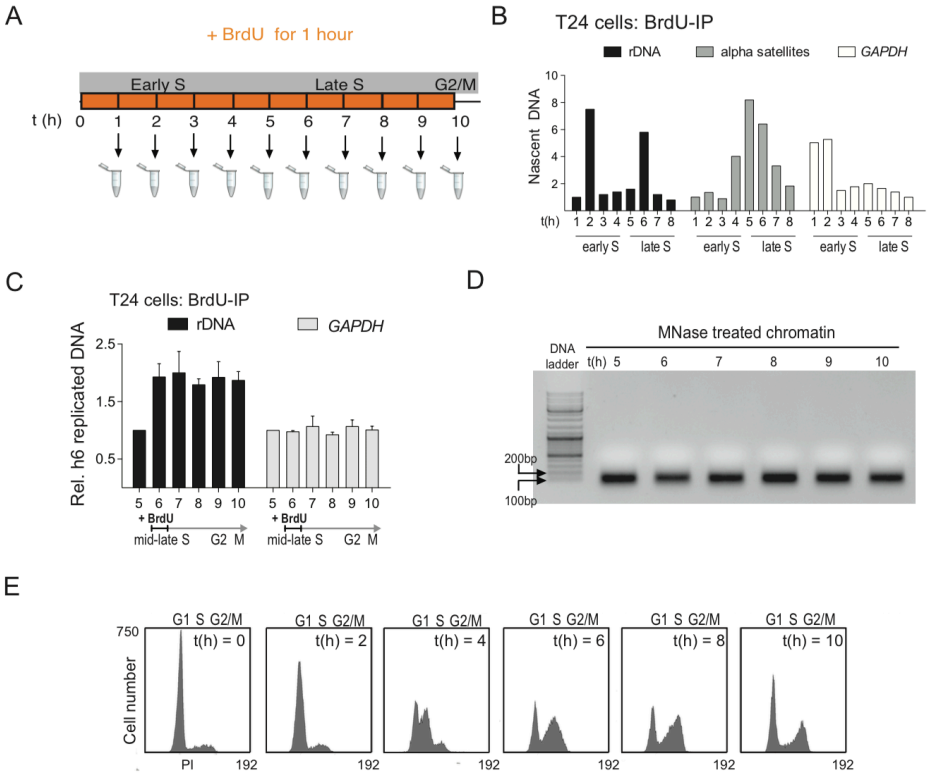

Supplementary Figure S2

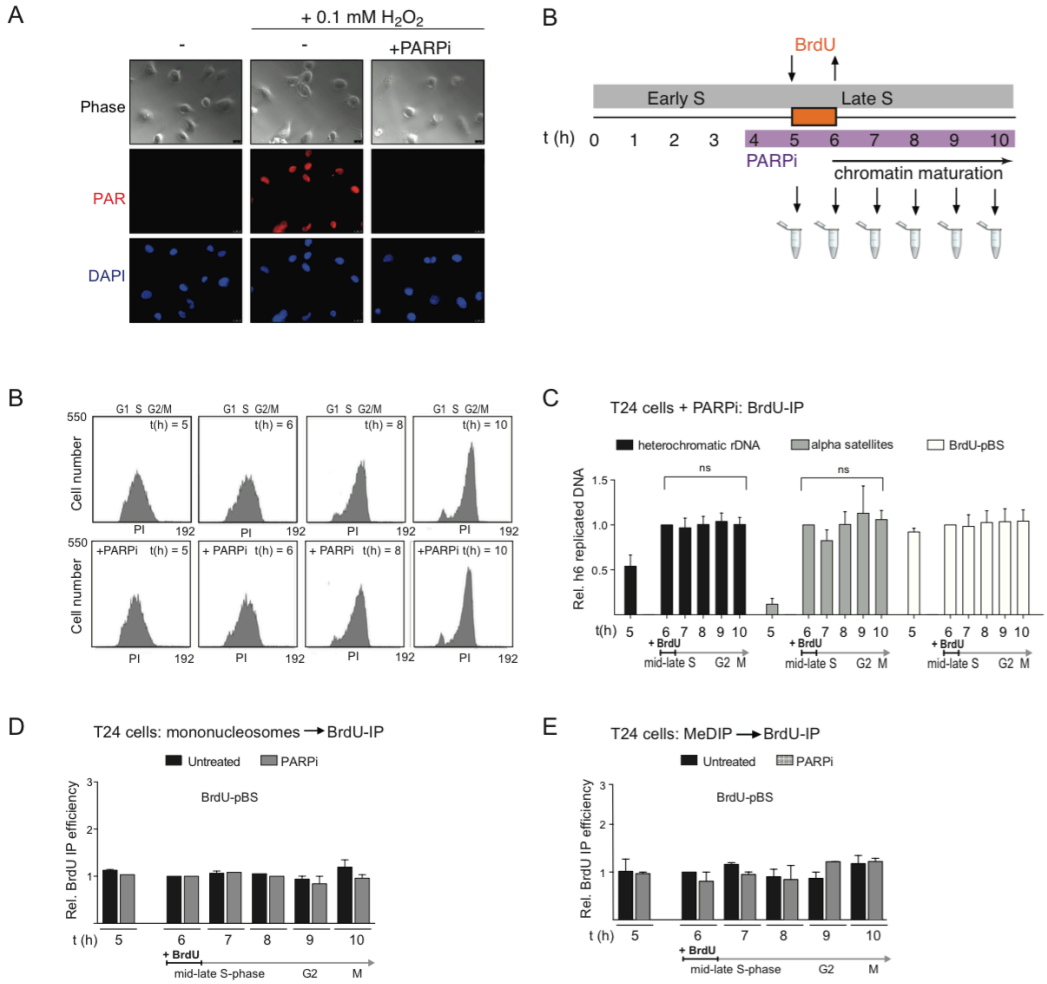

Supplementary Figure S3

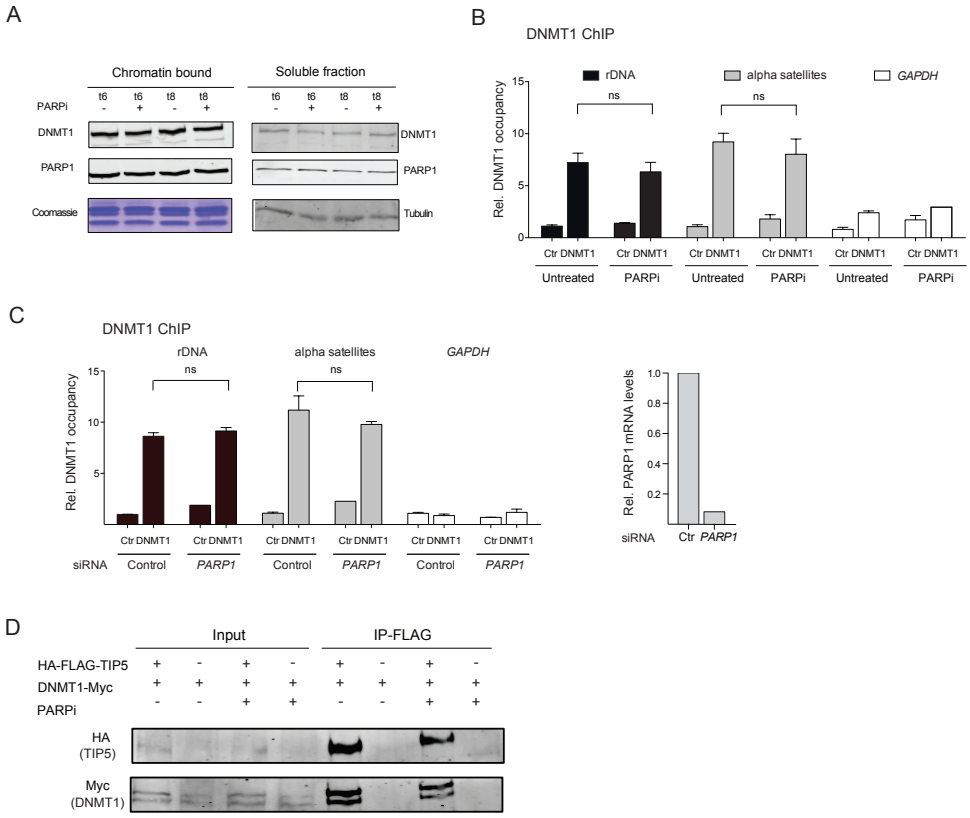

Supplementary Figure S4

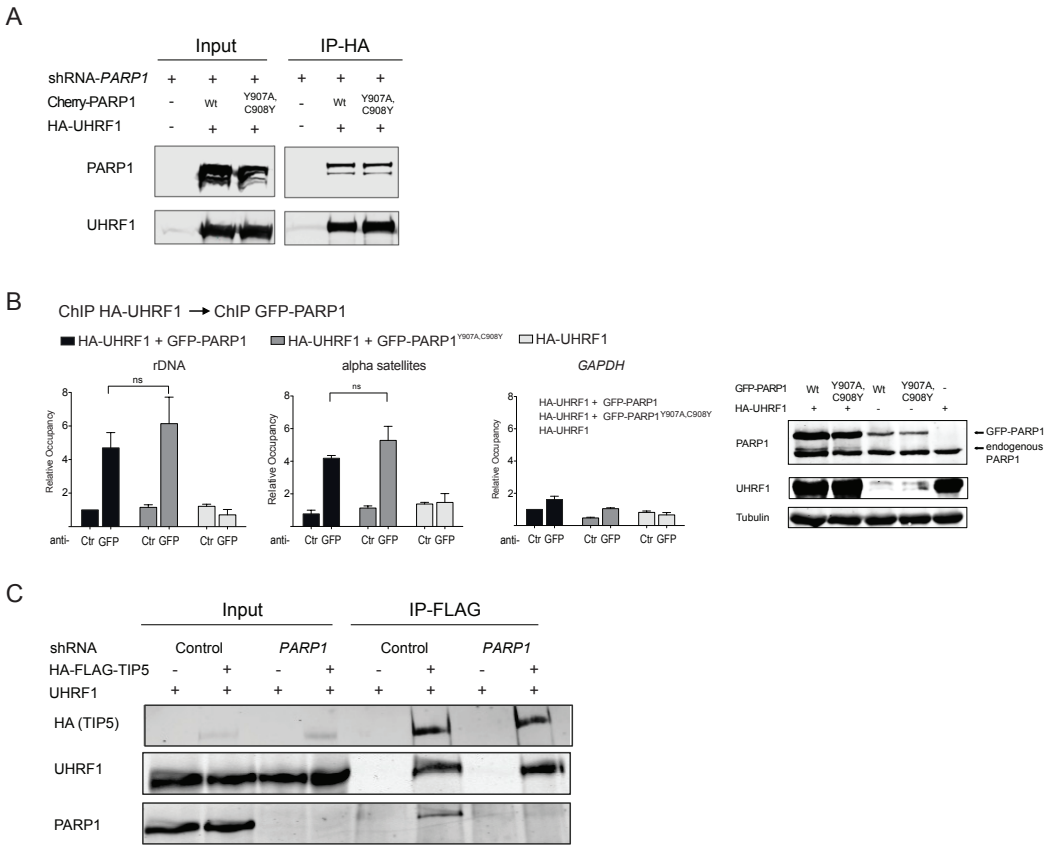

Supplementary Figure S5

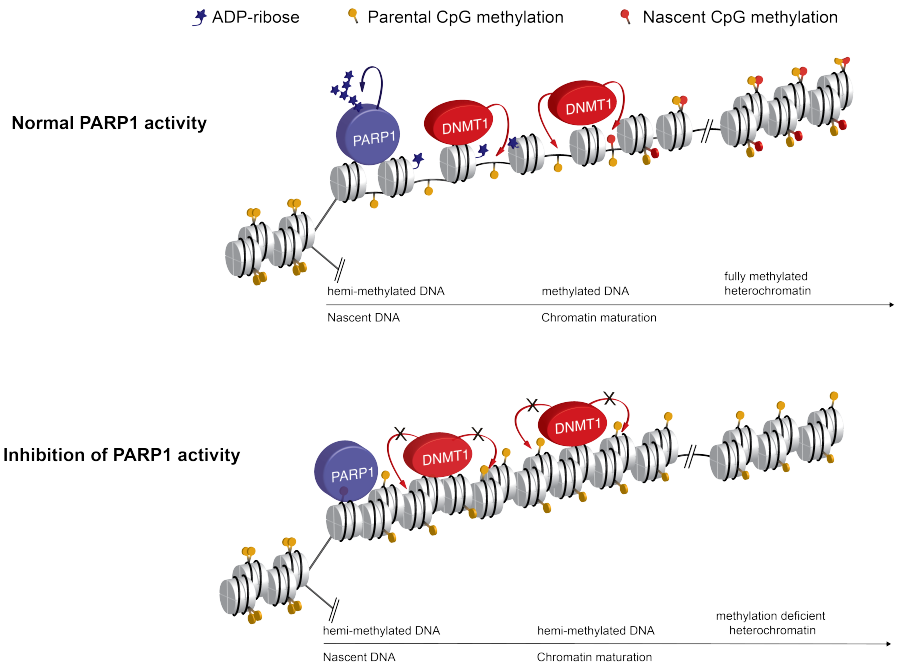

Supplementary information

Methods

Cell lines

T24 bladder tumor cells grown in McCoy's medium (Gibco) were arrested in G0 by contact inhibition (Jin et al., 1997). After 3 days of confluence, cells were seeded at a concentration of 5x $10^4/cm^2$ and reached G1/S phase boundary after 14 hours. NIH3T3 cells were grown in DMEM (Gibco) medium and arrested at G1/S boundary upon treatment with 2µg/ml aphidicolin for 18 hours (Guetg et al., 2010). Cell-cycle synchronization and progression was confirmed by flow cytrometry on a CyAn ADP Analyzer (Beckman Coulter) (FACS). HEK293T cells were grown in DMEM (Gibco) medium. HEK293T cells were selected with puromycin (0.4µg/ml; Gibco) for stable expression after transduction with retroviruses expressing shRNA-control and human *PARP1*-sequences (pLTR-PPT-RRE-H1-TetO2-$shRNA_{control}$-PGK-Puro and pLTR-PPT-RRE-H1-TetO2-$shRNA_{hPARP1}$-PGK-Puro.)

Chromatin Immunoprecipitation (ChIP) and re-ChIP

ChIP analysis was performed as previously described (Santoro, 2014). Briefly, formaldehyde 1% was added to cultured cells to cross-link proteins to DNA. Isolated nuclei were then lysed and sonicated using a Bioruptor ultrasonic cell disruptor to shear genomic DNA to an average fragment size of 200bp. 20µg chromatin was diluted to a total volume of 500µl with IP buffer (16.7 mM Tris-HCl pH 8.1, 167 mM NaCl, 1.2 mM EDTA, 0.01% SDS, 1.1% Triton X-100) and pre-cleared with 10µl packed Sepharose beads for 2 hours at 4°C. Pre-cleared chromatin was incubated overnight with the indicated antibodies. The next day, Dynabeads protein-A (or -G, Millipore) were added and incubated for 4 hours at 4°C. After washing, bound chromatin was eluted with the elution buffer (1% SDS, 100 mM $NaHCO_3$). Upon reversion of crosslinking (65°C, overnight), DNA was purified with phenol/chloroform, ethanol precipitated and quantified by qPCR.

For reChIP experiments, first-ChIP chromatin bound to Dynabeads protein-G was eluted with 10 mM DTT twice for 30 minutes at 37°C and the resulting eluate was diluted 40 times with IP buffer.

To dispose of potentially co-eluted antibodies from the first ChIP, chromatin was pre-cleared for 2 hours at 4°C with G-protein Sepharose beads. Pre-cleared chromatin was then incubated again over night with antibodies and immuno-precipitated as described above.

Micrococcal nuclease digestion

$7x10^6$ T24 cells were crosslinked in 1% formaldehyde for 10 minutes, harvested and washed 3 times in phosphate buffered saline (PBS) buffer. Cells were resuspended in 1.5 ml lysis buffer (10 mM Tris-HCl pH 7.4, 10 mM NaCl, 3 mM $MgCl_2$, 0.5% NP-40, 0.15 mM spermine, 0.5 mM spermidine) and incubated on ice for 5 minutes. After 10 minutes centrifugation at 850 rcf at 4°C, nuclei where respended in Micrococcal nuclease (MNase) digestion buffer (10 mM Tris-HCl pH 7.4, 15 mM NaCl, 60 mM KCl, 0.15 mM spermine, 0.5 mM spermidine), centrifuged again at 850 rcf at 4°C for 10 minutes and resuspended in 200µl MNase digestion buffer containing 1 mM $CaCl_2$. Nuclei were then incubated with 90 U of MNase (Roche) at 25°C for 20 minutes. The reaction was stopped with 260µl nuclease digestion buffer containing 20 mM EDTA, 2 mM EGTA, 250 mM NaCl and 1% SDS. Decrosslinking and protein digestion was achieved by incubation with 10µg Proteinase K at 42°C for one hour, followed by 65°C incubation over night. After treatment with RNase A (Thermo Scientific) for 30 minutes at 37°C, DNA was purified with phenol/chlorophorm and ethanol precipitated. Amounts and yield of pure DNA corresponding to mononucleosomes (DNA length of 150 bp) was always controlled on a 1% agarose gel.

BrdU-Immunoprecipitation

Cells were pulse labelled (1 hour) with 33 µM 5'-BrdU before sample collection (Guetg et al., 2010). Anti-BrdU IPs were performed using 2µg purified heat-denatured 200nt DNA fragments that were incubated at room temperature (RT) for 30 minutes with 1µg of anti-BrdU antibody (Roche) in 0.14 M NaCl, 10 mM Na-phosphate buffer, pH 7.2, 0.05% Triton X-100. DNA-antibody complexes were incubated with 40µg of anti-mouse IgGs (Sigma) for 30 minutes at room temperature and the precipitates were collected by centrifugation (21000 rcf, for 15 minutes at 25°C) and dissolved in 50 mM Tris-HCl, pH 8.0, 0.5% SDS, 1 M NaCl and 10 mM EDTA. Proteins

were digested over night at 42°C with 2µg Proteinase K and DNA was purified by phenol-chloroform extractions and ethanol precipitation. For BrdU-IPs following ChIP experiment, immuno-precipitated (ChIP) DNA was re-suspendend in 70µl H_2O_2. 50µl of ChIP-DNA was heat-denatured and incubated with 1µg anti-BrdU antibodies and purified as described above. To ensure similar IP efficiencies, BrdU-labeled pBS plasmid (BrdU-pBS) was added to each sample prior IP and *β-Lactamase* gene sequences were amplified by qPCR.

Methylated DNA immunoprecipitation (MeDIP)

200bp length DNA fragments were denatured and incubated over-night with 5mC-antibody (Diagenode) in 200µl IP buffer (10 mM Na-phosphate buffer, pH 7.0, 140 mM NaCl, 0.05% Triton X-100). The day after, 20µl protein-G Dynabeads (Millipore) were added and incubated for 2 hours at 4°C. Beads were then washed three times at RT for 10 minutes with the IP buffer and subsequently incubated with 250 µl Proteinase K digestion mix (50 mM Tris-HCl pH 8, 0.5% SDS, 10 mM EDTA, 2µg Proteinase K) over night at 42°C. The DNA was purified with phenol/chloroform, ethanol precipitated and quantified by qPCR.

Co-Immunoprecipitation

HEK293T cells were transfected with the Ca-phosphate method and the indicated plasmids. Nuclei were obtained by resuspending cells in hypotonic buffer (0.5% NP-40, 85 mM KCl, 5 mM HEPES, pH 7.4) and subsequent centrifugation at 6000 rcf for 10 minutes at 4°C. Nuclei were then resuspended in Nuclear extraction buffer (50 mM Tris-HCl pH 7.5, 0.15 M KCl, 5 mM $MgCl_2$, 0.2 mM EDTA, 20% Glycerol, 0.5 mM DTT and 0.5% NP-40) and sonicated 2 times 30 seconds with a Bioruptor ultrasonic cell disruptor. After DNaseI treatement for 1h at 4°C, extracts were sonicated again for 30 seconds and centrifuged for 10 minutes at 4°C with 3400 rcf. 0.5mg of protein from the resulting supernatant was immunoprecipitated overnight at 4°C using an immobilized antibody against HA (anti-HA-Agarose, Sigma) or M2 beads (anti-Flag, Sigma). 0.05mg (10%) of the extracts was later used to check for equal input material. Immuno-precipitates were washed three times at 4°C for 5 minutes with wash buffer (20 mM Tris-HCl pH

7.8, 150 mM KCl, 5 mM MgCl2, 0.2 mM EDTA, 10% glycerol, 0.1% Tween and 0.1 mM PMSF). Beads were pellet by centrifuging for 5 minutes at 4°C with 500 rcf. Proteins were eluted and denatured with 1xLämmli buffer, separated on SDS-polyacrylamide gel and analyzed by immunoblotting.

Immunofluorescence

T24 cells were pulsed labelled with 33 µM BrdU for 1 hour at the indicated time points of the cell cycle. BrdU incorporation assay was measured by growing T24 cells on polylysin-covered coverslips. Cells were pulse labelled with 33 µM BrdU for 1 hour at the indicated time points of the cell cycle and fixed with methanol (7 minutes, RT). DNA was denatured with 2 M HCl for 60 minutes at 37°C. After washing with PBS, cells were incubated with anti-BrdU antibodies (Roche) followed by Cy3-coniugated goat anti-mouse IgG (Jackson Immuno Research) and DAPI. Immunofluorescent images were digitally recorded and quantification was performed by counting BrdU positive cells relative to total cell number.

To measure PAR formation, T24 cells grown on polylysin-covered coverslips were treated with 10 µM ABT-888 for 1 hour. PAR-formation was induced with 0.1 mM H_20_2 in 1xPBS and 1 mM $MgCl_2$ for 10 minutes. Cells were fixed in methanol/acetic acid (3:1) on ice for 5 minutes, blocked in PBS with 5% milk powder and 0.05% Tween and incubated with 10H antibodies in blocking solution. After incubation with Cy3-coniugated goat anti-mouse IgG, cells were stained with DAPI. Immunofluorescent images were digitally recorded.

Chromatin Extraction

Chromatin bound proteins were isolated by incubating cells in chromatin extraction buffer (200 mM NaCl, 10 mM HEPES, 3 mM $MgCl_2$ and 0.5%Triton X-100) for 30 minutes at RT, followed by 10 minutes centrifugation at RT at 10600 rcf. The supernatant (unbound fraction) was denatured with 1xLämmli buffer and frozen at -20°C. The pellet (chromatin fraction) was resuspended in 100µl chromatin extraction buffer and sonicated 2 times 30 sec with a Bioruptor ultrasonic cell disruptor. After addition of 20µl 6xLämmli buffer and cooking 5 minutes at 95°C, chromatin

fraction was again centrifuged for 5 in at RT at 10600 rcf. The supernatant of this centrifugation represent the chromatin bound proteins. Proteins were separated on a 15% SDS-polyacrylamide gel (for histones) or a 6% SDS-polyacrylamide gel (for DNMT1 and PARP1) and analyzed by western blot. Bands were quantified using the Odyssey® software for quantification.

Antibodies

Anti-H3 (ab1791), anti-HA (ab9110), anti-GFP (ab290), anti-DNMT1 (ab13537) were purchased from Abcam. Anti-PARP1 (46D11) was from Cell Signaling anti-UHRF1 (MABE308), anti-H4K5ac (07-327), anti-H3K9me2 (17-648) and anti-H3S10p (06-570) were from Millipore, anti-Brdu (11 170 367 001) from Roche and anti-5mc (MAb-081-100) from Diagenode. Anti-UHRF1 (sc-373750), Anti-myc (sc49) and anti-PARP1 (sc53643) were obtained from Santa Cruz and Anti-HA (MMS-101P) from Covance

Plasmids

The following plasmids were used in this study: pLTR-PPT-RRE-CMV-HA-FLAG-TIP5-PGK-puro, pcDNA-FLAG-HA-UHRF1, pcDNA-HA-UHRF1, pcDNA-HA-PARP1, pEGFP-N1-PARP1, pEGFP-N1-PARP1Y907A;C908Y, pcDNA-cherry-PARP1, pcDNA-cherry-PARP1Y907A;C908Y, pcDNA-DNMT1-MYC, pLTR-PPT-RRE-H1-TetO2-shRNA$_{control}$-PGK-Puro and pLTR-PPT-RRE-H1-TetO2-shRNA$_{hPARP1}$-PGK-Puro.

qPCR Primers

Primers used to amplify human sequences:

rDNA promoter -150/-133	Fwd CGATGGTGGCGTTTTTGG
rDNA promoter +9/+21	Rev GACAGGTCGCCAGAGGACAGC
rDNA promoter -42/-22	Fwd TTTCGCTCCGAGTCGGCAATT (This primer was used for qPCR of mononucleosomal DNA)
alpha satellites	Fwd CTGCACTACCTGAAGAGGAC
alpha satellites	Rev GATGGTTCAACACTCTTACA

GAPDH	Fwd TGCACCACCAACTGCTTAGC
GAPDH	Rev GGCATGGACTGTGGTCATGAG
IP10	Fwd GGGAAATTCCGTAACTTGGA
IP10	Rev AAGCCATTTTCCCTCCCTAA

Primers used to amplify mouse sequences

rDNA promoter -105/-87	For CCCAGGTATGACTTCCAG
rDNA promoter -21/-1	Rev ACCTATCTCCAGGTCCAATAG
Major satellites	For GACGACTTGAAAAATGACGAAATC
Major satellites	Rev CATATTCCAGGTCCTTCAGTGTGC
Gapdh	For TGCACCACCAACTGCTTAGC
Gapdh	Rev GGCATGGACTGTGGTCATGAG

β-lactamase	Fwd CCTCCGATCGTTGTCAGAAG
β-lactamase	Rev GCAACTCGGTCGCCGCATAC

Supplementary References

Guetg, C., Lienemann, P., Sirri, V., Grummt, I., Hernandez-Verdun, D., Hottiger, M.O., Fussenegger, M., and Santoro, R. (2010). The NoRC complex mediates the heterochromatin formation and stability of silent rRNA genes and centromeric repeats. EMBO J *29*, 2135-2146.

Jin, Y., Xu, X.L., Yang, M.C., Wei, F., Ayi, T.C., Bowcock, A.M., and Baer, R. (1997). Cell cycle-dependent colocalization of BARD1 and BRCA1 proteins in discrete nuclear domains. Proc Natl Acad Sci U S A *94*, 12075-12080.

Santoro, R. (2014). Analysis of chromatin composition of repetitive sequences: the ChIP-Chop assay. Methods Mol Biol *1094*, 319-328.

Article

Cell Stem Cell

lncRNA Maturation to Initiate Heterochromatin Formation in the Nucleolus Is Required for Exit from Pluripotency in ESCs

Graphical Abstract

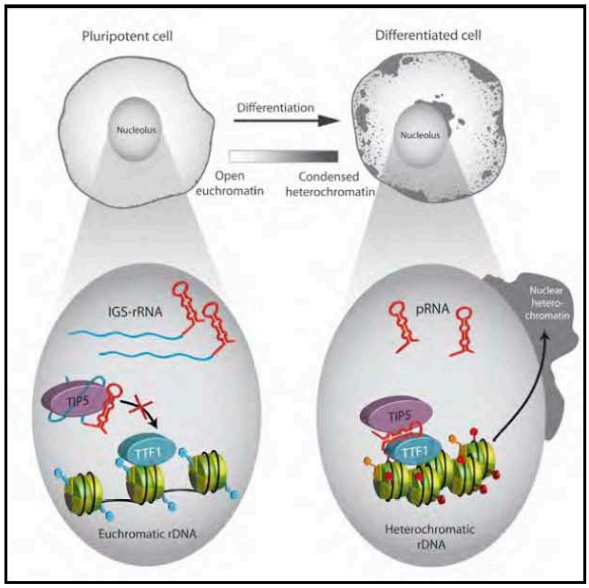

Highlights

rRNA genes (rDNA) acquire heterochromatin during ESC differentiation

Maturation of the lncRNA pRNA is required to establish rDNA heterochromatin

rDNA heterochromatin initiates heterochromatinization of ESC genomes

Inhibition of rDNA heterochromatin prevents ESC differentiation

Authors

Nataša Savić, Dominik Bär, ..., Paolo Cinelli, Raffaella Santoro

Correspondence

raffaella.santoro@vetbio.uzh.ch

In Brief

Savić et al. reveal that heterochromatin condensation in the nucleolus, where ribosomal genes are transcribed, triggers remodeling of the global open ESC chromatin into a highly condensed heterochromatic structure and that this mechanism is required for exit from pluripotency.

Savić et al., 2014, Cell Stem Cell 15, 720–734
December 4, 2014 ©2014 Elsevier Inc.
http://dx.doi.org/10.1016/j.stem.2014.10.005

CellPress

Cell Stem Cell
Article

lncRNA Maturation to Initiate Heterochromatin Formation in the Nucleolus Is Required for Exit from Pluripotency in ESCs

Nataša Savić,[1,2] Dominik Bär,[1] Sergio Leone,[1,2] Sandra C. Frommel,[1,2] Fabienne A. Weber,[2,3] Eva Vollenweider,[1,2] Elena Ferrari,[1] Urs Ziegler,[4] Andres Kaech,[4] Olga Shakhova,[5] Paolo Cinelli,[3,6,7] and Raffaella Santoro[1,6,*]
[1]Institute of Veterinary Biochemistry and Molecular Biology, University of Zurich, 8057 Zurich, Switzerland
[2]Molecular Life Science Program, Life Science Zurich Graduate School, University of Zurich, 8057 Zurich, Switzerland
[3]Institute of Laboratory Animal Science, University of Zurich, 8057 Zurich, Switzerland
[4]Center for Microscopy and Image Analysis, University of Zurich, 8057 Zurich, Switzerland
[5]Department of Oncology, University Hospital Zurich, 8952 Schlieren, Switzerland
[6]Center for Applied Biotechnology and Molecular Medicine, University of Zurich, 8057 Zurich, Switzerland
[7]Division of Trauma Surgery, Center for Clinical Research, University Hospital Zurich, 8091 Zurich, Switzerland
*Correspondence: raffaella.santoro@vetbio.uzh.ch
http://dx.doi.org/10.1016/j.stem.2014.10.005

SUMMARY

The open chromatin of embryonic stem cells (ESCs) condenses into repressive heterochromatin as cells exit the pluripotent state. How the 3D genome organization is orchestrated and implicated in pluripotency and lineage specification is not understood. Here, we find that maturation of the long noncoding RNA (lncRNA) pRNA is required for establishment of heterochromatin at ribosomal RNA genes, the genetic component of nucleoli, and this process is inactivated in pluripotent ESCs. By using mature pRNA to tether heterochromatin at nucleoli of ESCs, we find that localized heterochromatin condensation of ribosomal RNA genes initiates establishment of highly condensed chromatin structures outside of the nucleolus. Moreover, we reveal that formation of such highly condensed, transcriptionally repressed heterochromatin promotes transcriptional activation of differentiation genes and loss of pluripotency. Our findings unravel the nucleolus as an active regulator of chromatin plasticity and pluripotency and challenge current views on heterochromatin regulation and function in ESCs.

INTRODUCTION

The spatiotemporal organization of the genome has been recognized as an additional regulatory layer of chromatin, important for gene regulation and transcriptional competence (Gonzalez-Sandoval et al., 2013; Splinter and de Laat, 2011). Pluripotent stem cells such as embryonic stem cells (ESCs) are integral to the study of genome organization (Gorkin et al., 2014). Although ESCs organize their chromosomes into topological-associating domains that are largely invariant between cell types (Dixon et al., 2012; Nora et al., 2012), chromatin is generally less condensed and largely devoid of compact heterochromatin blocks compared to lineage-committed cells (Efroni et al., 2008; Jørgensen et al., 2007; Melcer et al., 2012; Meshorer et al., 2006). While ESC chromatin fibers occupy the entire nuclear volume, the highly compacted chromatin of differentiated cells is organized into discrete domains leading to large regions of the nucleus devoid of DNA (Fussner et al., 2010). Transcriptionally inactive chromatin in ESCs is unusually disorganized and tends to participate in fewer specific long-range interactions than in differentiated cells (de Wit et al., 2013). These results are consistent with a chromatin conformation that is particularly malleable and transcriptionally permissive in pluripotent cells and that may allow maintenance of a plastic state for the different transcriptional programs required for lineage specification (de Wit et al., 2013; Gaspar-Maia et al., 2011; Gorkin et al., 2014). Upon ESC differentiation, large-scale genome silencing takes place and ESC chromatin undergoes structural remodelling toward a highly condensed heterochromatic and transcriptionally repressed form (Bhattacharya et al., 2009; Meshorer and Misteli, 2006). These changes are also accompanied by alterations of nuclear architecture such as formation of large organized chromatin regions enriched in the heterochromatic and repressive histone modification H3K9 methylation (termed LOCKs) (Wen et al., 2009), maturation and compaction of constitutive heterochromatin (such as centric and pericentric repeats) and clustering of highly condensed heterochromatin either at the nucleolus or at the nuclear periphery (Aoto et al., 2006; Bártová et al., 2008a, 2008b; Efroni et al., 2008). However, how ESCs mediate the switch from a lower to a higher order chromatin structure remains elusive and calls for studies aimed at understanding the mechanism and function of this process.

An important component of nuclear architecture is the nucleolus, the compartment where transcription of hundreds of ribosomal RNA (rRNA) genes, rRNA processing, and ribosome subunit assembly take place (Moss and Stefanovsky, 2002). Clustering of highly condensed heterochromatin at nucleoli is a phenomenon known to occur in all somatic cells, yet neither the factors involved nor their physiological relevance is understood. Previous studies have however started to define a functional link between nuclear heterochromatin positioned in proximity to nucleoli and rRNA genes (rDNA), the genetic

component of the nucleolus. The nucleolar repressor factor TIP5 (TTF1-interacting protein 5, also known as BAZ2A) is required for heterochromatin formation of a fraction of rRNA genes through association with the long noncoding (lnc)RNA pRNA, DNA methyltransferases (DNMT1, DNMT3b), histone deacetylase HDAC1, and poly(ADP-ribose)-polymerase-1 (PARP1) (Guetg et al., 2012; Mayer et al., 2006; Santoro et al., 2002, 2010; Zhou et al., 2002). pRNA is a 250–300 nucleotide transcript corresponding to main rDNA promoter sequences and originates from processing of the 2 kb long IGS-rRNA (intergenic spacer rRNA) whose synthesis is driven by an alternative rDNA promoter located upstream of the main rDNA promoter (Mayer et al., 2006; Santoro et al., 2010). TIP5-pRNA interaction is necessary to form rDNA heterochromatin by mediating TIP5 nucleolar retention and association with rDNA and PARP1 (Guetg et al., 2012; Mayer et al., 2006). Depletion of TIP5 reduces silent epigenetic marks at rDNA and heterochromatic centric and pericentric repeats, and abrogates formation of condensed heterochromatic structures within and in proximity to the nucleolus (Guetg et al., 2010). Strikingly, this structural organization closely resembles the open chromatin of ESCs, prompting us to investigate if the chromatin state of the nucleolus regulates ESC chromatin plasticity and commitment to specific lineages.

RESULTS

Establishment of rDNA Heterochromatin Occurs during ESC Differentiation

We profiled the epigenetic state of the nucleolus, at rDNA, in ESCs and during differentiation into neural progenitor cells (NPCs) that are *Pax-6*, *Nestin*, and brain lipid-binding protein (*BLBP*) positive and do not express the pluripotency factor Nanog (Figure 1A; Figure S1A available online). Previous work showed that methylation of the two unique CpG dinucleotides at the mouse rDNA promoter distinguishes heterochromatic and silent rRNA genes from euchromatic, transcriptionally active rDNA (Santoro and Grummt, 2001). We quantified silent rDNA by measuring CpG methylation at rDNA promoter of ESCs, NPCs, and mouse somatic cells from brain tissue using HpaII digestion followed by qPCR, a method that accurately quantifies the amounts of silent rDNA (Santoro et al., 2002). Consistent with a previous bisulfite analysis (Schlesinger et al., 2009), rDNA promoter in ESCs displays very low meCpG levels, confirming the accuracy of our method. After 8 days of differentiation, a fraction of rRNA genes (25%–30%) acquired CpG methylation at levels comparable to brain tissue (Figure 1B). Similar results were obtained with a different ESC line and differentiation protocol (Figure S1B), indicating that rDNA is de novo methylated during early ESC differentiation. Consistent with these results, rDNA transcription levels were similar in NPCs and mouse fibroblast NIH 3T3 cells and lower than in ESCs (Figure 1C). Remarkably, rDNA methylation in induced pluripotent stem cells (iPSC) decreased to about one half when compared to the original fibroblasts (Figure 1D), implying a link between cell pluripotency and rDNA methylation levels. Upon differentiation, heterochromatin-related histone modifications H3K9me2, H3K9me3, and H3K27me3 increased at rDNA promoter and coding regions (Figure 1E; Figure S1C). In contrast, active histone modifications such as H3K4me2 and H3K4me3 were not greatly affected (Figure S1D). Consistent with previous reports, major and minor satellite repeats that compose centric and pericentric heterochromatin increased H3K9me3 levels during differentiation (Martens et al., 2005; Meshorer et al., 2006; Wong et al., 2009), whereas H3K9me2 occupancy was not greatly affected. These changes were accompanied by a reduction of major and minor satellite transcripts (Figure S1E), which are normally repressed in differentiated cells (Efroni et al., 2008). We conclude that formation of rDNA heterochromatin takes place during ESC-NPC transition and timely coincides with the switch to a higher condensed heterochromatic form of centric and pericentric repeats.

TIP5 Is Recruited to rDNA during ESC Differentiation

To determine how rDNA heterochromatin is established during ESC differentiation, we measured the association of upstream binding factor UBF, an essential rDNA transcription factor that exclusively binds to unmethylated, euchromatic rRNA genes, and of TIP5, which associates with methylated silent rDNA (Santoro and Grummt, 2001; Santoro et al., 2002). UBF occupancy at rDNA was lower in NPCs than in ESCs (Figure 1F), a further indication that the number of euchromatic active rRNA genes decreases during differentiation. In contrast, TIP5 binds to rDNA only in NPCs but not in ESCs (Figure 1F). Similarly, PARP1, previously shown to interact with TIP5 and implicated in the formation of rDNA heterochromatin (Guetg et al., 2012), increases its association with the rDNA promoter in NPCs. Thus, establishment of rDNA heterochromatin in ESC-NPC transcription is accompanied by a decrease in the association of factors specific to active genes and an increase in the binding of components of the rDNA silencing machinery.

TIP5 protein and mRNA levels were higher in ESCs than in NPCs (Figure 1G), implying that the lack of rDNA heterochromatin in ESC is independent of TIP5 amounts. We then analyzed the TIP5 cellular localization (Figure 1H; Figure S2). Consistent with previous results, TIP5 was exclusively localized within nucleoli of somatic MEFs, as indicated by the colocalization with the nucleolar protein UBF (Strohner et al., 2001). In contrast, the cellular localization of TIP5 in ESCs was predominantly nucleoplasmic and often excluded from the nucleoli. Upon differentiation, TIP5 was drastically reduced in the nucleoplasm and exclusively localized within the nucleoli of NPCs, showing a cellular localization that is characteristic of somatic cells (Figure 1H; Figure S2). We conclude that TIP5 association with rDNA is impaired in ESCs and its recruitment to rDNA is achieved upon ESC differentiation.

Processing of pRNA Mediates Formation of rDNA Heterochromatin

We reasoned that impairment of TIP5 binding to rDNA might be responsible for the lack of rDNA heterochromatin in ESCs. Previous studies implicated the lncRNA pRNA in TIP5 nucleolar retention and association with rDNA (Mayer et al., 2006). pRNA is a 250–300 nucleotide transcript corresponding to main rDNA promoter sequences and derives from processing of the 2 kb long IGS-rRNA (Mayer et al., 2006; Santoro et al., 2010) (Figure 2A). Measurements of pRNA sequences in ESCs and at different times of differentiation did not reveal remarkable differences between ESCs and NPCs (Figure 2B). However, this approach does not allow distinguishing between IGS-rRNA and mature pRNA.

Cell Stem Cell
The Nucleolus Regulates ESC Chromatin

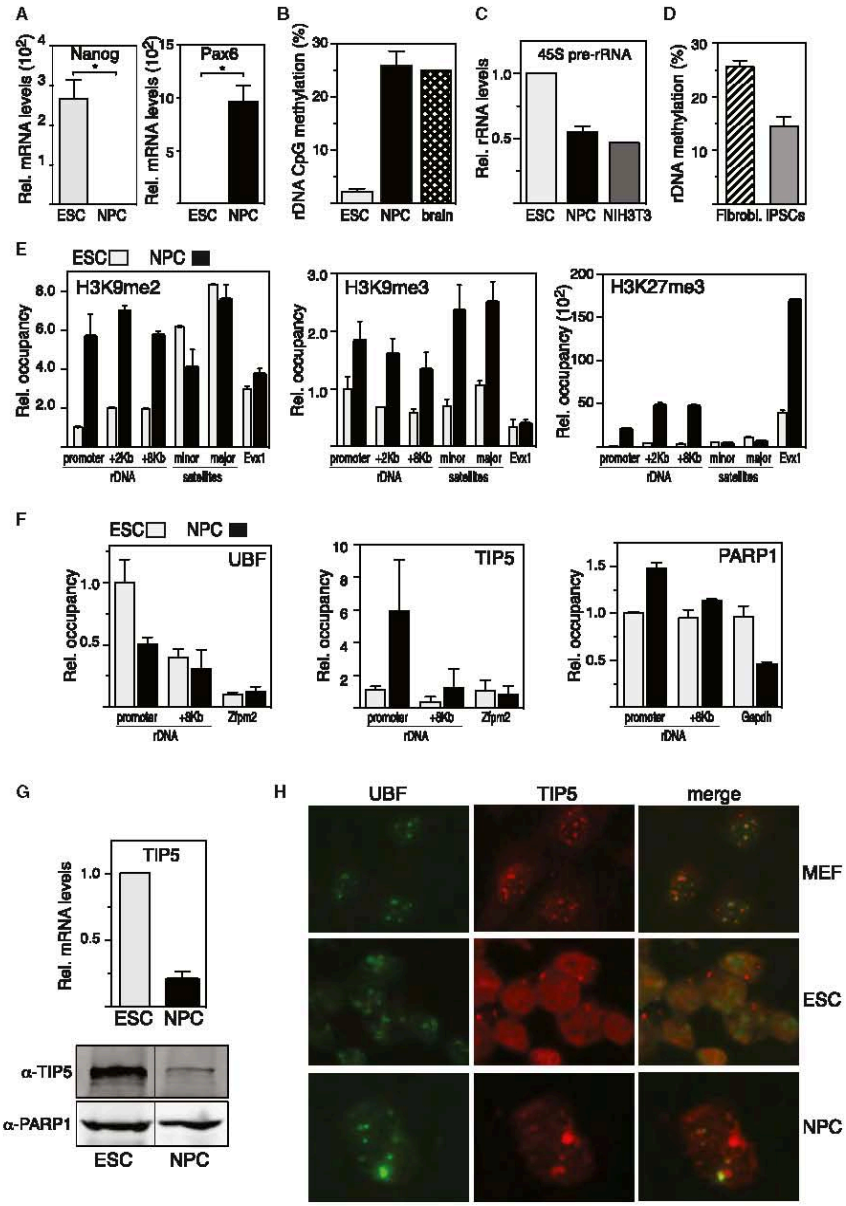

Figure 1. Establishment of rDNA Heterochromatin Occurs during ESC Differentiation and Correlates with the Recruitment of TIP5 to rDNA

(A) qRT-PCR. Nanog and Pax6 mRNA levels in ESCs and NPCs. Data were normalized to Rps12 mRNA.

(B) CpG methylation levels at rDNA promoter in ESCs, NPCs, and mouse brain tissues.

(legend continued on next page)

Quantification of 5′- and internal IGS-rRNA regions determined that unprocessed transcript levels were higher in ESCs than in NPCs (Figure 2B), suggesting that IGS-rRNA processing is less efficient in ESCs than in NPCs. To support these results, we measured ectopic IGS-rRNA and pRNA derived from an IGS-rRNA reporter gene plasmid that was transfected in NIH 3T3 cells, proficient for IGS-rRNA processing (Santoro et al., 2010), and in ESCs. Whereas ectopic IGS-rRNA was efficiently processed in NIH 3T3 cells (80%), maturation of pRNA was strongly reduced in ESCs (Figure 2C). Taken together, these results indicate that IGS-rRNA is not efficiently processed in ESCs and is thus less abundant in NPCs than in ESCs.

To test whether the lack of IGS-rRNA processing is the determinant that impairs formation of rDNA heterochromatin in ESCs, we transfected in vitro synthesized mature pRNA in ESCs and monitored TIP5 cellular localization, rDNA methylation, rDNA transcription, and H3K9me2 and H3K9me3 levels at rDNA (Figure 3). In ESCs transfected with pRNA, TIP5 decreased in the nucleoplasm and accumulated within nucleoli, as indicated by the colocalization with the nucleolar protein UBF (Figure 3A; Figure S3). Remarkably, the addition of pRNA in ESCs induced formation of heterochromatic rDNA as demonstrated by the reduction of rDNA transcription and the increase of both H3K9me2 and CpG methylation levels at the rDNA promoter (Figures 3B–3D; Figure S4). The modest increase in CpG methylation (from 1.7% to 4.4%) can also be attributed to the 2i conditions, recently described to lead to pronounced reduction in DNA methylation due to the downregulation of the de novo methyltransferases DNMT3a and DNMT3b (Leitch et al., 2013). Consistent with previous studies showing that TIP5 mediates dimethylation but not trimethylation of H3K9 at rRNA genes (Guetg et al., 2010; Santoro and Grummt, 2005), ectopic pRNA did not increase H3K9me3 levels at rDNA (Figure 3D; Figure S4). These results indicate that addition of pRNA in ESCs is sufficient to guide TIP5 to rDNA and to establish rDNA heterochromatin.

To determine how pRNA guides TIP5 to rDNA, we mutated pRNA sequences that were previously implicated in rDNA methylation and TIP5 association in somatic cells (Mayer et al., 2008; Schmitz et al., 2010). We mutated the T_0 element (pRNAΔT_0) that was previously described to form dsDNA:RNA triplex, a structure implicated in de novo rDNA methylation through recruitment of DNMT3b (Schmitz et al., 2010) and proposed as guiding module for TIP5 targeting to rDNA (Bierhoff et al., 2013). Similarly to wild-type pRNA, pRNAΔT_0 induced recruitment of TIP5 to nucleoli, promoted rDNA methylation and reduced rDNA transcription (Figures 3A–3C; Figure S3). Thus, pRNA-mediated nucleolar targeting of TIP5 and establishment of rDNA heterochromatin formation in ESCs is not mediated by rDNA:pRNA triplex. Accordingly, replacement of the 5′-pRNA region, including T_0 element, (hybrid, Control-pRNA) induced TIP5 nucleolar localization (Figure 3E; Figure S3). In contrast, replacement of 3′-pRNA sequences (hybrid, pRNA-Control), important for stem loop structure formation and the association with TIP5 in vitro (Mayer et al., 2008), impaired nucleolar localization of TIP5. Remarkably, point mutations that disrupt the stem loop structure (pRNA loop destroyed) were not efficient in recruiting TIP5 to the nucleoli whereas a compensatory mutation allowing hairpin formation did (pRNA loop recovered). Together, these results indicate that pRNA guides TIP5 to rDNA in *trans* through the hairpin structure and that addition of mature pRNA to ESCs is sufficient to establish rDNA heterochromatin. We conclude that the impairment of IGS-rRNA processing that abrogates formation of mature pRNA is the major determinant causing the euchromatic state of all rRNA genes in ESCs.

TIP5-TTF1 Association Is Mediated by pRNA and Impaired by IGS-rRNA

To determine why IGS-rRNA is unable to promote recruitment of TIP5 to rDNA, we determined whether TIP5 binds to IGS-rRNA using EMSA competition assays. Consistent with previous results, pRNA had a higher affinity for TIP5 compared to control RNA (Mayer et al., 2006) (Figure 4A). Surprisingly, TIP5 associates better with IGS-rRNA than with pRNA. To determine whether TIP5 preferentially associates with other IGS-rRNA sequences than pRNA, we analyzed TIP5 binding to IGS-rRNA sequences located upstream of the pRNA region. Spacer and enhancer RNA associate with TIP5 much less efficiently than pRNA (Figure S5A), suggesting that TIP5 binds to IGS-rRNA through the pRNA sequence and that upstream sequences might stabilize the complex through weak interactions. Together, these results indicate that TIP5 binds to IGS-rRNA and suggest that impairment of TIP5 recruitment to rDNA in ESCs might depend on the context of this interaction.

The requirement of the pRNA loop structure for nucleolar targeting of TIP5 (Figure 3) let us hypothesize that pRNA binding to TIP5 might favor the association with a docking protein for the recruitment to rDNA promoter and that IGS-rRNA might hinder this process. One important TIP5 interacting protein is the transcription terminator factor TTF1 (Németh et al., 2004; Strohner et al., 2001). TTF1 is a nucleolar protein that binds to terminator (T) elements, including the T_0 sequences at rDNA promoter, and is implicated in several rDNA regulatory processes (Evers and Grummt, 1995; Gerber et al., 1997; Längst et al., 1997). The association of TIP5 with TTF1 and its dependency on TTF1 for rDNA promoter binding proposed that TTF1 recruits TIP5 to rDNA (Németh et al., 2004; Santoro and Grummt, 2005; Strohner et al., 2001). However, whether and how pRNA is implicated in this process has so far not been investigated. TTF1 binds to RNA (Figure 4B), forming high-molecular-weight complexes. However, in contrast to TIP5, TTF1 did not display any

(C) qRT-PCR. rRNA transcription (45S pre-rRNA levels) in ESCs, NPCs, and NIH 3T3. Data were normalized to Rps12 mRNA.
(D) CpG methylation levels at rDNA promoter in mouse fibroblasts and iPSCs.
(E and F) ChIP. H3K9me2, H3K9me3 and H3K27me3, UBF, TIP5, and PARP1 occupancy. *Evx1*, *Zfpm2*, and *Gapdh* represent control genes. Data of two independent experiments were normalized to input and rDNA promoter value in ESCs.
(G) Tip5 mRNA (qRT-PCR) and protein levels (immunoblot) of ESCs and NPCs. Data were normalized to *Rps12* mRNA or PARP1 protein levels. Protein level titration was loaded and only the lanes with same protein amounts are shown.
(H) TIP5 cellular localization in MEFs, ESCs, and NPCs after 8 days of differentiation by immunofluorescence. Nucleoli are depicted by UBF signal.
All error bars represent the SD of two (when indicated) or three independent experiments. See also Figures S1 and S2.

Cell Stem Cell
The Nucleolus Regulates ESC Chromatin

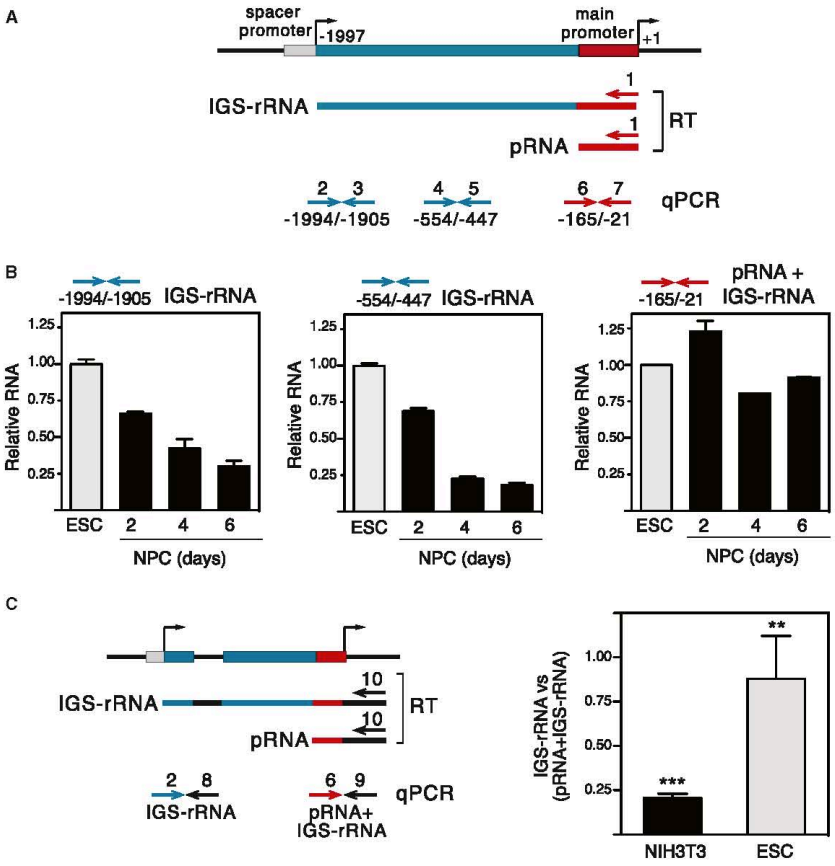

Figure 2. IGS-rRNA Is Not Efficiently Processed in ESCs

(A) Schema representing the mouse 5′-rDNA organization: Spacer promoter (gray), intergenic spacer region (blue), rDNA main promoter (red), and transcription start sites of IGS-rRNA (−1997) and 45S pre-rRNA (+1). Arrows represent primers used to perform RT (1; −20/−1) and to quantitatively amplify the indicated rDNA sequences (2–7).

(B) qRT-PCR. Levels IGS-rRNA and pRNA sequences of ESCs and NPCs (from days 2 to 6, from the beginning of differentiation). Data of two independent experiments were normalized to *Rps12* mRNA and to ESC values.

(C) Schema depicts the IGS-rRNA reporter plasmid. Black arrows represent primers used to perform RT (10) and to amplify plasmid sequences (8 and 9). Blue and red arrows (2 and 6) indicate primers hybridizing to rRNA sequences as described in (A). NIH 3T3 and ES cells were transfected with IGS-rRNA reporter plasmid. Data from three experiments are represented as values of amplifications with primers 2 and 8 (IGS-rRNA) normalized to amplifications with primers 6 and 9 (IGS-rRNA^{+}pRNA).

preferential binding to pRNA sequences (Figure 4C). In ESCs, TTF1 is bound to rDNA promoter and is localized within nucleoli as in differentiated cells (Figures S5B and S5C). To determine whether the association of TIP5 with TTF1 is regulated by pRNA or IGS-rRNA, we performed pull-down assays using purified RNA-free His-tagged TTF1 (aa.1-210, containing TIP5-interacting region) and GST-tagged-TIP5 (aa. 332-723, comprising the RNA- and TTF1-interacting regions) (Mayer et al., 2006; Németh et al., 2004). Immobilized GST-TIP5$_{332–723}$ was incubated with no RNA, or with equivalent moles of RNAs and analyzed for the interaction with His-TTF1$_{1–210}$. In the absence of RNA and in the presence of RNA control, TIP5 and TTF1 did not associate (Figure 4D). In contrast, TIP5-pRNA complexes displayed a strong interaction with TTF1, indicating that pRNA is required for TIP5-TTF1 association. Remarkably, TIP5 bound to IGS-rRNA did not interact with TTF1. Consistent with the role of 3′-pRNA sequences in TIP5 nucleolar targeting, this region was sufficient for TIP5-TTF1 interaction while the 5′-pRNA

Cell Stem Cell
The Nucleolus Regulates ESC Chromatin

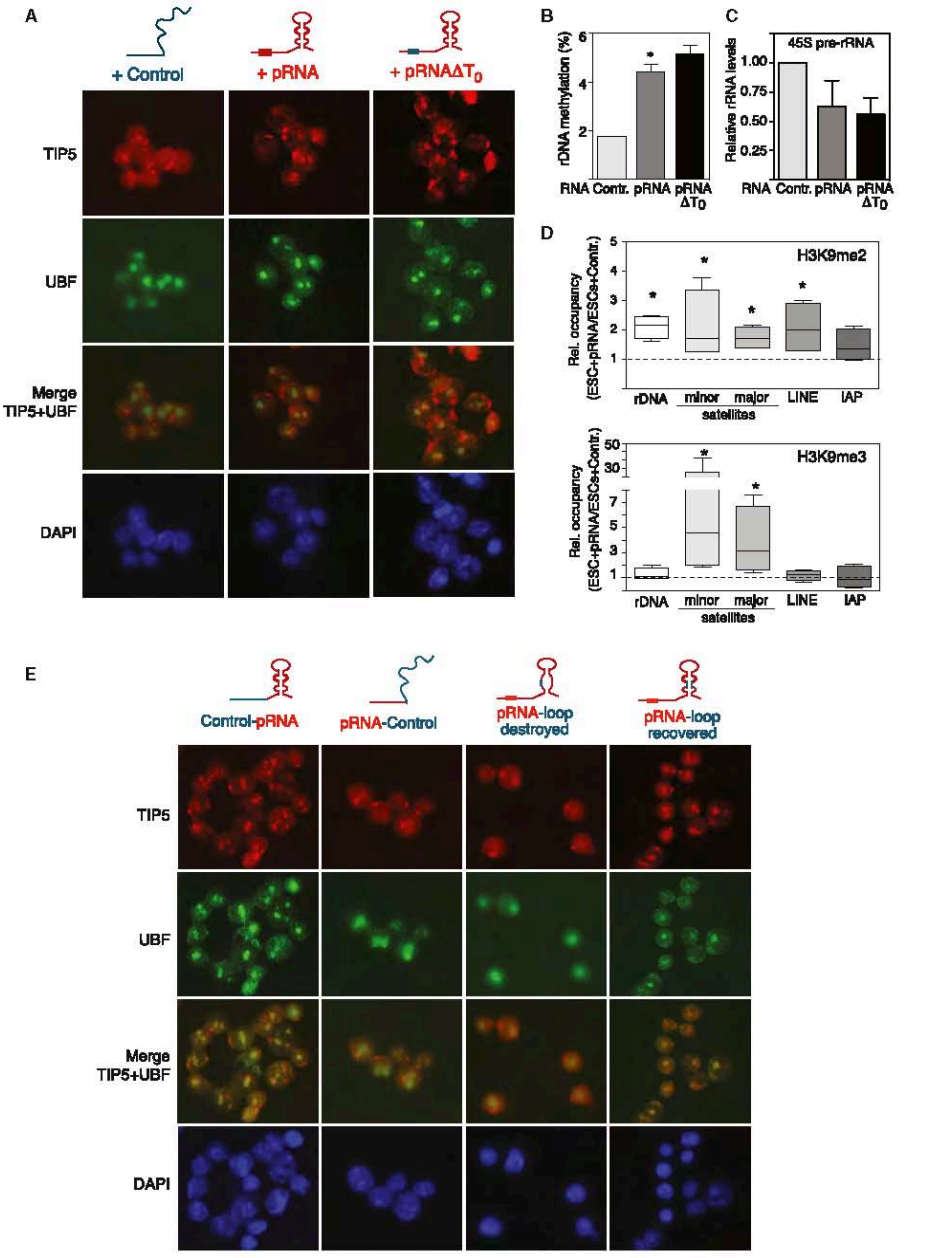

(legend on next page)

region was not. We conclude that pRNA mediates the association of TIP5 with TTF1 and that unprocessed IGS-rRNA prevents this interaction. Based on these results, we propose that the unprocessed IGS-rRNA in ESCs abolishes the interaction of TIP5 with TTF1, thus preventing TIP5 targeting to rDNA and nucleolar heterochromatin formation.

The Epigenetic State of Nucleolar Chromatin Affects ESC Chromatin and Pluripotency

Our previous studies showed that somatic cells depleted of TIP5 reduced silent epigenetic modifications at rDNA and at major and minor satellites and lack condensed heterochromatin adjacent to nucleoli (Guetg et al., 2010). Further structural alterations observed upon TIP5 knockdown, such as enlargement of nucleolar surfaces, reduction of nucleoli number, and formation of few decondensed DAPI-stained heterochromatic foci, resembled ESC chromatin organization (Figure 5A). To determine whether formation of rDNA heterochromatin affects the open chromatin of ESCs, we performed transmission electron microscopy to analyze and quantify the volume of heterochromatin associated to nucleoli in ESCs upon addition of pRNA (ESCs+pRNA) (Figure 5B; Figure S5D). Consistent with the loss of perinucleolar heterochromatin upon TIP5 knockdown in somatic cells (Guetg et al., 2010), ESCs+pRNA increased the amounts of condensed heterochromatin around nucleoli, displaying a structural organization like it is found in NPCs (Figure S5E). In line with these results, ESCs+pRNA increased H3K9me2 not only at rDNA, but also at major and minor repeats and at LINE elements while IAP transposons were not significantly affected (Figure 3D; Figure S4). H3K9me3 levels drastically increased at minor and major satellites while remaining unchanged at LINE L1 elements and IAP transposons and, as expected, at rDNA. Among the four performed experiments, we observed an inverse correlation between H3K9me2 and H3K9me3 levels at minor and major repeats (Figure S2), suggesting a two-step process that is initiated with H3K9me2 (the activity brought to rDNA by TIP5 (Santoro and Grummt, 2005)) and is further completed at major and minor satellite sequences with the establishment of H3K9me3. ESCs+pRNA increased the total amount of H3K9me2 to levels similar to those observed during ESC-NPC transition (Figure 5C). This result is in agreement with a previous work showing acquisition of large regions of H3K9 methylation during differentiation, which affects at least 30% of the genome (Wen et al., 2009). In contrast, the global H3K9me3 content was not altered in NPCs and ESCs+pRNA. Because terminally differentiated cells were previously described to contain elevated H3K9me3 levels (Hawkins et al., 2010), our results with NPCs most likely represent the epigenetic state at early differentiation time points. The elevated heterochromatic content of ESCs+pRNA was also accompanied by a reduction of minor satellites transcription as found during ESC differentiation (Figure S1E), whereas transcription of LINE and IAP elements was not greatly affected (Figure 5C). Taken together, these results suggest that tethering heterochromatin at rDNA via pRNA in ESCs initiates structural remodeling toward a highly condensed nuclear heterochromatin, a structure that ESCs normally acquire during differentiation.

We next addressed how the increased heterochromatic content mediated by pRNA affects ESC properties. ESCs+pRNA did not show alterations in important molecular features of the undifferentiated state such as cell proliferation, expression of the pluripotency genes *Oct4*, *Nanog*, and stage-specific embryonic antigen 1 (SSEA1), cell morphology, and alkaline phosphatase (AP) staining (Figures 6A–6D, and data not shown). To determine whether addition of pRNA affects pluripotency in vivo, we performed teratoma formation assays. ESCs+pRNA markedly decreased their capability to form teratoma compared to ESCs transfected with RNA control or with a pRNA mutant that is unable to recruit TIP5 to nucleoli (Figure 6E). Remarkably, teratomas derived from ESCs+pRNA showed a drastic reduced volume but displayed differentiation into all three germ layers (Figures S6A and S6B). Because ESCs were transiently transfected, we assume that teratomas obtained from ESCs+pRNA originated from untransfected cells, which is supported by the reduction in volume of these teratomas. To get insights into the loss of pluripotency, we analyzed transcription profiles of ESCs+pRNA and ESCs+RNA-control by RNaseq and found upregulation of 532 transcripts and downregulation of 509 transcripts in ESCs+pRNA (Table S1 available online). We carried out functional annotation analysis of transcripts whose levels were altered in ESCs+pRNA using DAVID tools (Huang et al., 2009) (Figure 6E; Table S1). The top eight gene ontology terms were all related to cell developmental and differentiation processes. Enrichment for these processes was particularly evident for transcripts upregulated in ESCs+pRNA, suggesting that addition of pRNA promotes expression of genes involved in cell differentiation and developmental processes. To exclude the possibility of pRNA off-target effects, we transfected a mutant pRNA unable to associate with TIP5 and analyzed transcription of *Btg3* and *Rdh10*, two genes upregulated in ESCs+pRNA and known to be implicated in neurogenesis and embryonic differentiation (Cammas et al., 2007; Yoshida et al., 1998). In contrast to pRNA, the pRNA mutant was unable to affect Btg3 and Rdh10 transcript levels (Figure S6C), indicating that upregulation of genes implicated in cell differentiation and the developmental processes is specifically mediated by a fully functional pRNA that is able to associate with TIP5, guide it to

Figure 3. Mature pRNA Is Required for the Establishment of rDNA Heterochromatin

(A) Mature pRNA induced recruitment of TIP5 to ESC nucleoli. Immunofluorescence with anti-TIP5 and anti-UBF antibodies in ESCs transfected with in vitro synthesized RNA control, pRNA, and pRNAΔT_0.

(B) Mature pRNA promotes rDNA promoter CpG methylation in ESCs. Error bars represent the SD of three independent experiments.

(C) Mature pRNA decreased rRNA synthesis in ESCs. rDNA transcription were measured by qRT-PCR and normalized to *Rps12* mRNA. Error bars indicate the SD of two independent experiments.

(D) Mature pRNA increased silent histone modifications at rDNA and centric-pericentric sequences of ESCs. Box-and-whisker plot of four independent ChIP experiments. Data are represented as bound over input in ESCs+pRNA normalized to values measured in ESCs+RNA control.

(E) pRNA loop structure mediates TIP5 recruitment to ESC nucleoli. Immunofluorescence with anti-TIP5 and anti-UBF antibodies of ESCs transfected with the indicated pRNA mutants.

See also Figure S3.

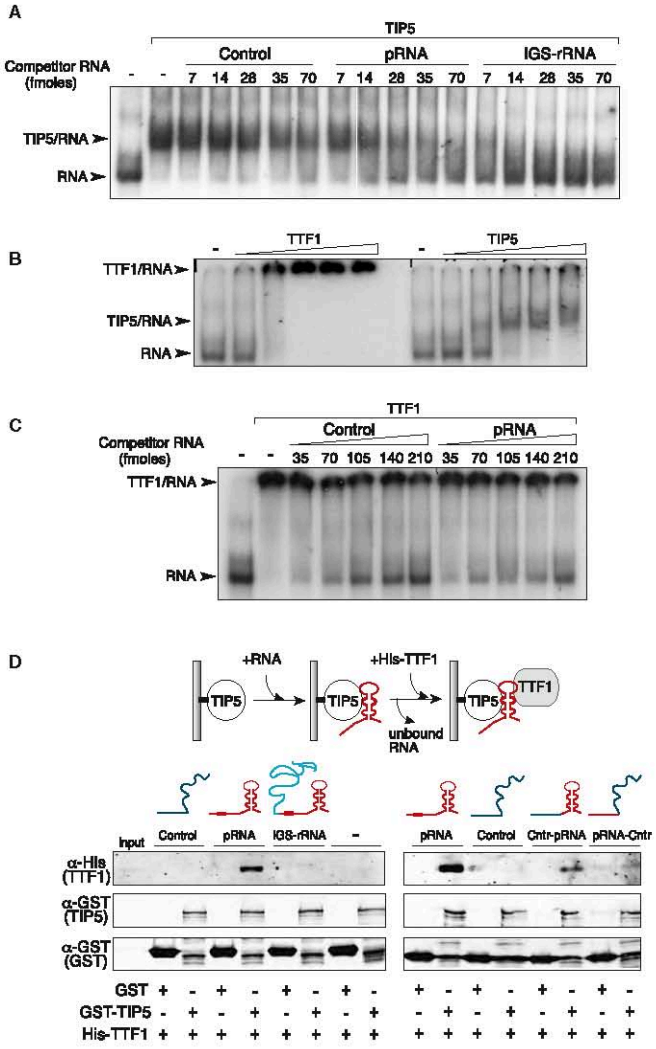

Figure 4. pRNA Mediates TIP5-TTF1 Interaction

(A) TIP5 binds to IGS-rRNA. Increasing equal moles of in vitro transcripts corresponding to control, pRNA, and IGS-rRNA sequences were used to compete for binding of $TIP5_{332-723}$ to radiolabelled run-off transcripts from pBluescript (MCS-RNA). RNA/protein complexes were analyzed by EMSA.

(B) TTF1 binds to RNA. Increasing equal moles of full-length TTF1 and $TIP5_{332-723}$ were analyzed for binding to radiolabeled MCS-RNA by EMSA.

(C) TTF1 does not show preferential binding to pRNA. Binding of full-length TTF1 to radiolabeled MCS-RNA was completed with increasing equal moles of RNA control and pRNA.

(D) TIP5-TTF1 interaction is mediated by pRNA and impaired by IGS-rRNA. Schema representing the GST-pull-down strategy used to analyze TIP5-TTF1 interaction in the presence of equivalent moles of RNAs. Pull-down assay. Bound proteins, GST, GST-TIP5, and His-TTF1, were detected with anti-GST and anti-His antibodies, respectively.

See also Figures S5A–S5C.

rDNA, and establish rDNA heterochromatin. Together, these results indicate that the elevated heterochromatic content induced by formation of nucleolar heterochromatin through pRNA impairs pluripotency and highlight the role of the nucleolus in the control of ESC chromatin plasticity that is required for the maintenance of the undifferentiated state.

To further explore the role of nucleolar chromatin in ESCs, we analyzed the differentiation capacity of cells depleted of TIP5. ESCs depleted of TIP5 by siRNA reduced TIP5 levels to 50% (Figures 7A and 7B). Upon TIP5 knockdown, ESCs proliferated less but displayed unaltered expression of *Oct4*, *Nanog*, and *Rex1*, exhibited the typical cell morphology of ESCs and were positive for AP staining (Figures 7B–7E). Similar results were obtained with other siRNA-TIP5 sequences (data not shown). To determine whether TIP5 depletion affects ESC differentiation, we treated an equal number of siRNA-control and -Tip5 treated ESCs with their respective siRNAs and induced monolayer differentiation upon withdrawal of 2i and LIF (Figure 7A). After 3 days, control cells displayed morphological structures typical of differentiated cells, whereas cells depleted of TIP5 underwent cell death and detached from the plate (Figures 7F–7H). The majority of the few siRNA-TIP5 cells that remained attached to plates showed ESC-like morphology and were positive for AP staining (Figures 7G and 7H; Figure S7). The effects observed with TIP5 depletion were specific for differentiated cells because ESCs double-treated with siRNA-Tip5 and cultured in 2i and LIF did not show any defect in viability (data not shown). These results indicate that TIP5 is required for ESC differentiation and suggest that the establishment of nucleolar heterochromatin is an event required for early differentiation.

DISCUSSION

The remodeling of the open and euchromatic genome structure of ESCs toward a highly condensed heterochromatic form

Cell Stem Cell
The Nucleolus Regulates ESC Chromatin

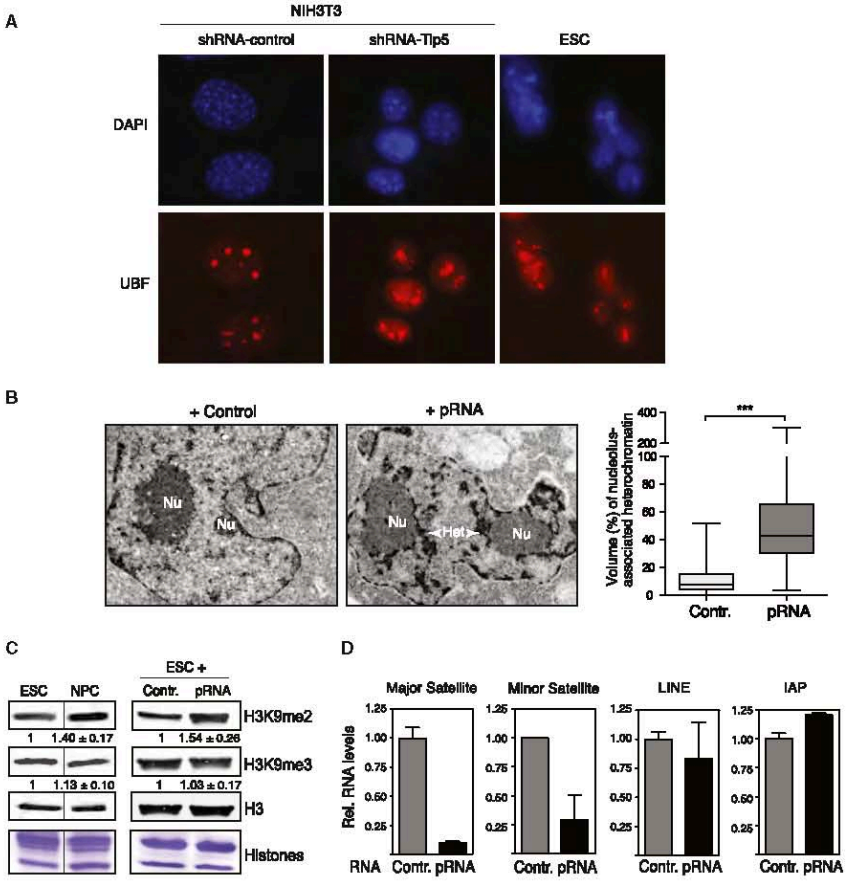

Figure 5. Mature pRNA Induces Global Remodelling toward Heterochromatic Structures

(A) Immunofluorescence showing heterochromatin (DAPI) and nucleoli (UBF) of NIH 3T3 cells stably expressing shRNA-control and -Tip5 sequences, and ESCs.

(B) Mature pRNA induced formation of condensed heterochromatin in ESCs. Transmission electron microscopy analysis. Representative images showing nucleolus-associated heterochromatin in ESCs+Control and ESCs+pRNA. The contrast procedure reveals in dark condensed heterochromatic structures (Het); 25–34 nucleoli of ESCs+RNA control and ESCs+pRNA of two independent experiments were selected at random. The volume of nucleolus-associated heterochromatin was expressed as a percentage of the volume of the nucleolus (Nu). Heteroscedastic two-tailed t test was used to compare the groups. See also Figures S5D and S5E.

(C) Immunoblot of H3K9me2, H3K9me3, and histone H3 of chromatin fractions of ESCs, NPCs, ESCs+RNA-control, and ESCs+pRNA. Values from three independent experiments were normalized to histone H3 levels. Protein level titration was loaded and only the lanes with same histone amounts are shown.

(D) qRT-PCR of major and minor satellite, LINE, and IAP retrotrasposon transcripts in ESCs+RNA-control and ESCs+pRNA. Values from two independent experiments were normalized to Rps12 mRNA.

characterizes the exit from pluripotency and the progression into differentiated states. ESC open chromatin correlates with a globally permissive transcriptional state contributing to the developmental plasticity and pluripotency of the ESC genome that has to have the ability to enter any distinct differentiation pathway (Gaspar-Maia et al., 2011). We determined here that the nucleolus is not only the place where ribosomes are produced, but it also plays a role in regulating genome architecture and pluripotency. Using mature pRNA as a mean to specifically tether heterochromatin at nucleoli of ESCs, we showed that the formation of heterochromatin at rRNA genes, the genetic component of nucleoli, has the ability to initiate the establishment of repressive chromatin structures at regions of the genome located outside of the nucleolus (Figure 7I). This process includes the formation of

Cell Stem Cell
The Nucleolus Regulates ESC Chromatin

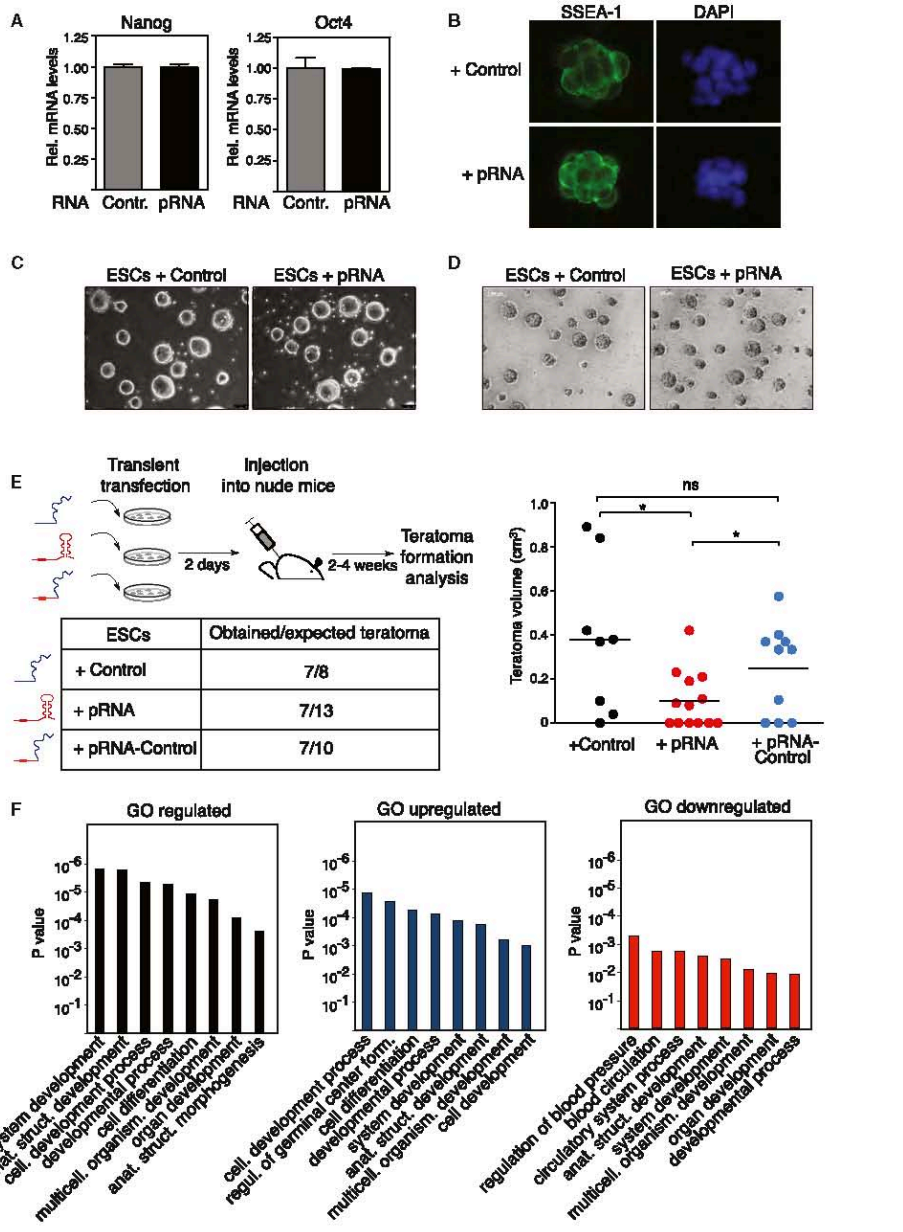

(legend on next page)

highly condensed heterochromatic structures clustering in proximity to nucleoli as found in differentiated cells. Such architectural remodeling is also evidenced by a global increase in H3K9me2, maturation of heterochromatin at repetitive sequences, and their transcriptional repression. These are characteristic features of the switch between pluripotency and differentiation. Although we cannot define which is the first event that globally initiates the formation of heterochromatin at the exit from pluripotency and entry into differentiation, our results place the nucleolus as an important regulator of this process. The establishment of rDNA heterochromatin during differentiation timely coincides with the formation of highly condensed heterochromatic structures and LOCKs (Meshorer and Misteli, 2006; Wen et al., 2009). This was particularly evident for the maturation of constitutive heterochromatin at major and minor satellite repeats, which displayed the same timing as rDNA for the acquisition of histone repressive marks and transcriptional repression upon ESC differentiation.

While showing some of the molecular outlines of the undifferentiated cells, pRNA-mediated heterochromatic ESCs transcribe genes implicated in differentiation processes and are no longer pluripotent. This observation highlights the role of the euchromatic organization in ESC identity and suggests that nucleolar chromatin is an important regulator of the pluripotent state. Likewise, impairing the formation of rDNA heterochromatin by TIP5 knockdown inhibits ESC differentiation, suggesting that the establishment of nucleolar heterochromatin is a necessary step for the switch from a lower to a higher order chromatin structure and lineage commitment.

How does the nucleolus influence heterochromatin formation? Due to the proximity of rDNA and centromeric sequences at rDNA-bearing chromosomes (Dev et al., 1977; Kurihara et al., 1994), the effect of rDNA heterochromatin on chromatin structures at major and minor repeats might in part be explained through spreading mechanisms. However, centromeres of chromosomes not containing rRNA genes also associate with the nucleolus at a frequency more than expected for a random distribution (Carvalho et al., 2001), indicating the existence of alternative mechanisms that establish heterochromatin at sequences that are further away from rDNA loci. In this case, the establishment of rDNA heterochromatin might allow the formation of a nucleolar/perinucleolar compartment enriched in chromatin repressor complexes that would be attractive for genomic regions that need to be repressed. Anchoring of heterochromatin at the nucleolus might have similar function like the ones described for the nuclear periphery that is responsible for the integrity of mammalian heterochromatin (Pinheiro et al., 2012; Towbin et al., 2012). Consistent with this, genomic regions localized at the lamina (LADs) were shown to relocate after cell division either at the lamina or at the nucleolus (Kind et al., 2013), suggesting interchangeable roles in establishing and maintaining heterochromatic states.

This study also provides evidence that rRNA genes do not only function in synthesizing rRNA. Silent rRNA repeats, present in all somatic cells, maintain their heterochromatic state independently of transcriptional activity, and are stably propagated throughout the cell cycle (Conconi et al., 1989). Our results indicated that the epigenetic state of rRNA genes contributes to nuclear architecture and cellular functions such as pluripotency and differentiation by controlling the balance between heterochromatin and euchromatin. Interestingly, rDNA deletions in *Drosophila* result in reduced heterochromatin elsewhere in the genome and the extent of the rDNA deletion correlates with the loss of silencing in much the same manner as mutations in known protein heterochromatin components (Paredes and Maggert, 2009).

Very little is understood about how specific lncRNAs selectively seek out interaction sites in the genome, the nature of lncRNA-chromatin interactions, and their possible functional roles (Rinn and Chang, 2012). This work underlined the role of lncRNA in targeting epigenetic regulatory processes at specific genomic loci leading to the establishment of chromatin conformation patterns that ultimately result in the fine control of genes. We show that the regulation of pRNA precursor IGS-rRNA processing is a key determinant for the control of the epigenetic state at rDNA and propose that the processing represents a mean of lncRNA regulation to modulate distinct functions of the same lncRNA. We determined that IGS-rRNA processing is a developmentally regulated process and that its impairment in ESCs prevents recruitment of TIP5 to rDNA and formation of rDNA heterochromatin. Although the mechanisms that impair IGS-rRNA processing in ESCs are yet to be determined, our results demonstrated that mature pRNA is necessary to establish rDNA heterochromatin. We showed that pRNA-mediated targeting of TIP5 occurs through DNA-protein recognition rules. Whereas IGS-rRNA abolishes the association of TIP5 with TTF1, pRNA promotes this interaction that serves to guide the complex to the rDNA promoter and to establish nucleolar heterochromatin. Thus, the same lncRNA can prevent or promote protein complex assembly and its processing controls the switch between these functions. Based on these results, it would not be surprising if processing emerges as a more general mechanism of lncRNA regulation.

In summary, our data underline the contribution of chromatin structure in ESC pluripotency and differentiation potential and indicate that the nucleolus is a key regulator of nuclear architecture and chromatin structure, which serves to control cell pluripotency and lineage commitment.

Figure 6. pRNA Impairs ESC Pluripotency

(A) Nanog and Oct4 mRNA levels in ESCs+RNA control and ESCs+pRNA (qRT-PCR). Values from two independent experiments were normalized to *Rps12* mRNA.

(B–D) (B) SSEA-1 immunostaining, (C) cell morphology, and (D) AP staining of ESCs+RNA control and ESCs+pRNA.

(E) ESCs+pRNA are not pluripotent. Efficiency of teratoma formation was assessed by the number of teratomas generated versus expected (injections) and by tumor volumes measured at the time when control animals were killed.

(F) Mature pRNA induced expression of genes implicated in cell differentiation and development. Top eight biological process gene ontology terms as determined using DAVID for genes regulated, and upregulated and downregulated in ESCs+pRNA.

See also Figure S6.

Cell Stem Cell
The Nucleolus Regulates ESC Chromatin

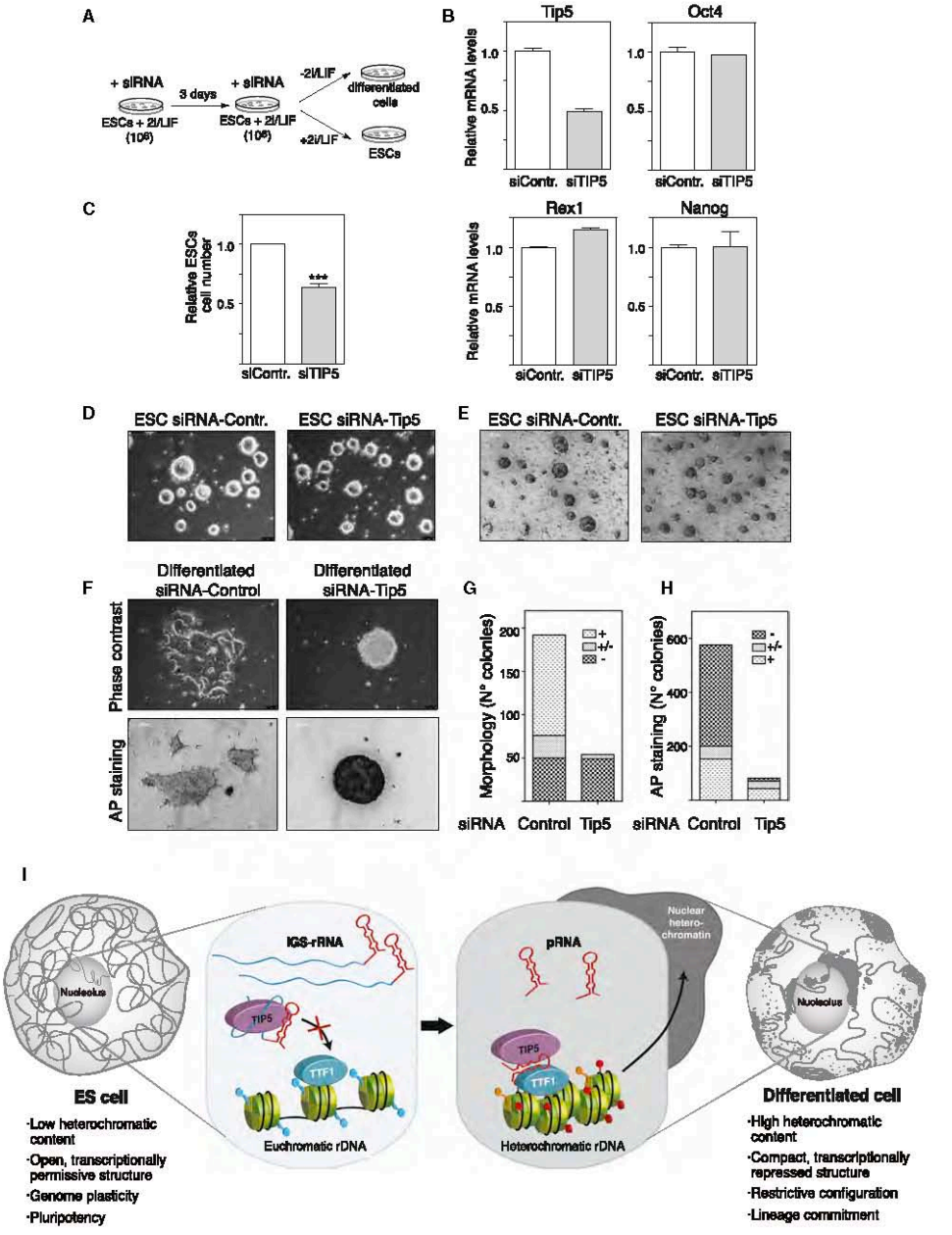

(legend on next page)

EXPERIMENTAL PROCEDURES

mESC Culture

One hundred twenty-nine mouse embryonic stem cells (E14 line) were cultured in N2B27 media (Dulbecco's modified Eagle's medium [DMEM] F12, neurobasal medium, N2/B27 supplements, 2 mM L-glutamine with Pen/Strep, β-Mercaptoethanol) supplemented with recombinant leukemia inhibitory factor, LIF (ESGRO, 1000 U/ml) and MEK and GSK3β inhibitors, 2i (Stemolecule CHIR99021 and PD0325901, 3 μM and 1 μM, respectively). Cells were seeded at a density of 50,000 cells/cm^2 in culture dishes (Corning CellBIND surface) treated with 0.1% gelatine without feeder layer. Propagation of cells was carried out every 2 days using Trypsin 0.5× for enzymatic cell dissociation.

mESC Differentiation

mESCs were differentiated to neural progenitor cells according to a previously established protocol (Bibel et al., 2004). In brief, differentiation used a suspension-based embryoid bodies formation (Bacteriological Petri Dishes, Bio-one with vents, Greiner). The neural differentiation media (DMEM, 10% fetal calf serum, 1× MEM NEAA, 2 mM L-glutamine with Pen/Strep, β-mercaptoethanol) was filtered through 0.22 μm filters and stored at 4°C. During the 8-day differentiation procedure, media was exchanged every 2 days. In the last 4 days of differentiation, the media was supplemented with 2 μM retinoic acid to generate neural precursors that are Pax-6-positive radial glial cells.

Immunocytochemistry

ESCs or differentiated cells were grown on gelatin-coated coverslips and permeabilized with 0.05% Triton X-100 in 20 mMTris-HCl (pH 8), 5 mM MgCl2, 0.5 mM EDTA, and 25% glycerol. After washing, cells were fixed with cold methanol (7 min) and stained with anti-TIP5 (Diagenode) and anti-UBF (SantaCruz) antibodies and DAPI (Molecular Probes), and immunofluorescent images were digitally recorded.

Transmission Electron Microscopy

Cells were first fixed with 2.5% glutaraldehyde, dehydrated in an ethanol series, transferred to methanol, and immersed into a freshly prepared mixture of methanol and acetic anhydride (5:1, v/v) at 25°C for 24 hr in the dark (Tandler and Solari, 1982; Testillano et al., 1991). Cells were then washed in pure methanol for 20 min, transferred in ethanol and embedded in Epon (Sigma). Ultrathin (50 nm) sections were contrasted with 5% aqueous uranyl acetate for 60 min at room temperature and examined with a CM100 transmission electron microscope (FEI).

The volume of nucleolus-associated heterochromatin was estimated using the Cavalieri-estimator (Gundersen et al., 1988; West, 2012). Volume estimates were performed for samples of 25 to 34 nucleoli selected at random from each electron microscopy sample of two independent experiments. Nucleoli were selected independent of their size or shape in the electron microscopy montages. The volume of nucleolus-associated heterochromatin was expressed as a percentage of the volume of the corresponding nucleolus. Due to unequal variances of heterochromatin volumes in control and experimental cells, a heteroscedastic two-tailed t test was used to compare the groups ($p = 7.6 \times 10^{-9}$).

EMSA

Radiolabeled MCS-RNA was synthesized by T7 RNA polymerase using pBluescript-KS(+)/EcoRI as template. After treatment with DNase I, transcripts were purified and 50,000 cpm of MCS-RNA were incubated for 15 min on ice with 40 ng recombinant TIP5 or TTF1 in EMSA buffer (20 mM Tris-HCl [pH 8.0], 5 mM MgCl2, 100 mM KCl, and 0.2 mM EDTA). Cold competitor RNA was added, and incubation was continued for 30 min. RNA-protein complexes were analyzed by electrophoresis on 6% (w/v) native polyacrylamide gels and depicted with autoradiography.

For detailed methods, list of antibodies, and tables of primers, see the Supplemental Experimental Procedures.

SUPPLEMENTAL INFORMATION

Supplemental Information includes Supplemental Experimental Procedures, seven figures, and one table and can be found with this article online at http://dx.doi.org/10.1016/j.stem.2014.10.005.

ACKNOWLEDGMENTS

The authors thank Ursula Luethi, Lutz Slomianka, and the Center for Microscopy and Image Analysis, University of Zurich for performing transmission electron microscopy analyses. This work was supported by the Swiss National Science Foundation (310003A-135801 and 31003A-152854 to R.S., 31003A-118361 to P.C., and 323530-133905 to F.A.W.), UBS-Promedica Stiftung (to R.S. and O.S.), Forschungskredit of the University of Zurich (to N.S. and E.V.), and the Mäxi Stiftung (to D.B. and R.S.).

Received: February 27, 2014
Revised: August 8, 2014
Accepted: October 16, 2014
Published: December 4, 2014

REFERENCES

Aoto, T., Saitoh, N., Ichimura, T., Niwa, H., and Nakao, M. (2006). Nuclear and chromatin reorganization in the MHC-Oct3/4 locus at developmental phases of embryonic stem cell differentiation. Dev. Biol. *298*, 354–367.

Bártová, E., Galiová, G., Krejcí, J., Harnicarová, A., Strasák, L., and Kozubek, S. (2008a). Epigenome and chromatin structure in human embryonic stem cells undergoing differentiation. Dev. Dyn. *237*, 3690–3702.

Bártová, E., Krejcí, J., Harnicarová, A., and Kozubek, S. (2008b). Differentiation of human embryonic stem cells induces condensation of chromosome territories and formation of heterochromatin protein 1 foci. Differentiation *76*, 24–32.

Bhattacharya, D., Talwar, S., Mazumder, A., and Shivashankar, G.V. (2009). Spatio-temporal plasticity in chromatin organization in mouse cell differentiation and during Drosophila embryogenesis. Biophys. J. *96*, 3832–3839.

Bibel, M., Richter, J., Schrenk, K., Tucker, K.L., Staiger, V., Korte, M., Goetz, M., and Barde, Y.A. (2004). Differentiation of mouse embryonic stem cells into a defined neuronal lineage. Nat. Neurosci. *7*, 1003–1009.

Figure 7. Depletion of TIP5 Impairs ESC Differentiation

(A) Schema showing the experimental strategy for TIP5 knockdown in ESCs.
(B) *Tip5*, *Oct4*, *Nanog*, and *Rex1* mRNA levels in ESCs depleted of TIP5.
(C) TIP5 knockdown affects ESC proliferation. Data represent relative cell numbers after 3 days of siRNA treatment.
(D and E) (D) Cell morphology and (E) AP staining of ESCs treated with siRNA-control and -*Tip5*.
(F–H) (F) Cell morphology and AP staining of cells after 3 days of differentiation. Quantifications are shown respectively in (G) differentiated (+), partially differentiated (+/−), and not differentiated (−); and (H) stained (+), partially stained (+/−), and not stained (−). See also Figure S7.
(I) Model showing the chromatin organization of the nucleus and nucleolus of ESCs (open, euchromatic) and differentiated cells (closed, heterochromatic). In ESCs, IGS-rRNA is not processed with consequent lack of mature pRNA. The unprocessed transcript impairs the association of TIP5 with TTF1, inhibiting TIP5 recruitment to rDNA and causing the euchromatic state of all rRNA genes. Upon differentiation, mature pRNA is produced and allows TIP5-TTF1 interaction that is productive for TIP5 targeting to rDNA and formation of heterochromatin at nucleoli. The arrow depicts the influence of rDNA heterochromatin in the formation of highly condensed and repressive chromatin structures at region outside the nucleolus. Establishment of compact heterochromatic structures abrogates genome plasticity of ESCs and set up a genome organization that favors cell lineage specification.

Bierhoff, H., Postepska-Igielska, A., and Grummt, I. (2013). Noisy silence: Non-coding RNA and heterochromatin formation at repetitive elements. Epigenetics *9*, 53–61.

Cammas, L., Romand, R., Fraulob, V., Mura, C., and Dolle, P. (2007). Expression of the murine retinol dehydrogenase 10 (Rdh10) gene correlates with many sites of retinoid signalling during embryogenesis and organ differentiation. Developmental dynamics *236*, 2899–2908.

Carvalho, C., Pereira, H.M., Ferreira, J., Pina, C., Mendonça, D., Rosa, A.C., and Carmo-Fonseca, M. (2001). Chromosomal G-dark bands determine the spatial organization of centromeric heterochromatin in the nucleus. Mol. Biol. Cell *12*, 3563–3572.

Conconi, A., Widmer, R.M., Koller, T., and Sogo, J.M. (1989). Two different chromatin structures coexist in ribosomal RNA genes throughout the cell cycle. Cell *57*, 753–761.

de Wit, E., Bouwman, B.A., Zhu, Y., Klous, P., Splinter, E., Verstegen, M.J., Krijger, P.H., Festuccia, N., Nora, E.P., Welling, M., et al. (2013). The pluripotent genome in three dimensions is shaped around pluripotency factors. Nature *501*, 227–231.

Dev, V.G., Tantravahi, R., Miller, D.A., and Miller, O.J. (1977). Nucleolus organizers in Mus musculus subspecies and in the RAG mouse cell line. Genetics *86*, 389–398.

Dixon, J.R., Selvaraj, S., Yue, F., Kim, A., Li, Y., Shen, Y., Hu, M., Liu, J.S., and Ren, B. (2012). Topological domains in mammalian genomes identified by analysis of chromatin interactions. Nature *485*, 376–380.

Efroni, S., Duttagupta, R., Cheng, J., Dehghani, H., Hoeppner, D.J., Dash, C., Bazett-Jones, D.P., Le Grice, S., McKay, R.D., Buetow, K.H., et al. (2008). Global transcription in pluripotent embryonic stem cells. Cell Stem Cell *2*, 437–447.

Evers, R., and Grummt, I. (1995). Molecular coevolution of mammalian ribosomal gene terminator sequences and the transcription termination factor TTF-I. Proc. Natl. Acad. Sci. USA *92*, 5827–5831.

Fussner, E., Ahmed, K., Dehghani, H., Strauss, M., and Bazett-Jones, D.P. (2010). Changes in chromatin fiber density as a marker for pluripotency. Cold Spring Harb. Symp. Quant. Biol. *75*, 245–249.

Gaspar-Maia, A., Alajem, A., Meshorer, E., and Ramalho-Santos, M. (2011). Open chromatin in pluripotency and reprogramming. Nat. Rev. Mol. Cell Biol. *12*, 36–47.

Gerber, J.K., Gögel, E., Berger, C., Wallisch, M., Müller, F., Grummt, I., and Grummt, F. (1997). Termination of mammalian rDNA replication: polar arrest of replication fork movement by transcription termination factor TTF-I. Cell *90*, 559–567.

Gonzalez-Sandoval, A., Towbin, B.D., and Gasser, S.M. (2013). The formation and sequestration of heterochromatin during development: delivered on 7 September 2012 at the 37th FEBS Congress in Sevilla, Spain. FEBS J. *280*, 3212–3219.

Gorkin, D.U., Leung, D., and Ren, B. (2014). The 3D genome in transcriptional regulation and pluripotency. Cell Stem Cell *14*, 762–775.

Guetg, C., Lienemann, P., Sirri, V., Grummt, I., Hernandez-Verdun, D., Hottiger, M.O., Fussenegger, M., and Santoro, R. (2010). The NoRC complex mediates the heterochromatin formation and stability of silent rRNA genes and centromeric repeats. EMBO J. *29*, 2135–2146.

Guetg, C., Scheifele, F., Rosenthal, F., Hottiger, M.O., and Santoro, R. (2012). Inheritance of silent rDNA chromatin is mediated by PARP1 via noncoding RNA. Mol. Cell *45*, 790–800.

Gundersen, H.J.G., Bendtsen, T.F., Korbo, L., Marcussen, N., Møller, A., Nielsen, K., Nyengaard, J.R., Pakkenberg, B., Sørensen, F.B., Vesterby, A., et al. (1988). Some new, simple and efficient stereological methods and their use in pathological research and diagnosis. APMIS *96*, 379–394.

Hawkins, R.D., Hon, G.C., Lee, L.K., Ngo, Q., Lister, R., Pelizzola, M., Edsall, L.E., Kuan, S., Luu, Y., Klugman, S., et al. (2010). Distinct epigenomic landscapes of pluripotent and lineage-committed human cells. Cell Stem Cell *6*, 479–491.

Huang, W., Sherman, B.T., and Lempicki, R.A. (2009). Systematic and integrative analysis of large gene lists using DAVID bioinformatics resources. Nat. Protoc. *4*, 44–57.

Jørgensen, H.F., Azuara, V., Amoils, S., Spivakov, M., Terry, A., Nesterova, T., Cobb, B.S., Ramsahoye, B., Merkenschlager, M., and Fisher, A.G. (2007). The impact of chromatin modifiers on the timing of locus replication in mouse embryonic stem cells. Genome Biol. *8*, R169.

Kind, J., Pagie, L., Ortabozkoyun, H., Boyle, S., de Vries, S.S., Janssen, H., Amendola, M., Nolen, L.D., Bickmore, W.A., and van Steensel, B. (2013). Single-cell dynamics of genome-nuclear lamina interactions. Cell *153*, 178–192.

Kurihara, Y., Suh, D.S., Suzuki, H., and Moriwaki, K. (1994). Chromosomal locations of Ag-NORs and clusters of ribosomal DNA in laboratory strains of mice. Mamm. Genome *5*, 225–228.

Längst, G., Blank, T.A., Becker, P.B., and Grummt, I. (1997). RNA polymerase I transcription on nucleosomal templates: the transcription termination factor TTF-I induces chromatin remodeling and relieves transcriptional repression. EMBO J. *16*, 760–768.

Leitch, H.G., McEwen, K.R., Turp, A., Encheva, V., Carroll, T., Grabole, N., Mansfield, W., Nashun, B., Knezovich, J.G., Smith, A., et al. (2013). Naive pluripotency is associated with global DNA hypomethylation. Nat. Struct. Mol. Biol. *20*, 311–316.

Martens, J.H., O'Sullivan, R.J., Braunschweig, U., Opravil, S., Radolf, M., Steinlein, P., and Jenuwein, T. (2005). The profile of repeat-associated histone lysine methylation states in the mouse epigenome. EMBO J. *24*, 800–812.

Mayer, C., Schmitz, K.M., Li, J., Grummt, I., and Santoro, R. (2006). Intergenic transcripts regulate the epigenetic state of rRNA genes. Mol. Cell *22*, 351–361.

Mayer, C., Neubert, M., and Grummt, I. (2008). The structure of NoRC-associated RNA is crucial for targeting the chromatin remodelling complex NoRC to the nucleolus. EMBO Rep. *9*, 774–780.

Melcer, S., Hezroni, H., Rand, E., Nissim-Rafinia, M., Skoultchi, A., Stewart, C.L., Bustin, M., and Meshorer, E. (2012). Histone modifications and lamin A regulate chromatin protein dynamics in early embryonic stem cell differentiation. Nat. Commun. *3*, 910.

Meshorer, E., and Misteli, T. (2006). Chromatin in pluripotent embryonic stem cells and differentiation. Nat. Rev. Mol. Cell Biol. *7*, 540–546.

Meshorer, E., Yellajoshula, D., George, E., Scambler, P.J., Brown, D.T., and Misteli, T. (2006). Hyperdynamic plasticity of chromatin proteins in pluripotent embryonic stem cells. Dev. Cell *10*, 105–116.

Moss, T., and Stefanovsky, V.Y. (2002). At the center of eukaryotic life. Cell *109*, 545–548.

Németh, A., Strohner, R., Grummt, I., and Längst, G. (2004). The chromatin remodeling complex NoRC and TTF-I cooperate in the regulation of the mammalian rRNA genes in vivo. Nucleic Acids Res. *32*, 4091–4099.

Nora, E.P., Lajoie, B.R., Schulz, E.G., Giorgetti, L., Okamoto, I., Servant, N., Piolot, T., van Berkum, N.L., Meisig, J., Sedat, J., et al. (2012). Spatial partitioning of the regulatory landscape of the X-inactivation centre. Nature *485*, 381–385.

Paredes, S., and Maggert, K.A. (2009). Ribosomal DNA contributes to global chromatin regulation. Proc. Natl. Acad. Sci. USA *106*, 17829–17834.

Pinheiro, I., Margueron, R., Shukeir, N., Eisold, M., Fritzsch, C., Richter, F.M., Mittler, G., Genoud, C., Goyama, S., Kurokawa, M., et al. (2012). Prdm3 and Prdm16 are H3K9me1 methyltransferases required for mammalian heterochromatin integrity. Cell *150*, 948–960.

Rinn, J.L., and Chang, H.Y. (2012). Genome regulation by long noncoding RNAs. Annu. Rev. Biochem. *81*, 145–166.

Santoro, R., and Grummt, I. (2001). Molecular mechanisms mediating methylation-dependent silencing of ribosomal gene transcription. Mol. Cell *8*, 719–725.

Santoro, R., and Grummt, I. (2005). Epigenetic mechanism of rRNA gene silencing: temporal order of NoRC-mediated histone modification, chromatin remodeling, and DNA methylation. Mol. Cell. Biol. *25*, 2539–2546.

Santoro, R., Li, J., and Grummt, I. (2002). The nucleolar remodeling complex NoRC mediates heterochromatin formation and silencing of ribosomal gene transcription. Nat. Genet. *32*, 393–396.

Santoro, R., Schmitz, K.M., Sandoval, J., and Grummt, I. (2010). Intergenic transcripts originating from a subclass of ribosomal DNA repeats silence ribosomal RNA genes in trans. EMBO Rep. *11*, 52–58.

Schlesinger, S., Selig, S., Bergman, Y., and Cedar, H. (2009). Allelic inactivation of rDNA loci. Genes Dev. *23*, 2437–2447.

Schmitz, K.M., Mayer, C., Postepska, A., and Grummt, I. (2010). Interaction of noncoding RNA with the rDNA promoter mediates recruitment of DNMT3b and silencing of rRNA genes. Genes Dev. *24*, 2264–2269.

Splinter, E., and de Laat, W. (2011). The complex transcription regulatory landscape of our genome: control in three dimensions. EMBO J. *30*, 4345–4355.

Strohner, R., Nemeth, A., Jansa, P., Hofmann-Rohrer, U., Santoro, R., Längst, G., and Grummt, I. (2001). NoRC—a novel member of mammalian ISWI-containing chromatin remodeling machines. EMBO J. *20*, 4892–4900.

Tandler, C.J., and Solari, A.J. (1982). Methanol-acetic anhydride: an efficient blocking agent for electron microscope cytochemistry. Its application to mouse testis and other tissues. Histochemistry *76*, 351–361.

Testillano, P.S., Sanchez-Pina, M.A., Olmedilla, A., Ollacarizqueta, M.A., Tandler, C.J., and Risueno, M.C. (1991). A specific ultrastructural method to reveal DNA: the NAMA-Ur. The journal of histochemistry and cytochemistry: official journal of the Histochemistry Society *39*, 1427–1438.

Towbin, B.D., González-Aguilera, C., Sack, R., Gaidatzis, D., Kalck, V., Meister, P., Askjaer, P., and Gasser, S.M. (2012). Step-wise methylation of histone H3K9 positions heterochromatin at the nuclear periphery. Cell *150*, 934–947.

Wen, B., Wu, H., Shinkai, Y., Irizarry, R.A., and Feinberg, A.P. (2009). Large histone H3 lysine 9 dimethylated chromatin blocks distinguish differentiated from embryonic stem cells. Nat. Genet. *41*, 246–250.

West, M.J. (2012). Estimating volume in biological structures. Cold Spring Harb Protoc. *2012*, 1129–1139.

Wong, L.H., Ren, H., Williams, E., McGhie, J., Ahn, S., Sim, M., Tam, A., Earle, E., Anderson, M.A., Mann, J., and Choo, K.H. (2009). Histone H3.3 incorporation provides a unique and functionally essential telomeric chromatin in embryonic stem cells. Genome Res. *19*, 404–414.

Yoshida, Y., Matsuda, S., Ikematsu, N., Kawamura-Tsuzuku, J., Inazawa, J., Umemori, H., and Yamamoto, T. (1998). ANA, a novel member of Tob/BTG1 family, is expressed in the ventricular zone of the developing central nervous system. Oncogene *16*, 2687–2693.

Zhou, Y., Santoro, R., and Grummt, I. (2002). The chromatin remodeling complex NoRC targets HDAC1 to the ribosomal gene promoter and represses RNA polymerase I transcription. EMBO J. *21*, 4632–4640.

Cell Stem Cell, Volume *15*
Supplemental Information

lncRNA Maturation to Initiate Heterochromatin Formation in the Nucleolus Is Required for Exit from Pluripotency in ESCs

Nataša Savić, Dominik Bär, Sergio Leone, Sandra C. Frommel, Fabienne A. Weber, Eva Vollenweider, Elena Ferrari, Urs Ziegler, Andres Kaech, Olga Shakhova, Paolo Cinelli, and Raffaella Santoro

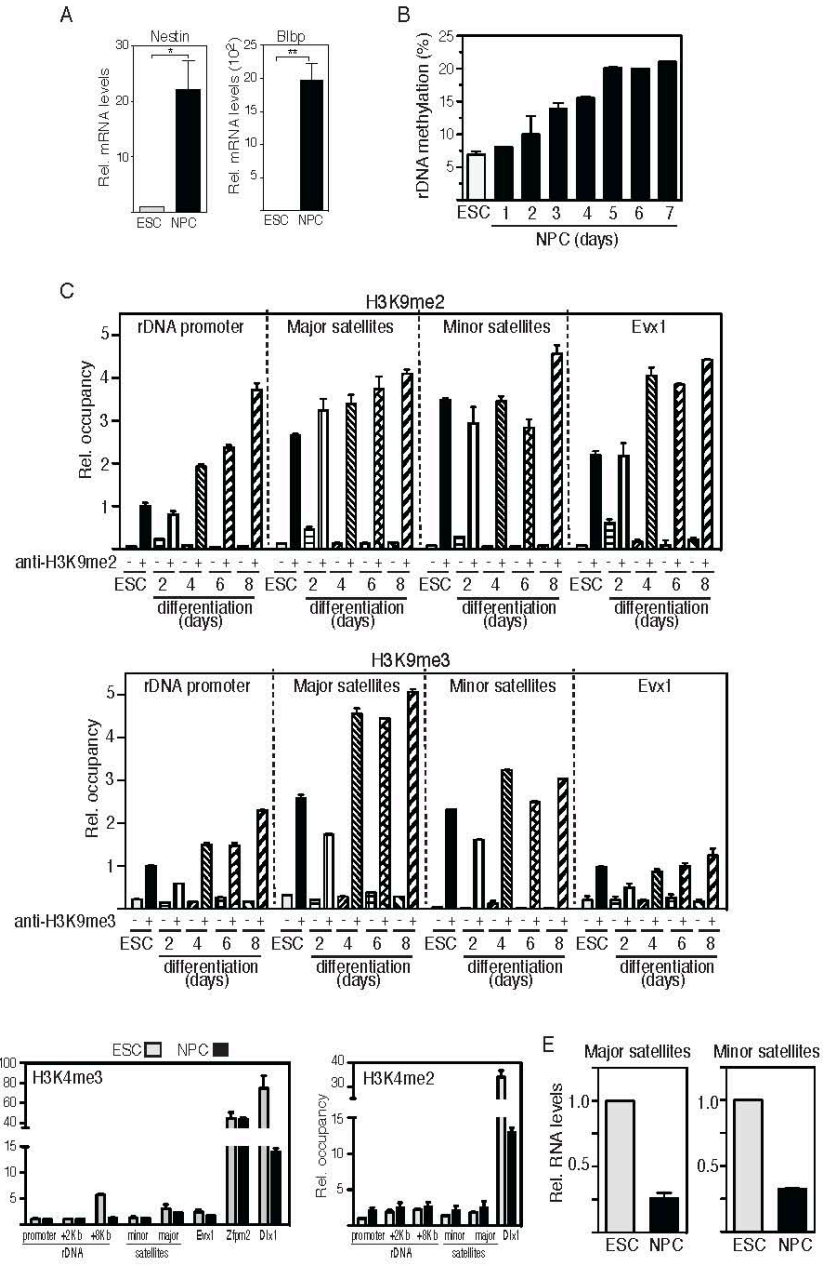
A
Nestin
Rel. mRNA levels
ESC NPC
Blbp
Rel. mRNA levels (10²)
ESC NPC
B
rDNA methylation (%)
ESC 1 2 3 4 5 6 7
NPC (days)
C
H3K9me2
rDNA promoter
Major satellites
Minor satellites
Evx1
Rel. occupancy
anti-H3K9me2
ESC 2 4 6 8
differentiation (days)
H3K9me3
rDNA promoter
Major satellites
Minor satellites
Evx1
Rel. occupancy
anti-H3K9me3
ESC 2 4 6 8
differentiation (days)
D
ESC NPC
H3K4me3
Rel. occupancy
promoter +2Kb +8Kb minor major Evx1 Zfpm2 Dlx1
rDNA
satellites
H3K4me2
Rel. occupancy
promoter +2Kb +8Kb minor major Dlx1
rDNA
satellites
E
Major satellites
Minor satellites
Rel. RNA levels
ESC NPC
ESC NPC

Figure S1

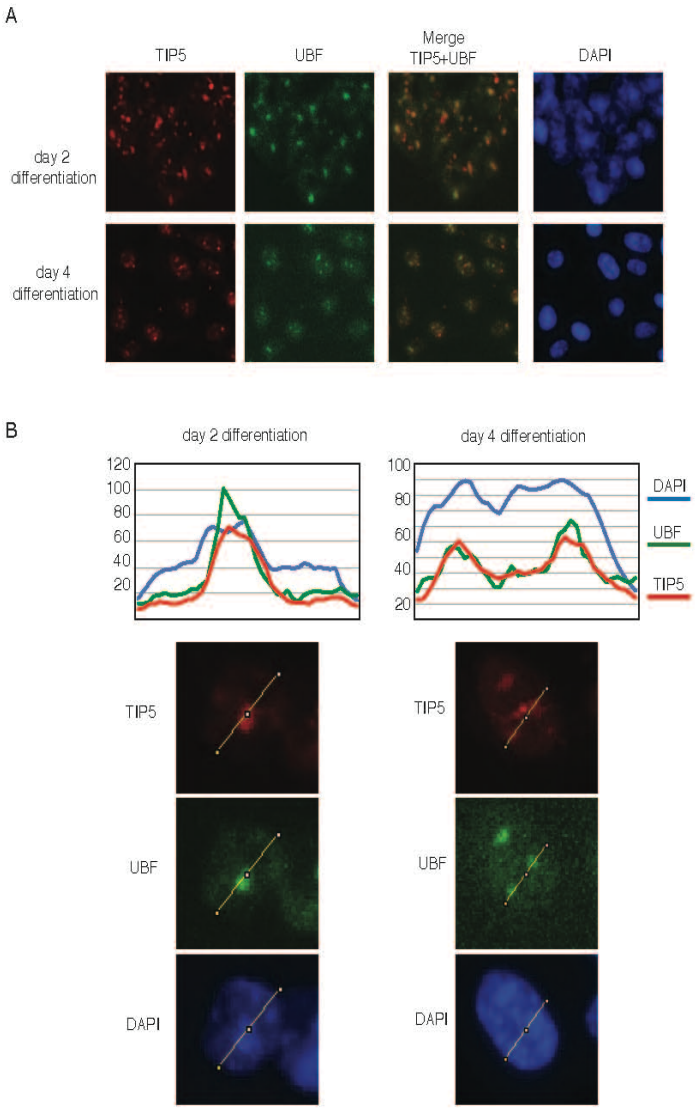
A
TIP5
UBF
Merge TIP5+UBF
DAPI
day 2 differentiation
day 4 differentiation
B
day 2 differentiation
day 4 differentiation
120
100
80
60
40
20
100
80
60
40
20
DAPI
UBF
TIP5
TIP5
UBF
DAPI
TIP5
UBF
DAPI

Figure S2

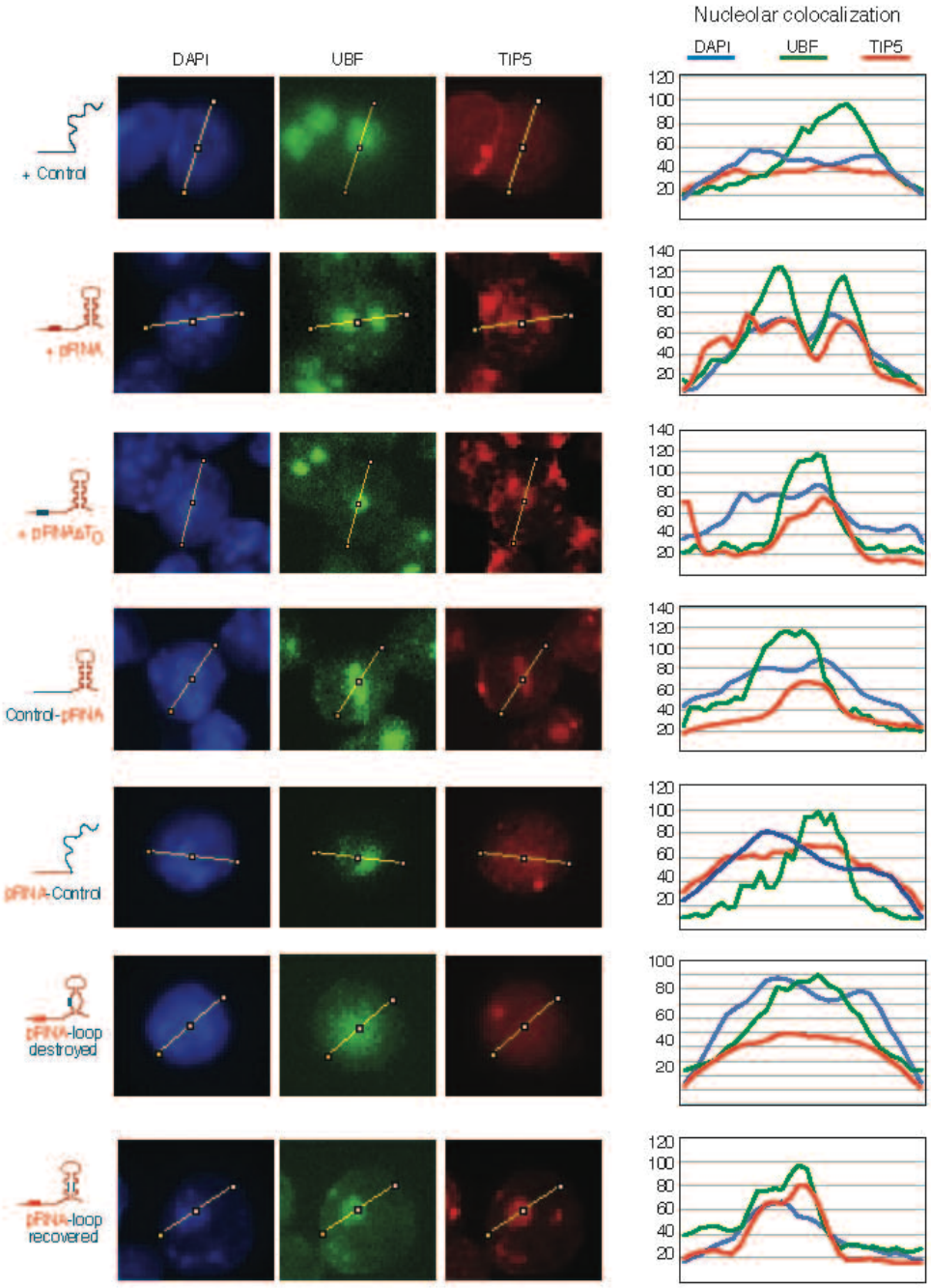
DAPI
UBF
TIP5
Nucleolar colocalization
DAPI
UBF
TIP5
+ Control
+ pRNA
+ pRNAΔT_D
Control-pRNA
pRNA-Control
pRNA-loop destroyed
pRNA-loop recovered

Figure S3

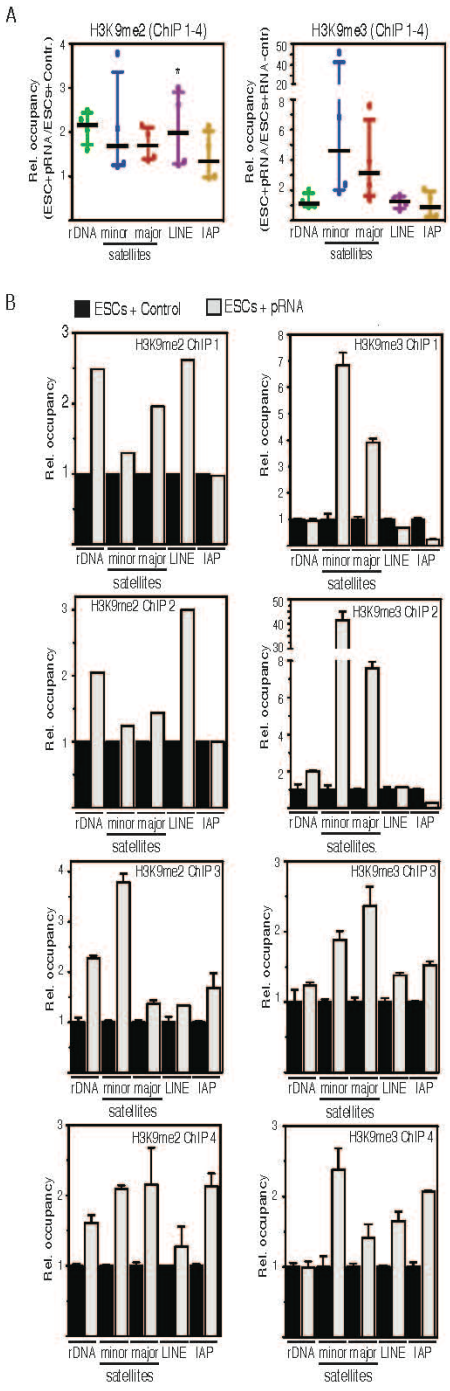
A
H3K9me2 (ChIP 1-4)
H3K9me3 (ChIP 1-4)
Rel. occupancy (ESC+pRNA/ESCs+Contr.)
Rel. occupancy (ESC+pRNA/ESCs+RtiA-cntr)
rDNA minor major LINE IAP
satellites
B
ESCs + Control
ESCs + pRNA
H3K9me2 ChIP 1
H3K9me3 ChIP 1
H3K9me2 ChIP 2
H3K9me3 ChIP 2
H3K9me2 ChIP 3
H3K9me3 ChIP 3
H3K9me2 ChIP 4
H3K9me3 ChIP 4
Rel. occupancy

Figure S4

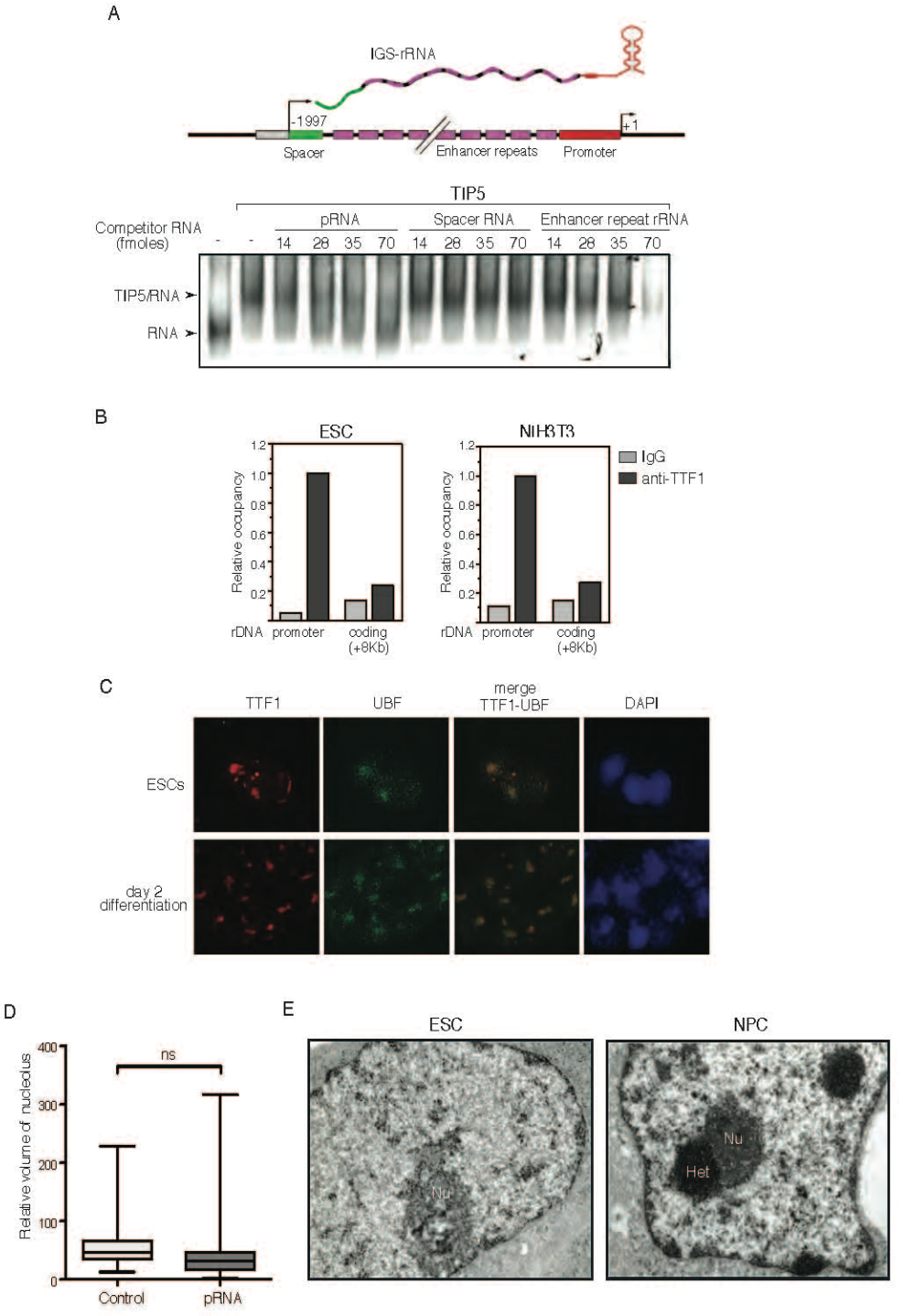
A
IGS-rRNA
-1997
+1
Spacer
Enhancer repeats
Promoter
TIP5
Competitor RNA (fmoles)
pRNA
Spacer RNA
Enhancer repeat rRNA
- - 14 28 35 70 14 28 35 70 14 28 35 70
TIP5/RNA
RNA
B
ESC
NIH3T3
IgG
anti-TTF1
Relative occupancy
rDNA promoter coding (+8Kb)
C
TTF1
UBF
merge TTF1-UBF
DAPI
ESCs
day 2 differentiation
D
ns
Relative volume of nucleolus
Control
pRNA
E
ESC
NPC
Nu
Het

Figure S5

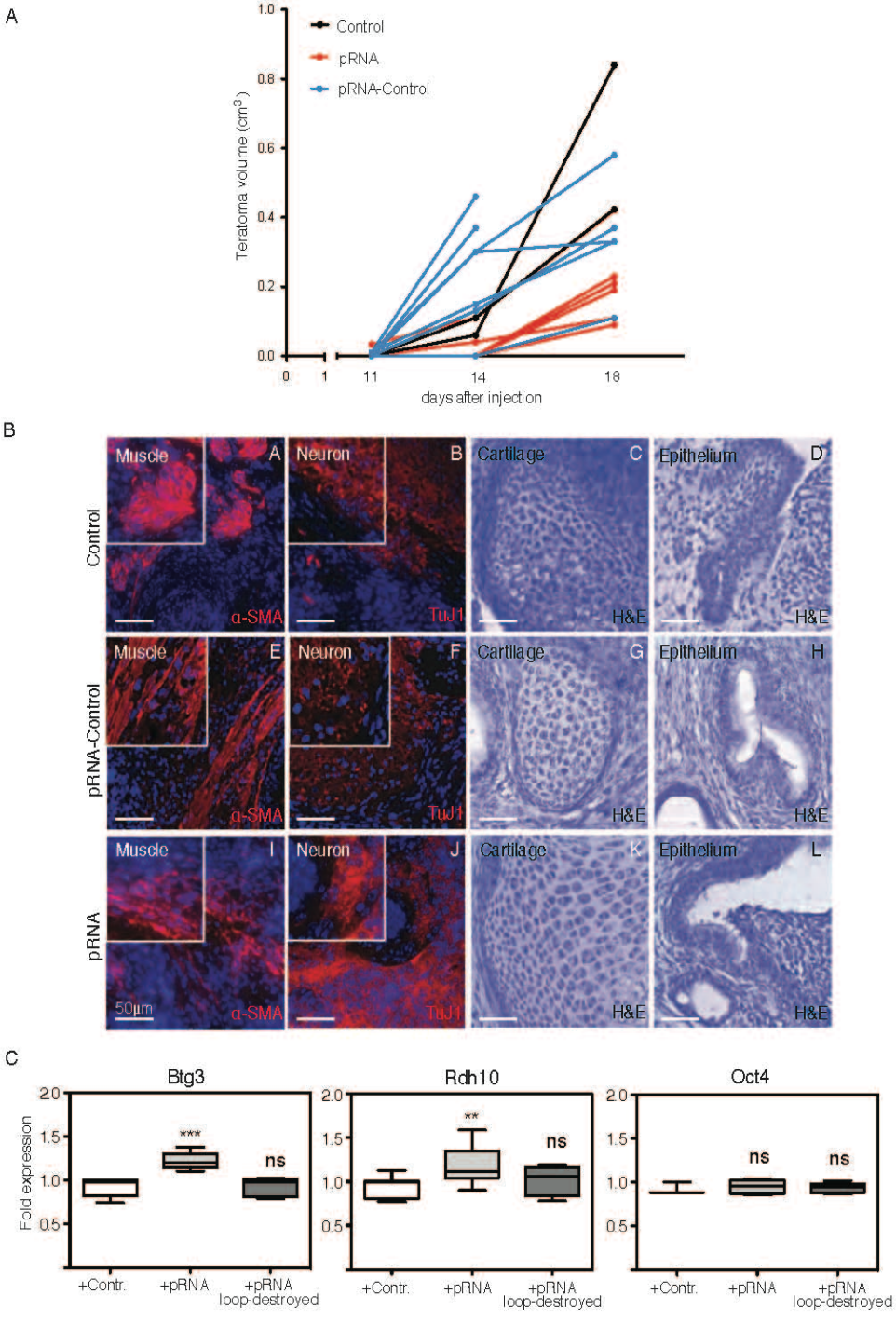
A
Control
pRNA
pRNA-Control
Teratoma volume (cm³)
days after injection
B
Control
pRNA-Control
pRNA
Muscle
Neuron
Cartilage
Epithelium
α-SMA
TuJ1
H&E
50µm
C
Btg3
Rdh10
Oct4
Fold expression
***
**
ns
+Contr.
+pRNA
+pRNA loop-destroyed

Figure S6

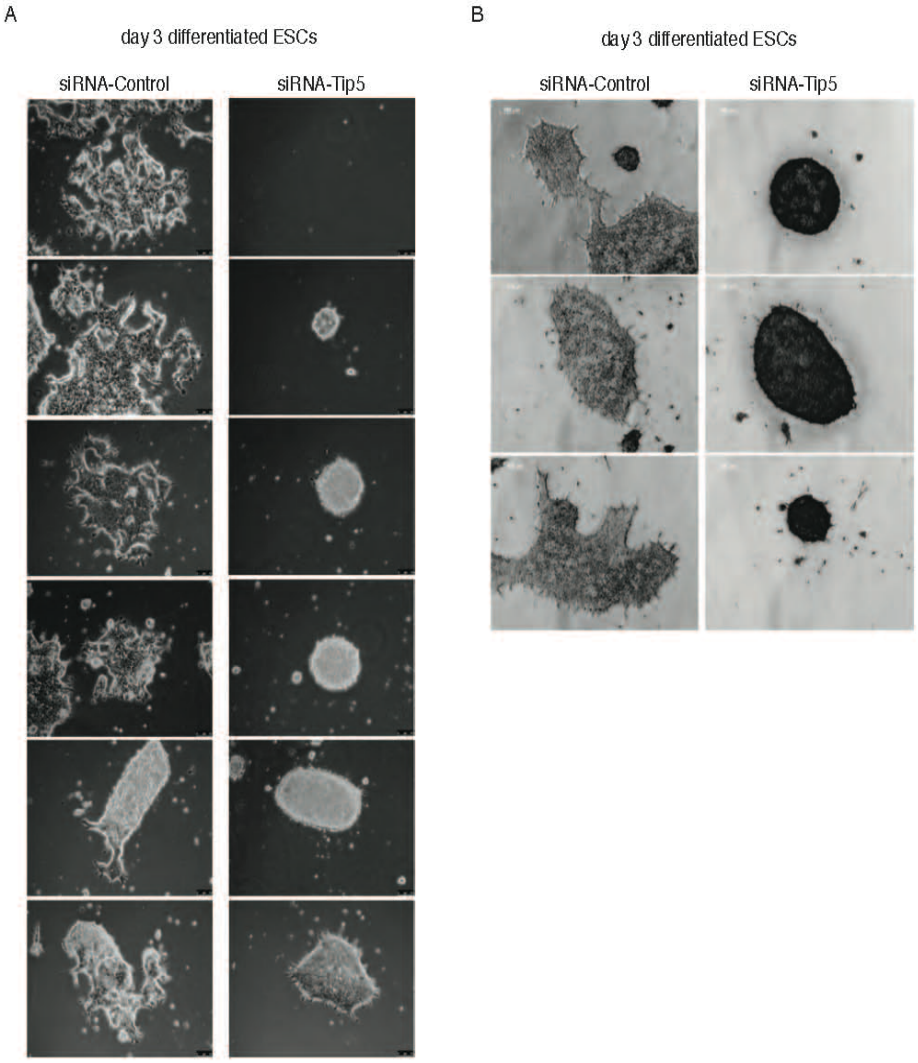
A
day 3 differentiated ESCs
siRNA-Control
siRNA-Tip5
B
day 3 differentiated ESCs
siRNA-Control
siRNA-Tip5

Figure S7

Supplemental Figure Legends

Figure S1. Establishment of rDNA heterochromatin occurs during ESC differentiation. Related to Figure 1.

(A) qRT-PCR. *Nestin* and *Blbp* (neural precursor markers) mRNA levels in ESCs and NPCs. Data were normalized to *Rps12* mRNA. Error bars indicate the SD of three independent experiments.

(B) CpG methylation levels at rDNA promoter in ESCs (JM8N4) and during 7 days of differentiation into NPCs. ESCs were cultivated on monolayer and differentiation was induced with N2B27 medium supplemented with RA. Error bars indicate the SD of two independent experiments.

(C) ChIP. H3K9me2 and H3K9me3 occupancy at rDNA promoter and coding sequences, major and minor satellites and control gene *Evx1* monitored during different time points (days) of differentiation. Data were normalized to input and rDNA promoter values in ESCs.

(D) ChIP. H3K4me2 and H3K4me3 occupancy in ESCs and NPCs. *Evx1*, *Zfpm2* and *Dlx1* represent control genes. Data were normalized to input and rDNA promoter values in ESCs.

(E) Major and minor satellite transcript levels in ESCs and NPCs were measured by qRT-PCR and normalized to *Rps12* mRNA. Error bars indicate the SD of two independent experiments.

Figure S2. Establishment of rDNA heterochromatin during ESC differentiation correlates with the recruitment of TIP5 to rDNA. Related to Figure 1.

(A) TIP5 localizes within nucleoli shortly after ESC differentiation. Immunofluorescence showing TIP5 nucleolar localization in ESCs after 2 and 4 days differentiation. Nucleoli are visualized by UBF signal.

(B) Quantification of TIP5, UBF and DAPI colocalization measured using Fiji image analysis software.

Figure S3. The stem-loop structure of pRNA is sufficient to target TIP5 to nucleoli. Related to Figure 3.

Quantification of nucleolar localization of TIP5 in ESCs transfected with RNA Control, pRNA, pRNA and pRNA mutants (pRNAΔT_0, Control-pRNA, pRNA-Control, pRNA-loop destroyed and pRNA-loop recovered). TIP5, UBF and DAPI signals were measured using Fiji image analysis software.

Figure S4. Mature pRNA increases H3K9me2 and H3K9me3 at rDNA and centric-pericentric heterochromatin in ESCs. Related to Figure 3.

(A) Scatter plot of the four ChIP experiments shown in Figure 3D.

(B) Results of the single four ChIP experiments showing an inverse correlation in the enrichment between H3K9me2 and H3K9me3 levels at minor and major repeats in ESCs+pRNA when compared to ESCs+RNA-control. Data are represented as bound over input in ESCs+pRNA normalized to values measured in ESCs+RNA-control.

Figure S5. Mature pRNA mediates TIP5-TTF1 interaction and induces global remodelling toward heterochromatic structures pRNA. Related to Figure 4 and 5.

(A) TIP5 binds to IGS-rRNA and it has a stronger affinity for pRNA sequences. Increasing equal moles of *in vitro* transcripts corresponding to pRNA, spacer promoter and enhancer repeat RNA were used to compete for binding of $TIP5_{332-723}$ to radiolabelled run-off transcripts from pBluescript (MCS-RNA). RNA/protein complexes were analyzed by EMSA.

(B) TTF1 binds to the rDNA promoter of ESCs. ChIP showing association of TTF1 with rDNA promoter in ESCs and NIH3T3 cells. Data of two independent experiments were normalized to input and rDNA promoter values. The low levels of TTF1 association with +8 Kb rDNA sequences (that do not contain T elements) demonstrated the specificity of the assay.

(C) TTF1 is localized within nucleoli of ESCs and differentiated cells. Immunofluorescence showing TTF1 nucleolar localization in ESCs and 2 days after differentiation. Nucleoli are visualized by UBF signal.

(D) Box-and-whisker plot of nucleoli size in ESCs+Control and ESCs+pRNA. 25 to 34 nucleoli of ESCs+RNA control and ESCs+pRNA of two independent experiments were selected at random

and independent of their size or shape in the EM montages. Volumes were estimated using the Cavalieri-estimator (Gundersen et al., 1988; West, 2012). Nucleoli volumes did not differ among control and ESCs+pRNA while heterochromatin associated to nucleoli did. The volume of nucleolus-associated heterochromatin was expressed as a percentage of the volume of the nucleolus (Nu) that was associated with and shown in main Figure 5B.

(E) Transmission electron microscopy analysis of ESCs and NPCs. The contrast procedure reveals in dark condensed heterochromatic structures (Het) and nucleoli (Nu).

Figure S6. pRNA impairs ESC pluripotency. Related to Figure 6.

(A) Kinetics of teratoma growth from the time of injection to euthanasia of control animals. In this experiment, tumors derived from ESCs+RNA-control (2), ESCs+pRNA (6) and ESCs+mutant pRNA-Control (7) were analysed.

(B) Histological analysis of teratomas derived from ESCs transfected with RNA-control, pRNA and mutant pRNA-Control revealed that ESCs differentiate into all three germ layers as shown by the presence of ectoderm (B, F, J), endoderm (C) and mesoderm (A,E,I). C,D,G,H,K,L haematoxylin staining. Immunostaining for bIII tubulin (TuJ1) (B,F,J), and smooth muscle actin (SMA) (A,E,I). Inserts show higher magnification. Scale bars, 50 μm.

(C) Box-and-whisker plot of three independent experiments showing mRNA levels of *Btg3, Rdh10* and *Oct4* measured in ESCs transfected with RNA-control, pRNA and mutant pRNA loop-destroyed. *Btg3* and *Rdh10* are known to be implicated in neurogenesis and embryonic differentiation (Cammas et al., 2007; Yoshida et al., 1998). Consistent with the results of Fig. 6A, *Oct4* mRNA levels remained unaffected in all three conditions.

Figure S7. Depletion of TIP5 impairs ESC differentiation. Related to Figure 7.

(A) Cell morphology and (B) AP staining of differentiated ESCs treated with siRNA-control and -*Tip5*.

Supplemental Table Legends

Supplemental Table S1. Related to Figure 6.

Total RNA of ESCs+RNA-Control and ESCs+pRNA from two biological replicates were purified and analyzed by RNA seq. The table includes the list of genes whose transcript levels were altered in ESCs+pRNA when compared to control cells (defined as regulated, upregulated and downregulated) and gene onthology analysis using DAVID tools.

Supplemental Experimental procedures

Reprogramming into iPSC

Reprogramming was performed as previously described (Weber et al., 2013). Breifly, mouse embryonic fibroblasts (MEF) were isolated from 14.5 day-pregnant C57BL/6 mice and cultured in DMEM supplemented with 10% FBS (PAA) and 1% L-glutamin/penicillin/streptomycin (10,000 U/ml penicillin G sodium; 10,000µg /ml streptomycin sulphate; 29.2mg/ml L-glutamine; 10mM sodium citrate in 0.14% NaCl, Gibco). The reprogramming of the MEFs was performed according to Yamanaka's protocol (Takahashi et al., 2007) using the pMXs retroviral vectors producing murine *Oct4*, *Sox2*, *Klf4* and *c-Myc* (Addgene, cat. nos. 13366, 13367, 13370 and 13375). Two days after infection, MEFs were cultured in DMEM containing 15% FBS, 1% L-glutamin/penicillin/streptomycin, 1x MEM non-essential amino acids (GIBCO) and 50 mM ß-mercaptoethanol (GIBCO) supplemented with 1000 U/ml ESGRO murine Leukemia inhibitory factor (LIF, Chemicon Int.). The iPSC cell line used for the experiment of Figure 1D has the ability to generate teratoma (data not shown).

Transfections

ESCs were seeded at a density of 20,000 cells/cm^2 and transfected with the indicated siRNAs (50 nM siRNA) or synthetic RNAs (1 mg/ml) using Lipofectamine® RNAiMAX (Life Techonlogies) in Opti-MEM® GlutaMAX™ (GIBCO) reduced-serum medium. Analysis of differentiated transfected ESCs was performed using consecutive transfections. Three days after the first transfection, equal amounts of ESCs (e.g. siRNA-control and siTIP5 treated cells) were again transfected and induced to differentiate in complete media (G-MEM, 10%FCS, Sodium Pyruvate 100mM, 1xMEM NEAA, L-Glutamine) by withdrawal of LIF and 2i. Efficiencies of siRNA-mediated depletions and synthetic RNA levels were monitored by qRT-PCR 3-4 days post-transfection.

In Vitro Transcription

The indicated pRNA and control sequences were cloned by PCR into pJET1/2 plasmids. pRNA : mrDNA from -232 to -1; Control-pRNA: control sequences at 5', mrDNA from -140 to -1 at 3';

pRNA-Control: mrDNA from -232 to -140 at 5', control sequences at 3' ; pRNA-loop destroyed: mrDNA from -232 to -1 sequences where GGG (-115/-113) were replaced with AAA; pRNA-loop recovered: mrDNA from -232 to -1 sequences where CCC (-60/-58) were replaced with TTT. All plasmids were verified by sequencing. Synthetic RNAs were synthesized using T7 polymerase and as substrate Xba I linearized pJET1/2 vectors containing the indicated sequences. After treatment with DNase I, transcripts were double purified using TRIzol reagent (Invitrogen) according to the manufacture's protocol.

Chromatin Immunoprecipitation

The chromatin immunoprecipitation (ChIP) protocol was previously described (Santoro, 2014). Briefly, formaldehyde 1% was added to cultured cells to cross-link proteins to DNA. Isolated nuclei were then lysed in 300µl lysis buffer (50 mM Tris-HCl [pH 8.1], 10 mM EDTA, 1% SDS) and sonicated using a Bioruptor ultrasonic cell disruptor to shear genomic DNA to an average fragment size of 200bp. 20 to 40 mg chromatin was diluted tenfold with IP buffer (16.7 mM Tris-HCl [pH 8.1]), 167 mM NaCl, 1.2 mM EDTA, 0.01% SDS, 1.1% Triton X-100) and than immunoprecipitated overnight with ChIP-grade antibodies. After elution and reversion of crosslinks, the precipitated DNA was purified with phenol/chloroform, ethanol precipitated and than quantified by qPCR. rDNA, major and minor satellite sequences were amplified with previously reported primers (Martens et al., 2005) (Martens et al., 2005; Santoro et al., 2002). Primers are listed in Table S2.

RNA Extraction, reverse transcription and quantitative PCR (RT-qPCR)

RNA was purified with Trizol reagent (Life Technologies) . Residual contaminating genomic DNA was removed with Ambion® TURBO™ DNase according to manufacture's instructions. RNA was primed with random hexamers and reverse-transcribed to first-strand cDNA. Reverse transcription of pRNA and IGS-rRNA was performed using DNA oligo -20/-1 Rev or random primers. qRT-PCR was performed with SensiMix SYBR Hi-ROX Mix (Bioline) on a Rotor-Gene Q (Qiagen). Amplification of samples without reverse transcriptase assured absence of DNA (data

not shown). The relative transcription levels were determined by normalizing to Rps12 mRNA levels. Statistical significance (P-values) of the difference in expression levels between genes was calculated using the two-sample paired t-test. Primer sequences used in qRT-PCR are listed in Table S2.

CpG methylation

rDNA CpG methylation was measured as previously described (Santoro, 2014; Santoro et al., 2002)). 2 μg genomic DNA were digested with HpaII (NEB) in the presence of 5 ng of unmethylated pBluescript KS(+) plasmid. rDNA CpG methylation levels were measured by quantitative amplification using primer pairs (-165/-145 Forw and -20/-1 Rev) that flank the restriction sites CCGG at -142 of rDNA promoter or primers that amplify neighbouring sequences lacking HpaII sites (+1/+20 Forw and +111/+130 Rev). Values were obtained using logarithmic dilutions of mouse genomic DNA as standard curve. CpG methylation levels were calculated as resistance to HpaII digestion by normalizing the amounts of rDNA amplified from -165 to -1 to the levels of amplicons from +1 to +130. To verify HpaII digestion efficiency, pBluescript KS(+) plasmid was analyzed by qPCR using one forward primer that is complementary to sequences upstream of the CCGG site of β-lactamase gene (at 2580) and two different reverse primers that map upstream and downstream the HpaII sites (see Table S2). All analyzed samples displayed 96-98% digestion efficiency.

GST-Pulldown

5 μg of GST-TIP5$_{235-741}$ were incubated with 15μl of GST beads (Glutathione Sepharose 4B, GE Healthcare) in AM100 buffer (100mM KCl, 20mM Tris-HCl pH 8.0, 5mM $MgCl_2$, 0.2mM EDTA, 1X Protease Inhibitor (Roche)) for 12-16 hours at 4°C. After two washes with EMSA buffer containing 3% Glycerol, bound GST-TIP5$_{235-741}$ was incubated with 25 nmoles of the indicated RNAs for 1h at 4°C. After a double wash with AM200 buffer (200mM KCl, 20mM Tris-HCl pH 8.0, 5mM $MgCl_2$, 0.2mM EDTA, 1X cOmplete Protease Inhibitor Cocktail (Roche)), bound GST-TIP5/RNA complexes were incubated with 0.5 μg of His-TTF1$_{1-210}$ for 2h at 4°C. Samples were then washed

three times with EBC buffer (250mM NaCl, 50mM Tris-HCl pH8.0, 0.5% NONIDET P-40, 5mM DTT, 1X cOmplete Protease Inhibitor Cocktail), run on a 12% SDS polyacrylamide gel and analyzed by Western blot with anti-GST and anti-RGS.HIS antibodies.

AP staining

Cells were fixed in 4% paraformaldehyde for 10min, washed with AP Buffer (100mM TrisCl pH 9.5, 100mM NaCl, 50mM MgCl2) and then incubated for 30 min in AP Buffer containing NBT (37 mg/ml) and 3.5µl BCIP (175 mg/ml). The staining was blocked with Tris-EDTA (Sigma) for 10min.

Whole-Transcriptome Shotgun Sequencing (RNA-Seq) and Data Analyses

Total RNA of ESCs+Control-RNA and ESCs+pRNA from two biological replicates were purified and analyzed by RNA seq. 100bp paired-end reads have been sequenced with illumina Hiseq. The reads were quality filtered and submitted to RSEM for expression quantitation (Li and Dewey, 2011). Expression counts were further analyzed with the glm method in the edgeR package to compute the significance of differential expression (Robinson et al., 2010).

Teratoma analysis

Teratoma samples were fixed in 4% buffered paraformaldehyde and embedded in paraffin. For immunostainings, 5 µm thickness paraffin sections were deparaffinized and rehydrated and subsequently subjected to the antigen retrieval (Citrate buffer pH 6.0 for 10 minutes at 110°C in rapid microwave histoprocessor, Milestone, USA). The following primary antibodies were used: anti-bIII tubulin (Sigma), anti-GFAP (DAKO) and anti-SMA (Sigma). Nuclei were stained with DAPI and slides were mounted with Fluorescent Mounting Medium (DAKO) to avoid bleaching. Images were captured with a Leica DMI 6000B Microscope and using LAS AF (Leica Application Suite Advanced Fluorescence) software. Animal experiments were performed in accordance with Swiss law and have been approved by the veterinary authorities of Zurich.

Antibodies

The following antibodies were used: anti-TIP5 (CS-090-100-Diagenode); anti-UBF (sc-13125), anti-GST (sc-459) and anti-PARP1 (sc-53643) from Santa Cruz; anti-H3K9me2 (17-648), anti-H3K9me3 (17-625), and anti-H3K27me3 (17-622) and anti-SSEA-1 from Millipore; anti-H3 (ab1791) from Abcam; anti-RGS.HIS (34610) from Qiagen. Anti-TTF1 antibody was produced with Genosphere.

List of primers

mouse rDNA CpG methylation primers		
Name	**For/Rev**	**Sequence**
rDNA promoter -165/-145	For	GACCAGTTGTTCCTTTGAGG
rDNA promoter -21/-1	Rev	ACCTATCTCCAGGTCCAATAG
rDNA coding +1/+20	For	ACTGACACGCTGTCCTTTCC
rDNA coding +111/+130	Rev	GACAGCTTCAGGCACCGCGA

mouse cDNA primers		
Name	**For/Rev**	**Sequence**
Tip5	For	AAGATGTGTGGCTACAATGG
Tip5	Rev	TCTGCACCCATCAGCTCCG
Nanog	For	AAGCAGAAGATGCGGACTGT
Nanog	Rev	ATCTGCTGGAGGCTGAGGTA
Pax6	For	GCACATGCAAACACACATGA
Pax6	Rev	ACTTGGACGGGAACTGACAC
Nestin	For	AGGCTGAGAACTCTCGCTTGC
Nestin	Rev	GGTGCTGGTCCTCTGGTATCC
Blbp	For	AGGTGGCAAAGTGGTGATCC
Blbp	Rev	TCCAACCGAACCACAGACTTAC
Minor satellites	For	CATGGAAAATGATAAAAACC
Minor satellites	Rev	CATCTAATATGTTCTACAGTGTGG
Major satellites	For	GACGACTTGAAAAATGACGAAATC
Major satellites	Rev	CATATTCCAGGTCCTTCAGTGTGC
rDNA spacer -1994/1975	For	GCAGACCGAGTTGCTGTAC
rDNA spacer -1922/1905	Rev	GGGTAGGACTTAAGCCTT
rDNA enhancer -554/-535	For	GAAGCCCTCTTGTCCCCGTC
rDNA enhancer -466/-447	Rev	GATCCAAAGCTCCAGCTGAC
rDNA promoter -165/-145	For	GACCAGTTGTTCCTTTGAGG
rDNA promoter -21/-1	Rev	ACCTATCTCCAGGTCCAATAG
45S pre-rRNA +550/570	For	CTCTTGTTCTGTGTCTGCC
45S pre-rRNA +745/765	Rev	GCCCGCTGGCAGAACGAGAAG
Line L1 ORF2	For	TTTGGGACACAATGAAAGCA
Line L1 ORF2	Rev	CTGCCGTCTACTCCTCTTGG
IAPgag	For	AGCAGGTGAAGCCACTG
IAPgag	Rev	CTTGCCACACTTAGAGC
Btg3	For	AAGGTCAGGCCTACAGATGC
Btg3	Rev	GGTCACCTTATCCAGAGCCC
Rdh10	For	GAAATCCTGCCCCCGTGTAA

Rdh10	Rev	TAGTGGTCCAGAAGTGTGCG
Oct-4	For	GGCGTTCGCTTTGGAAAGGTGTTC
Oct-4	Rev	CTCGAACCACATCCTTCTCT
Rex1	For	AGAAAGCAGGATCGCCTCAC
Rex1	Rev	AGGGAACTCGCTTCCAGAAC
Rps12	For	GAAGCTGCCAAAGCCTTAGA
Rps12	Rev	AACTGCAACCAACCACCTTC
Gapdh	For	TGCACCACCAACTGCTTAGC
Gapdh	Rev	GGCATGGACTGTGGTCATGAG

ChIP primers		
Name	**For/Rev**	**Sequence**
rDNA promoter -165/-145	For	GACCAGTTGTTCCTTTGAGG
rDNA promoter -21/-1	Rev	ACCTATCTCCAGGTCCAATAG
rDNA coding +2251/70	For	GCATCGGTGTGTCGGCATCG
rDNA coding +2346/65	Rev	CTGAGCAGTCCCACCACACC
rDNA coding +8124/145	For	GCGACCTCAGATCAGACGTGG
rDNA coding +8203/224	Rev	CTGTTCACTCGCCGTTACTGAG
Minor satellites	For	CATGGAAAATGATAAAAACC
Minor satellites	Rev	CATCTAATATGTTCTACAGTGTGG
Major satellites	For	GACGACTTGAAAAATGACGAAATC
Major satellites	Rev	CATATTCCAGGTCCTTCAGTGTGC
Evx1 TSS	For	TACACAGCATCTGGGGAGTG
Evx1 TSS	Rev	GTGTGCTGGGTTAAGGGAGA
Zfpm2 TSS	For	GGATGAAGTTCTCAGAGCTGGT
Zfpm2 TSS	Rev	GCGCGAACTTTTACACCTACTT
Dlx1 TSS	For	ATGTCTCCTTCTCCCATGTCC
Dlx1 TSS	Rev	ACTGCACGGAACTGATGTAGG
Gapdh promoter	For	GGTTGCTGTGTCACTACCGAAGAA
Gapdh promoter	Rev	AAATGGAGAAGTGTGGGTCTCCCT
Line L1 ORF2	For	TTTGGGACACAATGAAAGCA
Line L1 ORF2	Rev	CTGCCGTCTACTCCTCTTGG
IAPgag	For	AGCAGGTGAAGCCACTG
IAPgag	Rev	CTTGCCACACTTAGAGC

Supplemental References

Cammas, L., Romand, R., Fraulob, V., Mura, C., and Dolle, P. (2007). Expression of the murine retinol dehydrogenase 10 (Rdh10) gene correlates with many sites of retinoid signalling during embryogenesis and organ differentiation. Developmental dynamics : an official publication of the American Association of Anatomists *236*, 2899-2908.
Gundersen, H.J.G., Bendtsen, T.F., Korbo, L., Marcussen, N., Møller, A., Nielsen, K., Nyengaard, J.R., Pakkenberg, B., Sørensen, F.B., Vesterby, A., *et al.* (1988). Some new, simple and efficient stereological methods and their use in pathological research and diagnosis. Apmis *96*, 379-394.
Li, B., and Dewey, C.N. (2011). RSEM: accurate transcript quantification from RNA-Seq data with or without a reference genome. BMC Bioinformatics *12*, 323.
Martens, J.H., O'Sullivan, R.J., Braunschweig, U., Opravil, S., Radolf, M., Steinlein, P., and Jenuwein, T. (2005). The profile of repeat-associated histone lysine methylation states in the mouse epigenome. EMBO J *24*, 800-812.
Robinson, M.D., McCarthy, D.J., and Smyth, G.K. (2010). edgeR: a Bioconductor package for differential expression analysis of digital gene expression data. Bioinformatics *26*, 139-140.
Santoro, R. (2014). Analysis of chromatin composition of repetitive sequences: the ChIP-Chop assay. Methods Mol Biol *1094*, 319-328.
Santoro, R., Li, J., and Grummt, I. (2002). The nucleolar remodeling complex NoRC mediates heterochromatin formation and silencing of ribosomal gene transcription. Nat Genet *32*, 393-396.
Takahashi, K., Tanabe, K., Ohnuki, M., Narita, M., Ichisaka, T., Tomoda, K., and Yamanaka, S. (2007). Induction of pluripotent stem cells from adult human fibroblasts by defined factors. Cell *131*, 861-872.
Weber, F.A., Bartolomei, G., Hottiger, M.O., and Cinelli, P. (2013). Artd1/Parp1 regulates reprogramming by transcriptional regulation of Fgf4 via Sox2 ADP-ribosylation. Stem Cells *31*, 2364-2373.
West, M.J. (2012). Estimating volume in biological structures. Cold Spring Harb Protoc *2012*, 1129-1139.
Yoshida, Y., Matsuda, S., Ikematsu, N., Kawamura-Tsuzuku, J., Inazawa, J., Umemori, H., and Yamamoto, T. (1998). ANA, a novel member of Tob/BTG1 family, is expressed in the ventricular zone of the developing central nervous system. Oncogene *16*, 2687-2693.

Pramel7 mediates naïve pluripotency through proteasomal-epigenetic combined pathways

Urs Graf[1,2,3], Elisa A. Casanova[1], Eva Vollenweider[3,4], Sarah Wyck[3,4], Fabienne A. Weber[2,3], Sameera S. Patel[2,3], Jiwen Li[5], Jafar Sharif[6], Guido A. Wanner[1], Haruhiko Koseki[6], Jiemin Wong[5], Raffaella Santoro[4,7] and Paolo Cinelli[1,2,7]*

[1]Division of Trauma Surgery, Center for Clinical Research, University Hospital Zurich, University of Zurich, Sternwartstrasse 14, CH-8091 Zurich

[2]Institute of Laboratory Animal Science, University of Zurich, Winterthurerstrasse 190, CH-8057 Zurich

[3]Life Science Zurich Graduate School, University of Zurich, Winterthurerstrasse 190, CH-8057 Zurich

[4]Institute of Veterinary Biochemistry and Molecular Biology, University of Zurich, Winterthurerstrasse 190, CH-8057 Zurich

[5]Shanghai Key Laboratory of Regulatory Biology, Institute of Biomedical Sciences and School of Life Sciences, East China Normal University, Shanghai 200241, China

[6]Developmental Genetics Laboratory, RIKEN Center for Integrative Medical Sciences, 1-7-22 Suehiuro-cho, Tsurumi-ku, Yokohama City, Kanagawa 230-0045, Japan

[7]Center for Applied Biotechnology and Molecular Medicine, University of Zurich, Winterthurerstrasse 190, CH-8057 Zurich

*Corresponding author: Dr. Paolo Cinelli
Division of Trauma Surgery
Center for Clinical Research
University Hospital Zurich
Sternwartstrasse 14
CH-8091 Zurich
Tel.: +41 44 255 3678
FAX: +41 44 255 4741
Email: paolo.cinelli@usz.ch

Abstract

Ground state naïve pluripotency is established in the inner cell mass (ICM) of the mature blastocyst and is present only transiently. Embryonic stem cells (ESCs) can be derived at this stage and represent the immortalization of the pluripotent state by acquiring the capacity for infinite self-renewal. The precise molecular changes accompanying the arrest of the normal developmental program during ICM/ESC transition remain to be fully elucidated. Compared to ESCs, naïve pluripotency of ICM has been associated with global DNA hypomethylation and a generally low repressive epigenetic state that might serve for a greater flexibility to undergo rapid and transient phenotypic and developmental changes (Tang et al., 2010). Here we show that Pramel7 (Preferentially Expressed Antigen in Melanoma-like 7), a protein exclusively expressed in ICM but present only at low levels in ESCs, functions as a substrate recognition component of the proteasome system by targeting degradation of Uhrf1 (Ubiquitin-like, containing PHD and RING finger domains, 1), a key factor for the maintenance of DNA methylation. Enhancing the expression of Pramel7 in ESCs reduces Uhrf1 levels and causes remodeling into an active epigenetic state, which resembles the one of ICM cells, including global DNA hypomethylation. Expression of Pramel7 locks ESCs in pluripotency and destabilizes terminal differentiation by maintaining elevated expression of pluripotent genes through inhibition of *de novo* DNA methylation. Together these findings reveal an as-yet-unappreciated dynamic nature of DNA methylation through the control of proteasome pathway. Moreover, they offer important insights for the establishment of the unique epigenotype of naïve pluripotency that might help in establishing more physiological ESC culture conditions to reproduce *in vitro* the *in vivo* ground state pluripotency.

Introduction

Embryonic stem cells (ESCs) are derived from the inner cell mass (ICM) of mouse blastocysts and can be expanded indefinitely *in vitro* (Zwaka and Thomson, 2005). When injected into host blastocyst pluripotent E3.5-E4.5 epiblast cells and ESCs can both contribute to the formation of all three germ layers and to the germ line (Niwa, 2007). However, only ESCs cultured *in vitro* have the capacity for unlimited self-renewal while pluripotent cells of the early mammalian embryo only briefly proliferate before acquiring a more restricted developmental potential (Niwa, 2007; Zwaka and Thomson, 2005). Consequently, during the conversion of ICM cells to ESCs, there is an evident arrest of a normal developmental program, which *in vitro* is subverted in favor of a potential for unrestricted self-renewal while retaining pluripotency (Tang et al., 2010). The precise molecular changes accompanying this transition remain to be clarified. The aspiration to exploit *ex vivo* pluripotent ESCs for biomedical benefit presupposes the elucidation of their precise nature and relationship to pluripotent cells in the embryo (Nichols and Smith, 2009). Evidences suggest that epigenetic mechanisms may have an important role during ICM/ESC transition. ICM cells have a lower content of DNA methylation than ESCs cultivated in fetal calf serum (FCS) (Smith et al., 2012)(Habibi et al., 2013) These results are consistent with recent single-cell transcriptomic analyses showing that most of the epigenetic regulators increasing their expression in ESC versus ICM are linked to a repressive epigenetic status, including components of the DNA methylation machinery (Tang et al., 2010). Conversely, a large proportion of the epigenetic modifiers known to confer an active epigenetic state show higher expression in ICM. These data indicate that ICM cells may require a greater epigenetic flexibility to undergo rapid and transient phenotypic and developmental changes in the course of early postimplantation development. By contrast, the more repressive epigenetic status of ESCs may be important for maintenance and propagation of their undifferentiated pluripotent state while retaining the capacity for infinite self-renewal (Tang et al., 2010). However, hampered by the limited number of cells available for analysis, it remains to be clarified how epigenetic features of the ICM are established.

We and others have recently found that Pramel7, a member of the Preferentially Expressed Antigen in Melanoma (PRAME) family, is expressed at high levels at morula stage and in ICM, at lower levels in ESCs, but is completely absent in post-implantation embryos and in somatic tissues (Bortvin et al., 2003; Casanova et al., 2011; Cinelli et al., 2008). Constitutive overexpression of Pramel7 induces embryonic death at E6.5 upon generation of chimera (Casanova et al., 2011). In ESCs, ablation of Pramel7 induces differentiation, whereas its overexpression impairs teratoma formation and is sufficient to suppress differentiation in the absence of exogenous LIF (Casanova et al., 2011). This process is reversible, as upon Pramel7 transgene excision cells revert to a LIF-dependent state and regain their capacity to form chimeric mice. The considerably higher expression of Pramel7 in ICM than in ESCs and its requirement to sustain pluripotency suggested an important role in naïve pluripotent cells.

Results

Expression of Pramel7 induces remodeling of ESC chromatin into a more open and transcriptionally permissive state

To determine whether Pramel7 is implicated in pluripotency through epigenetic and chromatin related processes, we analyzed ESCs expressing high Pramel7 levels. We made use of a previously established E14-ESC line that expresses Pramel7 under the control of CAG promoter and contains a *Pramel7*-IRES-*Puro* cassette flanked by loxP sites followed by *EGFP* sequences (P7-ESCs) (**Fig. 1a**) (Casanova et al., 2011). To assess whether elevated expression of Pramel7 affects the epigenetic state of ESCs, we performed immunocytochemistry using 5-methylcytosine antibodies and compared DNA methylation content between control ESCs and P7-ESCs. As shown in **Figure 1b**, intense methylcytosine staining at DAPI-dense pericentric heterochromatin regions found in control ESCs was significantly reduced in P7-ESCs. We then examined the level of global DNA methylation by analyzing the resistance of the DNA to the methylation-sensitive restriction enzyme HpaII and found that global CpG methylation was substantially reduced in P7-ESCs (**Fig. 1c**). We obtained similar results when comparing the resistance of DNA to digestion with McrBC, an endonuclease that cleaves DNA containing only methylcytosine on one or both strands (**Fig.**

1d). To determine whether DNA methylation content in ESCs was dependent on Pramel7 expression levels, we deleted Pramel7 transgene with Cre-recombinase (Cre) with consequent expression of EGFP ($P7^-/EGFP^+$) (**Fig. 1a, e**). Upon P7 transgene deletion, DNA methylation levels reverted to levels found in control cells, indicating that DNA methylation content depends on Pramel7 expression levels (**Fig. 1e**). Since DNA methylation and histone modifications act together to influence chromatin structure, we compared active and repressive histone mark content in control ESCs and P7-ESCs (**Fig. 1f**). The levels of H4ac, H3K9ac, H3K27ac and H3K4me3, epigenetic modifications characteristic of open and transcriptional active chromatin states, were higher in P7-ESCs than in control cells whereas the repressive mark H3K27me3 was more abundant in control cells. Thus, elevated expression of Pramel7 induces remodeling of ESC chromatin into a more open and transcriptionally permissive state resembling the epigenetic landscape of the ICM (Smith et al., 2012; Tang et al., 2010)(Habibi et al., 2013)

Pramel7 interacts with UHRF1 and the Cullin2 RING E3 ubiquitin ligase complex

To identify factors implicated in Pramel7-mediated remodeling of ESC chromatin into a more active epigenetic state, we performed a yeast two-hybrid screen using a full-length Pramel7-LexA fusion protein as a bait to screen an E14 ESCs cDNA library (**Fig. 2a**). Three out of five isolated clones displayed a strong LacZ signal, all expressing Uhrf1 (Ubiquitin-like, with PHD and RING finger domains 1). Uhrf1 specifically recognizes and binds to hemimethylated DNA at replication forks and is crucial for the transmission of DNA methylation marks during cell division (Bostick et al., 2007; Liu et al., 2013; Sharif et al., 2007). Anti-FLAG co-immunoprecipitation (co-IP) analysis in ESCs expressing FLAG-Pramel7 (FP7-ESCs) confirmed the interaction of Pramel7 with Uhrf1 (**Fig. 2b**). Pramel7-Uhrf1 association was also detected in HEK293T cells, which do not express Pramel7, after anti-FLAG co-IP of cells transfected with plasmids expressing FLAG-Pramel7 (FP7) (**Fig. 2c**). Consistent with these results, mass-spectrometry analysis of Pramel7 co-immunoprecipitated proteins in HEK293T cells again identified Uhrf1 as Pramel7-interacting protein (**Fig. 2d**). In addition, we also detected various types of histones, such as the canonical histones H2A and H4 and the histone variant H3.3, suggesting a role of Pramel7 that is linked to chromatin. The association

with histones was also determined for Uhrf1 in HEK293T cells with or without ectopic expression of Pramel7, indicating that Pramel7 does not interfere with the interaction of Uhrf1 with chromatin (Extended Data **Fig 1**). Remarkably, we also identified ElonginC (TCEB1) and polyubiquitin as Pramel7-interacting proteins, both components of the Cullin2 RING E3 ubiquitin ligase (CRL) complex that is involved in polyubiquitination and subsequent proteasomal degradation of target substrates (Hotton and Callis, 2008) (**Fig. 2d**). Interestingly, we found ubiquitin associated with Uhrf1 whereas the interaction with Elongin C was detected only in the presence of Pramel7 (**Supplemental Fig 1**). Western blot and mass-spectrometry analyses of Pramel7-interacting proteins in Uhrf1$^{-/-}$ ESCs revealed Pramel7 association with several CRL components such as ElonginB, ElonginC and Cullin2, indicating that the association of Pramel7 with CRL complex does not depend on Uhrf1 (**Fig. 2e, f**). Together, these results indicate that Pramel7 associates with Uhrf1 and components of CRL complex.

Interaction with Pramel7 mediates the proteasomal degradation of UHRF1

The above findings prompted to investigate whether Pramel7 targets Uhrf1 for proteasomal degradation. We compared Uhrf1 protein levels in control E14 and FP7-ESCs by immunofluorescence analysis and found a significant reduction of Uhrf1 signal corresponding to DAPI-dense pericentric heterochromatin regions in FP7-ESCs, which in contrast could be easily detected in control ESCs (**Fig. 3a**). Similarly, Western blotting indicated that Uhrf1 levels were drastically reduced in FP7-ESCs, a result also obtained in HEK293T cells after 48h of ectopic expression of Pramel7 (**Fig. 3b**). The reduction in Uhrf1 protein levels was not mediated through the inhibition of *Uhrf1* gene expression, as *Uhrf1* mRNA levels in FP7 ESCs were comparable to control ESCs (**Fig. 3c**). This is also consistent with a previous analysis showing no remarkable alterations of *Uhrf1* mRNA levels in ICM and ESC cells (Tang et al., 2010).

To get insight into the Pramel7-mediated degradation of Uhrf1, we excised the FLAG-Pramel7 cassette in FP7-ESCs by Cre-recombinase simultaneously bringing *EGFP* under the control of the CAG promoter. Clones were selected for EGFP positive (FP7$^-$/EGFP$^+$) and negative (FP7$^+$/EGFP$^-$) signal. Immunocytochemistry with anti-Uhrf1 antibodies indicated that Uhrf1 expression was significantly reduced in FP7$^+$/EGFP$^-$ when compared to FP7$^-$/EGFP$^+$

(**Fig. 3d**). The dependency of Uhrf1 moieties on Pramel7 expression levels was also evident by Western blotting of cell lysates from five $FP7^-/EGFP^+$ and one $FP7^+/EGFP^-$ clones (**Fig. 3e**). This observation was further supported by a partial decrease in Uhrf1 levels in cells derived from a clone ($FP7^-/EGFP^+$, 3) that displayed a mixed population of recombined ($FP7^-/EGFP^+$) and non-recombined ($FP7^+/EGFP^-$) cells. To independently verify these findings, we monitored Uhrf1 levels for 5 days in HEK293T cells after transfection of Flag-Pramel7-expression plasmid (from 8h to 120h post-transfection) (**Fig. 3f**). Pramel7 expression was first detected 24h post-transfection, a time point that coincides with the initial reduction in Uhrf1 levels. After 72h, when Pramel7 expression started to decline, Uhrf1 levels again increased and, concomitant with the disappearance of Pramel7 (96h and 120h), Uhrf1 levels were restored to similar protein amounts found in control cells.

The 26S-proteasome mediates the final step in the degradation of polyubiquitin-tagged proteins. To assess whether the degradation of Uhrf1 mediated by Pramel7 occurs via the 26S-proteasome, we monitored Uhrf1 levels in HEK293T cells expressing FLAG-Pramel7 and 18h post-transfection treated with the proteasome inhibitor MG132 (**Fig. 3g**). Compared to untreated cells, addition of MG132 significantly impaired Pramel7-dependent degradation of Uhrf1, suggesting that the 26S-proteasome is implicated in this process. Taken together, these results indicate that Uhrf1 stability depends on Pramel7 expression levels and suggest that Pramel7 targets Uhrf1 for degradation via the 26S-proteasome pathway.

The Pramel7-LRR and Uhrf1 SRA and RING domains are necessary for the Pramel7-UHRF1 interaction and UHRF1 degradation

We then analyzed whether the interaction of Pramel7 with Uhrf1 is required for Uhrf1 degradation. Pramel7 contains 3 leucine-rich repeat (LRR) motifs, which in general are implicated in the formation of protein-protein interactions (Kobe and Kajava, 2001). Analysis of Uhrf1 degradation in HEK293T cells transfected with Pramel7-LRR deletion mutants indicated that deletion of the first LRR (ΔLRR1) was sufficient to impair Pramel7-mediated degradation of Uhrf1 (**Fig. 4a, b**). Similar results were obtained with further deletions of the second (ΔLRR1/2) and third LRR (ΔLRR1/2/3). To determine whether degradation of Uhrf1 depends on the interaction with Pramel7, we performed anti-FLAG co-IP in HEK293T cells

overexpressing FLAG-Pramel7 and Uhrf1 (F**ig. 4c**). Overexpression of Uhrf1 was intended to increase Uhrf1 signal and obtain a better detection of Uhrf1-Pramel7 interaction. Deletion of the first LRR motif was already sufficient to impair Uhrf1 interaction with Pramel7. Thus, Pramel7-mediated degradation of Uhrf1 requires the association of Uhrf1 with Pramel7 that is mediated by the first LRR motif. To further support these results, we analysed the degradation and Pramel7 association of Uhrf1 mutants lacking the C-terminal region, including PHD, SRA and RING (ΔPSR) domains or only the SRA and RING motifs (ΔSR) (**Fig. 4d-f**). These regions were previously implicated in hemimethylated DNA recognition, ubiquitination of histone H3K23 and association with the histone methyltransferase G9a (Achour et al., 2009; Arita et al., 2008; Nishiyama et al., 2013). Deletion of SRA and RING regions was sufficient to impair degradation of Uhrf1 and both ΔPSR and ΔSR Uhrf1 mutants showed a drastic reduction in the interaction with Pramel7 (**Fig. 4e, f**). Uhrf1 associates with histones and, consistent with previous reports (Gelato et al., 2014), this interaction is abolished upon deletion of PSR domains whereas the ΔSR Uhrf1 mutant still retained the ability to associate with histones (**Fig. 4g**). Similar to Uhrf1, Pramel7 in ESCs also associated with histones (**Figs. 2d and 4h**) and exhibited a preferential association with chromatin, which as expected was also enriched in Uhrf1 (**Fig. 4i**). We conclude that Pramel7-LRR and Uhrf1 SRA and RING domains are implicated in Pramel7-Uhrf1 interaction, which is required to target Uhrf1 to the 26S proteasome. Furthermore, this association is most likely occurring on chromatin sites.

Pramel7 maintains the pluripotency state by repressing DNA methylation through regulation of Uhrf1 stability

Upon differentiation, ESC chromatin remodels into a condensed and repressed structure, an event that signals the transition from a pluripotent to a restrictive lineage committed state (Savić et al., 2014). DNA methylation was shown to be crucial for permanent restriction of developmental fate during differentiation (Schmidt et al., 2012). To determine whether the expression of Pramel7 upon ESC differentiation impairs terminal differentiation, we tested the ability of FP7 ESCs to differentiate into a stable state. We differentiated FP7-ESCs upon withdrawal of LIF and feeders for 14 days and observed that control E14 ESCs developed

into a homogeneous layer of cells whereas FP7-ESCs formed less differentiated and more compact colonies (**Fig. 5a**). Moreover, differentiated FP7 cells still expressed the pluripotency markers Oct4 and stage-specific embryonic antigen-1 (SSEA1). As expected, Uhrf1 levels were lower in differentiated cells than in ESCs, reflecting a lower proliferation rate of cells in the differentiated state (**Fig. 5b**) (Bonapace et al., 2002). Pramel7-mediated degradation of Uhrf1 was still active during differentiation as evident by lower Uhrf1 levels and DNA methylation content in FP7 differentiated cells than in differentiated E14 control cells (**Fig. 5b, c**). Remarkably, pluripotent genes *Oct4*, *Nanog* and *Rex1* in differentiated FP7 cells were expressed at higher levels, suggesting that transcriptional silencing was not as efficient as in differentiated control ESCs (**Fig. 5d**). Consistent with the hypomethylated state of FP7 genome, methylation of *Oct4* promoter was lower in differentiated FP7 cells than in control-differentiated cells (**Fig. 5e**). To determine whether expression of Pramel7 affects the stable terminally differentiated state, we tested the ability of 14 days-differentiated FP7-ESCs to reconvert to a pluripotent state (**Fig. 5f**). Differentiated cells seeded at the density of 10-cells/well in 96-well plates were cultured for 7 days upon conditions supporting pluripotency (+LIF) and screened for the expression of the pluripotency marker alkaline phosphatase (AP). AP positive (AP^+) colonies were present in only 2.7% of E14-ESC wells (5/182) whereas 80.8% (147/182) of wells with FP7-ESCs contained AP^+ colonies. FP7-ESC reconverted clones maintained FLAG-Pramel7 expression and low Uhrf1 levels (**Supplemental Fig. 2a**), and expressed the pluripotency markers Oct4, Nanog, Rex1 and SSEA1 (**Supplemental Fig. 2b,c**). We conclude that Pramel7 maintains the pluripotency state by repressing DNA methylation through regulation of Uhrf1 stability.

Discussion

During *in vitro* ESC derivation, ICM cells of the blastocyst replace their normal developmental program by acquiring the capacity for infinite self-renewal and pluripotency. The low DNA methylation content in ICM has been proposed to be a characteristic feature of cells with the inherent ability to generate pluripotency and to undergo rapid and transient phenotypic and developmental changes in the course of early postimplantation development (Leitch et al., 2013; Tang et al., 2010). Downregulation of Pramel7 expression does not only mark the

transition of ICM cells to more restricted developmental lineages but also the conversion to *in vitro* pluripotent ESCs (Bortvin et al., 2003; Casanova et al., 2011; Cinelli et al., 2008) which, as recently suggested, might represent a more differentiated status (Marks and Stunnenberg, 2014; McEwen et al., 2013; Nichols and Smith, 2009). Here we show that elevated expression of Pramel7 in ESCs caused remodeling into a euchromatic epigenetic state that resembles the one of the ICM (Habibi et al., 2013; Smith et al., 2012; Tang et al., 2010). Downregulation of both *de novo* DNA methyltransferases Dnmt3a and Dnmt3b has been considered a way to protect the ICM genome from DNA methylation (Leitch et al., 2013). The post-transcriptional control of Uhrf1 levels mediated by Pramel7 might represent an additional regulatory pathway to establish a low repressive epigenetic state, creating greater epigenetic flexibility required by ICM cells to undergo rapid and transient developmental changes. ESCs cultured in the presence of the two inhibitors (2i), PD0325901 and CHIR99021, that target mitogen-activated protein kinase (MEK) and glycogen synthase kinase-3 (GSK3), have been recently proposed to represent the ground state of pluripotency (Ying et al., 2008). Remarkably, compared to ESCs cultured in FCS, 2i-ESCs display CpG hypomethylation that parallels the one observed in the preimplantation epiblast (Habibi et al., 2013; Leitch et al., 2013). Thus, an inducible system that modulates expression of *Pramel7 in vitro* cultured pluripotent ESCs might represent an attractive more physiological alternative to reproduce *in vitro* the *in vivo* ground state pluripotency.

Our results also suggest that controlling the maintenance of DNA methylation through modulation of Uhrf1 stability has the potential to regulate cell fate and might be indicative of an as-yet-unappreciated dynamic nature of DNA methylation. Indeed, although Uhrf1 is implicated in the maintenance of DNA methylation patterns during replication, *de novo* methylation of the pluripotent gene *Oct4* upon differentiation depends on Pramel7 and Uhrf1 levels. Moreover, retrieval of Uhrf1 levels upon Pramel7 transgene deletion was sufficient to revert genome-wide DNA methylation to levels found in control cells. Whether residual me-C moieties still maintained by DNMT1 or other epigenetic modifications represent a memory mark guiding Uhrf1 to restore full methylation patterns will be an issue of our future studies.

The post-transcriptional control of Uhrf1 levels mediated by Pramel7 joins together two pathways, proteasome and epigenetics, which independently have been implicated in the

maintenance of pluripotency. Previous studies have suggested a role of the proteasome in pluripotent ESCs. Inhibition of proteolytic activity or the depletion of distinct proteasomal subunits prevents aberrant transcriptional initiation on specific regulatory regions in ESCs or affects transcription of pluripotency associated genes (Atkinson et al., 2012; Schröter and Adjaye, 2014; Szutorisz et al., 2006). Regulation of Uhrf1 turnover by proteasome degradation has recently been described during cell cycle and upon DNA damage, suggesting that maintaining an appropriate level of Uhrf1 is important for processes such as cell proliferation and DNA damage response (Chen et al., 2013; Felle et al., 2011; Ma et al., 2012; Mistry et al., 2010). Our results indicate that controlling Uhrf1 levels through Pramel7-mediated targeting for proteasome degradation is an important molecular pathway for the regulation of epigenetic states linked to naïve pluripotency. Since PRAME and PRAME family members are expressed in a wide range of human tumours and are often correlating with poor clinical outcome (Ikeda et al., 1997; Oberthuer et al., 2004; van Baren et al., 1998; van t Veer et al., 2002), our data also offer important insights into how developmental programs might be undermined, leading to the formation of diseased tissues, including cancers.

Material and Methods

Cell lines and culture media

ESCs were routinely cultivated on mitotically inactivated mouse embryonic fibroblasts (MEFs) in complete medium (GMEM (Sigma), 10% FCS, 10mM Sodium Pyruvate, 1x NEAA, 1x Pen/Strep/Glu, 0.1mM 2-Mercaptoethanol) supplemented with 1000U/ml Leukemia Inhibitory Factor (LIF, Millipore) (CM+LIF). HEK293T cells and MEFs were grown in DMEM (Life Technologies) supplemented with 10% FCS, 1x Pen/Strep/Glu and 10mM Sodium Pyruvate. Establishment of Pramel7-ESCs (P7-ESC) was described in(Casanova et al., 2011).

Immunofluorescent detection and alkaline phosphatase staining

Cells were fixed in 4% formalin. For confocal analysis formalin was supplemented with 1:555 100% TritonX-100 (Sigma). Primary antibodies were diluted in PBST (PBS + 0.1% Tween-20) and 4% horse serum and cells were incubated either over night at 4°C or at room temperature for 2-4h. Nuclei were stained with DAPI (Roche) or Hoechst. Wide field images were taken on a Zeiss Axiovert 40 CFL and processed using AxioVision 4.6 software (Zeiss) and Adobe Photoshop CS6. Confocal pictures were taken in the Center for Microscopy and Image Analysis (ZMB) of the University of Zurich and processed with IMARIS 7.6 software. For alkaline phosphatase staining cells were fixed in 4% formalin washed 2x with AP-buffer (0.1M Tris-HCl, 0.1M NaCl, 20mM MgCl2, pH 9.5) incubated with AP staining solution (AP Buffer + 0.5µl/ml NBT (Roche) and 3.5µl/ml BCIP (Roche)). Staining reaction was stopped with 1x Tris-EDTA (20mM Tris-HCl, 5mM EDTA).

Isolation of genomic DNA and DNA methylation analysis

Cells were incubated with Proteinase K over night at 50°C followed by treatment with RNAseA (Fermentas) for 30' at 37°C. genomic DNA (gDNA) was purified with 25:24:1 phenol:chloroform:isoamyl alcohol and subsequently precipitated by addition of NH4Ac/EtOH. 4 μg of gDNA were digested over night with 20U HpaII or McrBC in 20 µl total reaction volume containing 0.5ng of pBluescript plasmid DNA for testing the efficiency of the HpaII digest. Digested gDNA was loaded on a 0.8% agarose gel and gDNA fragments were separated by electrophoresis. Quantification of DNA signal was measured using Fiji image

analysis software. To verify HpaII digestion efficiency, pBluescript KS(+) plasmid was analyzed by qPCR using one forward primer that is complementary to sequences upstream of the CCGG site of β-lactamase gene (at 2580) and two different reverse primers that map upstream and downstream the HpaII sites. All analyzed samples displayed 96-98% digestion efficiency. Bisulfite conversion was performed using the EpiTect Bisulfite Kit (Qiagen) according to the manufacturer's protocol. *Oct4* promoter region was amplified from bisulfite treated DNA, cloned in pCR®II-TOPO® (Life technologies) and sequenced. Amplification were performed with nested touchdown PCR program with a 0.5°C decrease in the annealing temperature after each cycle. Primers were described in(Takahashi and Yamanaka, 2006) and are listed in **Supplementary Table 1**.

Yeast two-hybrid assay

Pramel7 was used as bait and cDNA library of E14 ESCs as pool of prey proteins. The bait was cloned into a lexA-expression vector and tested for self-activation and successful expression. cDNA library was transformed and co-expressed with the bait plasmid. Positive clones were selected and library plasmids were isolated. Finally positive clones were sequenced and BLAST analysis was performed. The exact procedure can be obtained here: http://www.dualsystems.com/fileadmin/user_upload/z_download/manuals/P01004_DUALhybrid.pdf.

Co-immunoprecipitation and proteomic analysis

Cell pellets were resuspended in IP Buffer (50mM Tris-HCl pH 7.5, 150mM KCl, 5mM MgCl2, 0.2mM EDTA, 20% (v/v) Glycerol, 0.5mM DTT, 0.1% (v/v) NP-40, Proteinase inhibitor cocktail (Roche)), sonicated and DNase treated. .1mg of nuclear protein was subjected to immunoprecipitation overnight at 4 °C using ANTI-FLAG M2 affinity gel, Sigma). Precipitates were washed three times with IP buffer, separated on a 6% SDS-polyacrylamide gel and analyzed by immunoblot. For proteomic analysis, immunoprecipitated proteins were eluted twice using 100 μl M2 FLAG-peptide (Sigma). Eluates were precipitated with trichloro-acetic acid (TCA), washed with cold acetone and shortly dried at 95°C. Proteomic analysis was carried out at the Functional Genomics Centre Zurich (University and ETH Zurich).

RNA extraction, reverse transcription and quantitative real-time PCR

RNA was extracted using the RNeasy Mini Kit (Qiagen). 500ng or 1 μ g of RNA were reverse transcribed using Oligo(dT)12–18 Primer (Life Technologies), 10mM dNTP Mix (Life Technologies), RNAsin Plus RNAse Inhibitor (Promega) and SuperscriptIII Reverse Transcriptase (Life Technologies). Real Time PCR was performed with the Rotor-Gene SYBR Green PCR Kit (FAST) (Qiagen). Primer sequences are listed in **Supplementary Table 2**.

Transfection of HEK293T cells and electroporation of ESCs

Transfection of HEK293T with plasmid DNA was performed either using CaCl2 and BES solution (50mM BES, 280mM NaCl, 1.5mM Na2HPO4, pH 7.0) or Xtremegene HP (Roche) transfection reagent. For stable integration of plasmid pCAG-FLAG-Pramel7-PGK-puro in E14 ESCs, cells were first separated from feeder layer by trypsinisation, incubated with plasmid DNA and electroporated at 500 μ F capacitance and 240V using a Bio Rad Gene Pulser II. Antibiotic selection was started 24-48h after electroporation and continued for 4 subsequent days (puromycin, 1µg/ml). After selection medium was changed to standard conditions (CM+LIF), selected colonies were grown and clonally expanded.

For time course experiment in HEK293T cells, HEK293T cells were transfected with FLAG-Pramel7 expression plasmid. Samples were collected 8, 12, 24, 36, 48, 72, 96 and 120h after transfection and analysed for FLAG-Pramel7 and Uhrf1 protein levels by Western blotting. For time course experiment with MG132, HEK293T cells were transfected with FP7 plasmid DNA using Xtremegene HP transfection reagent (Roche). 18h after transfection, MG132 was added in a final concentration of 20µM. Samples were collected 1h, 2h, 4h, 6h and 8h after MG132 addition and Pramel7 and Uhrf1 levels were analysed by Western blotting.

Differentiation and reconversion of control E14 and FP7-ESCs

E14 and FP7-ESCs were separated from feeder layer and seeded on gelatinized feeder-free culture dishes in complete medium without LIF. To avoid confluence, cells were passaged after 6 and 10 days. After 14 days, cells were seeded on two 96-well plates containing feeder cells and LIF in a dilution of 10cells/well and cultured for further 7 days. 14 days differentiated

cells and cells cultured in the presence of LIF were harvested and analyzed for the expression of Pramel7 and Uhrf1 and of pluripotency factors Oct4 and SSEA1.

Antibodies

For immunofluorescence analysis, the following antibodies were used: anti-5mC (Diagenode C15200081), anti-OCT-3/4 (Santa Cruz sc-9081), anti-SSEA1 (Developmental studies Hybridoma bank, University of Iowa), anti-Uhrf1 (Santa Cruz sc-98817). For western blot analyses the following antibodies were used: anti-H3 (Abcam), anti-H3K9ac (Cell Signaling 9649), anti-H3K27ac (Cell Signaling 4729), anti-H4ac (Millipore 06-866) anti-H3K4me3 (Cell Signaling 9751), anti-H3K27me3 (Cell Signaling 9756), anti-Tubulin (Sigma T8203), anti-FLAG (Sigma F7425) anti-Uhrf1 (Santa Cruz sc-98817), anti-ElonginB (Santa Cruz sc-11447), anti-ElonginC (Santa Cruz sc-1559), anti-Cullin2 (Invitrogen 51-1800).

Acknowledgments

The authors thank Dominik Bär for technical assistance, Wojciech Piwko and Olga Shakhova for discussions and reagents. This work was supported by the Olga Mayenfisch Foundation (to P.C.), the Novartis Foundation for Medical-Biological Research (to P.C.), the Theodor und Ida Herzog-Egli Foundation (to P.C and R.S.), the Stiftung für wissenschaftliche Forschung an der Universität Zürich (to P.C. and R.S.), the Swiss National Science Foundation (310003A-135801 and 31003A-152854 to R.S), the UBS-Promedica Stiftung (to R.S.) and the Forschungskredit of the University of Zurich (to E.V. and U.G.).

References

Achour, M., Fuhrmann, G., Alhosin, M., Rondé, P., Chataigneau, T., Mousli, M., Schini-Kerth, V.B., and Bronner, C. (2009). UHRF1 recruits the histone acetyltransferase Tip60 and controls its expression and activity. In Biochem Biophys Res Commun, pp. 523-528.

Arita, K., Ariyoshi, M., Tochio, H., Nakamura, Y., and Shirakawa, M. (2008). Recognition of hemi-methylated DNA by the SRA protein UHRF1 by a base-flipping mechanism. In Nature, pp. 818-821.

Atkinson, S.P., Collin, J., Irina, N., Anyfantis, G., Kyung, B.K., Lako, M., and Armstrong, L. (2012). A putative role for the immunoproteasome in the maintenance of pluripotency in human embryonic stem cells. In Stem Cells (Wiley Subscription Services, Inc., A Wiley Company), pp. 1373-1384.

Bonapace, I.M., Latella, L., Papait, R., Nicassio, F., Sacco, A., Muto, M., Crescenzi, M., and Di Fiore, P.P. (2002). Np95 is regulated by E1A during mitotic reactivation of terminally differentiated cells and is essential for S phase entry. In J Cell Biol, pp. 909-914.

Bortvin, A., Eggan, K., Skaletsky, H., Akutsu, H., Berry, D., Yanagimachi, R., Page, D., and Jaenisch, R. (2003). Incomplete reactivation of Oct4-related genes in mouse embryos cloned from somatic nuclei. In Development, pp. 1673-1680.

Bostick, M., Kim, J.K., Estève, P.-O., Clark, A., Pradhan, S., and Jacobsen, S.E. (2007). UHRF1 plays a role in maintaining DNA methylation in mammalian cells. In Science, pp. 1760-1764.

Casanova, E.A., Shakhova, O., Patel, S.S., Asner, I.N., Pelczar, P., Weber, F.A., Graf, U., Sommer, L., Bürki, K., and Cinelli, P. (2011). Pramel7 mediates LIF/STAT3-dependent self-renewal in embryonic stem cells. In Stem Cells, pp. 474-485.

Chen, H., Ma, H., Inuzuka, H., Diao, J., Lan, F., Shi, Y.G., Wei, W., and Shi, Y. (2013). DNA damage regulates UHRF1 stability via the SCF(beta-TrCP) E3 ligase. Mol Cell Biol *33*, 1139-1148.

Cinelli, P., Casanova, E.A., Uhlig, S., Lochmatter, P., Matsuda, T., Yokota, T., Rülicke, T., Ledermann, B., and Bürki, K. (2008). Expression profiling in transgenic FVB/N embryonic stem cells overexpressing STAT3. In BMC Dev Biol, pp. 57.

Felle, M., Joppien, S., Nemeth, A., Diermeier, S., Thalhammer, V., Dobner, T., Kremmer, E., Kappler, R., and Langst, G. (2011). The USP7/Dnmt1 complex stimulates the DNA methylation activity of Dnmt1 and regulates the stability of UHRF1. Nucleic Acids Res *39*, 8355-8365.

Gelato, K.A., Tauber, M., Ong, M.S., Winter, S., Hiragami-Hamada, K., Sindlinger, J., Lemak, A., Bultsma, Y., Houliston, S., Schwarzer, D., *et al.* (2014). Accessibility of different histone H3-binding domains of UHRF1 is allosterically regulated by phosphatidylinositol 5-phosphate. In Mol Cell, pp. 905-919.

Habibi, E., Brinkman, A.B., Arand, J., Kroeze, L.I., Kerstens, H.H.D., Matarese, F., Lepikhov, K., Gut, M., Brun-Heath, I., Hubner, N.C., *et al.* (2013). Whole-genome bisulfite sequencing of two distinct interconvertible DNA methylomes of mouse embryonic stem cells. In Cell Stem Cell, pp. 360-369.

Hotton, S.K., and Callis, J. (2008). Regulation of cullin RING ligases. In Annu Rev Plant Biol (Annual Reviews), pp. 467-489.

Ikeda, H., Lethé, B., Lehmann, F., van Baren, N., Baurain, J.F., de Smet, C., Chambost, H., Vitale, M., Moretta, A., Boon, T., *et al.* (1997). Characterization of an antigen that is recognized on a melanoma showing partial HLA loss by CTL expressing an NK inhibitory receptor. In Immunity, pp. 199-208.

Kobe, B., and Kajava, A.V. (2001). The leucine-rich repeat as a protein recognition motif. In Curr Opin Struct Biol, pp. 725-732.

Leitch, H.G., McEwen, K.R., Turp, A., Encheva, V., Carroll, T., Grabole, N., Mansfield, W., Nashun, B., Knezovich, J.G., Smith, A., *et al.* (2013). Naive pluripotency is associated with global DNA hypomethylation. Nat Struct Mol Biol *20*, 311-316.

Liu, X., Gao, Q., Li, P., Zhao, Q., Zhang, J., Li, J., Koseki, H., and Wong, J. (2013). UHRF1 targets DNMT1 for DNA methylation through cooperative binding of hemi-methylated DNA and methylated H3K9. In Nat Commun, pp. 1563.

Ma, H., Chen, H., Guo, X., Wang, Z., Sowa, M.E., Zheng, L., Hu, S., Zeng, P., Guo, R., Diao, J., *et al.* (2012). M phase phosphorylation of the epigenetic regulator UHRF1 regulates its physical association with the deubiquitylase USP7 and stability. Proc Natl Acad Sci U S A *109*, 4828-4833.

Marks, H., and Stunnenberg, H.G. (2014). Transcription regulation and chromatin structure in the pluripotent ground state. Biochim Biophys Acta *1839*, 129-137.

McEwen, K.R., Leitch, H.G., Amouroux, R., and Hajkova, P. (2013). The impact of culture on epigenetic properties of pluripotent stem cells and pre-implantation embryos. Biochem Soc Trans *41*, 711-719.

Mistry, H., Tamblyn, L., Butt, H., Sisgoreo, D., Gracias, A., Larin, M., Gopalakrishnan, K., Hande, M.P., and McPherson, J.P. (2010). UHRF1 is a genome caretaker that facilitates the DNA damage response to gamma-irradiation. Genome Integr *1*, 7.

Nichols, J., and Smith, A. (2009). Naive and primed pluripotent states. Cell Stem Cell *4*, 487-492.

Nishiyama, A., Yamaguchi, L., Sharif, J., Johmura, Y., Kawamura, T., Nakanishi, K., Shimamura, S., Arita, K., Kodama, T., Ishikawa, F., *et al.* (2013). Uhrf1-dependent H3K23 ubiquitylation couples maintenance DNA methylation and replication. In Nature, pp. 249-253.

Niwa, H. (2007). How is pluripotency determined and maintained? Development *134*, 635-646.

Oberthuer, A., Hero, B., Spitz, R., Berthold, F., and Fischer, M. (2004). The tumor-associated antigen PRAME is universally expressed in high-stage neuroblastoma and associated with poor outcome. In Clin Cancer Res, pp. 4307-4313.

Savić, N., Bär, D., Leone, S., Frommel, S.C., Weber, F.A., Vollenweider, E., Ferrari, E., Ziegler, U., Kaech, A., Shakhova, O., *et al.* (2014). lncRNA Maturation to Initiate Heterochromatin Formation in the Nucleolus Is Required for Exit from Pluripotency in ESCs. In Cell Stem Cell, pp. 720-734.

Schmidt, C.S., Bultmann, S., Meilinger, D., Zacher, B., Tresch, A., Maier, K.C., Peter, C., Martin, D.E., Leonhardt, H., and Spada, F. (2012). Global DNA hypomethylation prevents consolidation of differentiation programs and allows reversion to the embryonic stem cell state. PLoS One *7*, e52629.

Schröter, F., and Adjaye, J. (2014). The proteasome complex and the maintenance of pluripotency: sustain the fate by mopping up? In Stem Cell Res Ther, pp. 24.

Sharif, J., Muto, M., Takebayashi, S.-i., Suetake, I., Iwamatsu, A., Endo, T.A., Shinga, J., Mizutani-Koseki, Y., Toyoda, T., Okamura, K., *et al.* (2007). The SRA protein Np95 mediates epigenetic inheritance by recruiting Dnmt1 to methylated DNA. In Nature, pp. 908-912.

Smith, Z.D., Chan, M.M., Mikkelsen, T.S., Gu, H., Gnirke, A., Regev, A., and Meissner, A. (2012). A unique regulatory phase of DNA methylation in the early mammalian embryo. In Nature, pp. 339-344.

Szutorisz, H., Georgiou, A., Tora, L., and Dillon, N. (2006). The proteasome restricts permissive transcription at tissue-specific gene loci in embryonic stem cells. In Cell, pp. 1375-1388.

Takahashi, K., and Yamanaka, S. (2006). Induction of pluripotent stem cells from mouse embryonic and adult fibroblast cultures by defined factors. Cell *126*, 663-676.

Tang, F., Barbacioru, C., Bao, S., Lee, C., Nordman, E., Wang, X., Lao, K., and Surani, M.A. (2010). Tracing the derivation of embryonic stem cells from the inner cell mass by single-cell RNA-Seq analysis. In Cell Stem Cell, pp. 468-478.

van Baren, N., Chambost, H., Ferrant, A., Michaux, L., Ikeda, H., Millard, I., Olive, D., Boon, T., and Coulie, P.G. (1998). PRAME, a gene encoding an antigen recognized on a human melanoma by cytolytic T cells, is expressed in acute leukaemia cells. In Br J Haematol, pp. 1376-1379.

van t Veer, L.J., Dai, H., van de Vijver, M.J., He, Y.D., Hart, A.A.M., Mao, M., Peterse, H.L., van der Kooy, K., Marton, M.J., Witteveen, A.T., *et al.* (2002). Gene expression profiling predicts clinical outcome of breast cancer. In Nature, pp. 530-536.

Ying, Q.L., Wray, J., Nichols, J., Batlle-Morera, L., Doble, B., Woodgett, J., Cohen, P., and Smith, A. (2008). The ground state of embryonic stem cell self-renewal. Nature *453*, 519-523.

Zwaka, T.P., and Thomson, J.A. (2005). A germ cell origin of embryonic stem cells? Development *132*, 227-233.

Figure Legends

Figure 1: Elevated expression of Pramel7 induces remodeling of ESC chromatin into a more open and transcriptionally permissive state. **a**, Schema representing the construct used to establish Pramel7-ESCs. **b**, DNA methylation defects in Pramel7-ESCs (P7-ESCs) in comparison with the wild-type E14 cells as revealed by immunofluorescent staining using anti-5-mC antibody. Scale bar: 10µm. **c**,**d,** CpG methylation levels measured by digestion of genomic DNA from E14 and Pramel7-ESCs with the methylation-sensitive restriction enzymes HpaII and McrBC. Quantification of DNA signal was measured using Fiji image analysis software. M: DNA ladder. **e**, Defects in DNA methylation depends on Pramel7 expression levels. CpG methylation levels in Cre-recombined ($P7^+/EGFP^-$) and non-recombined ($P7^+/EGFP^-$) ESC clones. **e**, Western blot of active and repressive histone marks in whole cell lysates of E14 and P7-ESCs. Quantification was performed using ImageJ software.

Figure 2: Pramel7 associates with Uhrf1 and components of the Cullin2 RING E3 ubiquitin ligase (CRL) complex. **a**, Yeast two-hybrid assay using Pramel7 as a bait and a whole transcriptome cDNA library of E14 ESCs as prey. 3 clones displayed a strong LacZ signal and all expressed Uhrf1. **b**, **c,** FLAG immunoprecipitation from FP7-ESCs and HEK293T cells transfected with FLAG-Pramel7 (FP7) expressing plasmids. Immunoblots show association of Pramel7 with Uhrf1. d, Mass-spectrometry analysis of proteins co-immunoprecipitated with FLAG-Pramel7 in HEK293T cells. **e**, FLAG co-immunoprecipitation of components of the Cullin2 RING E3 ubiquitin ligase (CRL) complex (ElonginB, ElonginC, Cullin2) in $Uhrf^{-/-}$ ESCs expressing FLAG-Pramel7. **f**, Mass-spectrometry analysis of proteins FLAG-immunoprecipitated in $Uhrf^{-/-}$ ESCs expressing FLAG-Pramel7.

Figure 3: Pramel7 expression affects Uhrf1 stability and leads to Uhrf1 degradation via the 26S-proteasome pathway. **a**, Immunofluorescent labeling of Uhrf1 protein in E14 and FP7-ESCs. Scale bar: 10µm. **b**, Western blot for Pramel7 and Uhrf1 in whole cell lysates of E14 and FP7-ESCs and in HEK293T cells 48h after transient transfection with FP7 plasmid. Tubulin is shown as loading control. **c**, *Uhrf1* gene expression in E14 and FP7-ESCs were

measured by qRT-PCR and normalized to Actin mRNA. **d**, Immunofluorescence showing mutually exclusive Uhrf1 and EGFP expression in $FP7^-/EGFP^+$ (Cre-recombined) and $FP7^+/EGFP^-$ (non-recombined) ESC colonies; Scale bar: 200µm. **e**, Uhrf1 and Pramel7 levels measured by Western blotting analysis of cell lysates from five $FP7^-/EGFP^+$ and one $FP7^+/EGFP^-$ ESC clones. **f**, Monitoring Uhrf1 levels in HEK293T cells during 5 days after transient transfection of FP7 plasmid DNA (8h to 120h post-transfection). **g**, Monitoring Pramel7-mediated Uhrf1 degradation after addition of the proteasome inhibitor MG132. WT: HEK293T cells 18h after control transfection with pBluescript plasmid.

Figure 4: Pramel7 LRRs and Uhrf1 SRA and RING domains are implicated in Pramel7-Uhrf1 interaction and Uhrf1 stability. **a**, Schema representing the domain organization of Pramel7 and the analyzed ΔLRR mutants. LRR: Leucine-rich repeat. **b**, Western blot of Uhrf1 in HEK293T cells 48h after transfection of FLAG-Pramel7 (FP7) and FP7-ΔLRR mutants; Tubulin is shown as loading control. **c**, FLAG-immunoprecipitation from HEK293T cells expressing FP7-ΔLRR mutants and mouse Uhrf1. **d**, Schematic representation of FLAG-Uhrf1 and Uhrf1 mutant constructs: ΔSR (deletion of SRA and RING domains) and ΔPSR (deletion of PHD, SRA and RING domains). **e**, Western blot of Uhrf1 WT and mutants in HEK293T cells 48h post-transfection of Uhrf1 and Pramel7 expression plasmids. **f**, FLAG-immunoprecipitation from HEK293T cells transfected with FLAG-Uhrf1 WT and mutants and Pramel7 expression plasmids. **g**,**h** Association of Uhrf1 and Pramel7 with histone H3 shown by FLAG immunoprecipitation from HEK293T expressing FLAG-Uhrf1 WT or FLAG-Uhrf1 mutants (**g**) and FLAG-Pramel7 (**h**). **i**, Uhrf1 and Pramel7 associate with chromatin of ESCs. Chromatin-bound and soluble fractions of equivalent cell number of E14 and FP7-ESCs were analyzed by western blot for Uhrf1 and Pramel7 levels. Tubulin is shown as loading and fractionation control.

Figure 5: Pramel7 maintains the pluripotent state by repressing DNA methylation through regulation of Uhrf1 stability. **a**, Immunofluorescence analysis of pluripotency markers Oct4 and SSEA1 in 14 days differentiated E14 and FP7-ESCs. **b**, Uhrf1 and FLAG-Pramel7 (FP7) protein levels from whole cell lysates of E14 and FP7-ESCs in self-renewing conditions (+LIF)

and after 14 days of differentiation. **c**, DNA methylation levels of 14 days differentiated E14 and FP7-ESCs measured by digestion with HpaII and McrBC. **d**, Expression of pluripotency-associated genes Oct4, Nanog and Rex1 in differentiated cells were measured by qRT-PCR and normalized to actin mRNA. Data are represented as fold expression in FP7-ESCs compared to E14-ESCs. **e**, Bisulfite genomic sequencing analysis of the *Oct4* promoter in MEFs, E14-ESCs and differentiated E14 and FP7 cells Open and closed circles indicate nonmethylated and methylated CpG's, respectively. **f**, Alkaline phosphatase (AP) staining assay of 14 days differentiated E14 and FP7 ESCs re-exposed to self-renewing conditions (+LIF) for 7 days. Representative images of AP-stained 96 well plates and of an AP^- colony typical for E14-ESCs and an AP^+ colony characteristic for FP7 ESCs are shown. Scale bar: 100µm. Right panel shows average numbers of wells containing AP^+ colonies. **g**, Model showing the role of Pramel7 in naïve pluripotency of ICM. Transition of ICM to *ex vivo* immortalized pluripotent ESCs is marked by the reduction of Pramel7 expression and CpG methylation content. Pramel7 induces global hypomethylation by targeting Uhrf1 for proteasomal degradation and establishes an active epigenetic state that might be required by ICM to undergo rapid and transient developmental changes.

Supplemental Data Figures and Table

Supplemental data Figure 1: Mass spectrometry analysis of FLAG-Uhrf1 interacting proteins in the presence or absence of Pramel7 in HEK293T cells.

Supplemental data Figure 2: FP7 reconverted clones still exhibit decreased levels of Uhrf1 and express markers associated with pluripotency. a, Uhrf1 protein levels of 3 reconverted clones expanded in self-renewing conditions (CM+LIF). ReC: Reconverted clone. CM+LIF: Complete medium supplemented with leukemia inhibitory factor. FP7: FLAG-Pramel7. b, Representative immunofluorescent labeling of an FP7 reconverted clone with the pluripotency markers Oct4 and SSEA1. SSEA1: Stage-specific embryonic antigen-1. Scale bar: 200µm. ReC: Reconverted clone. FP7: FLAG-Pramel7. c, Expression of pluripotency-associated genes Nanog, Oct4 and Rex1 in FP7 reconverted clones normalized to E14 ESCs all

cultivated in self-renewing conditions (CM+LIF). ReC: Reconverted clone. FP7: FLAG-Pramel7.

Supplemental data Table 1

List of primers and PCR programs used for bisulfite analysis.

Supplemental data Table 2

List of primers used for qRT-PCR.

Figure 1

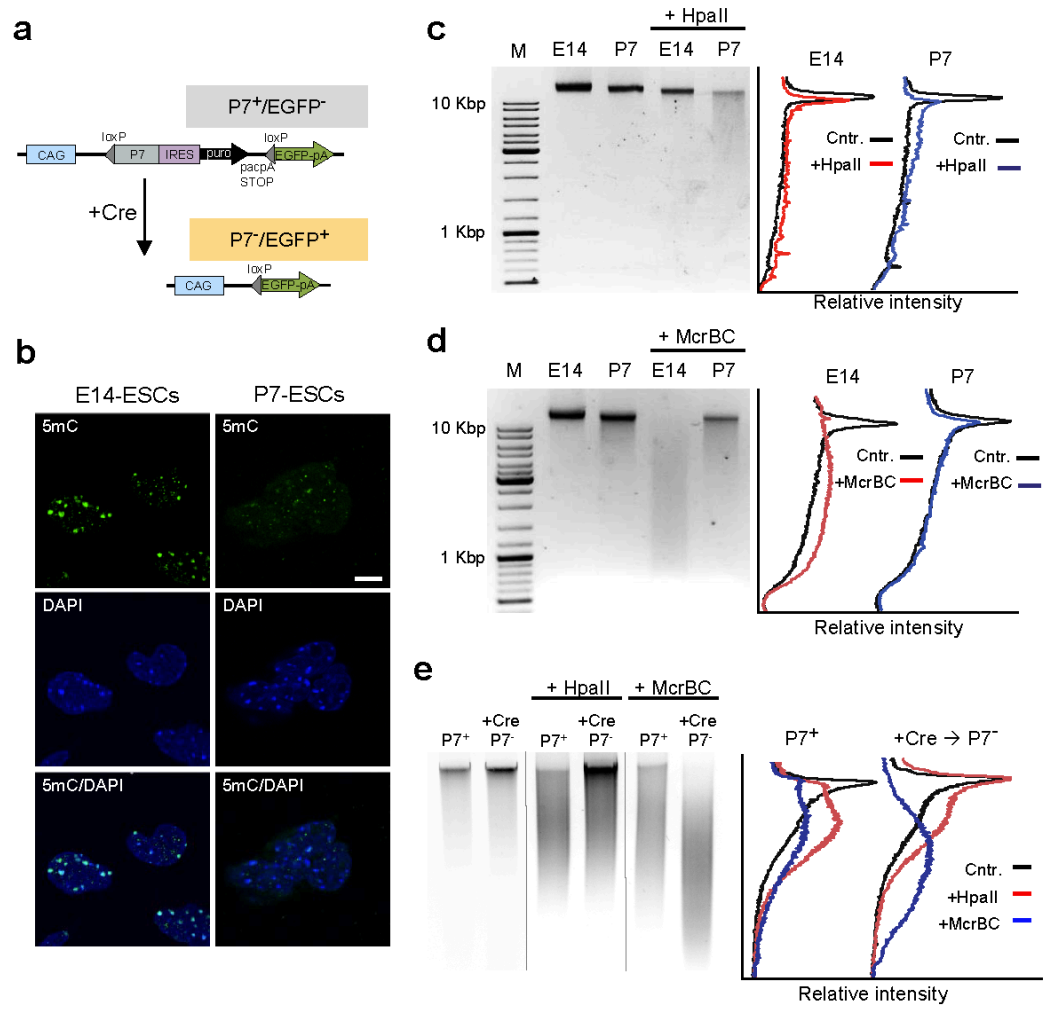
a
P7+/EGFP-
loxP
CAG
P7
IRES
puro
loxP
EGFP-pA
pacpA
STOP
+Cre
P7-/EGFP+
loxP
CAG
EGFP-pA
b
E14-ESCs
P7-ESCs
5mC
5mC
DAPI
DAPI
5mC/DAPI
5mC/DAPI
c
+ HpaII
M
E14
P7
E14
P7
10 Kbp
1 Kbp
E14
P7
Cntr.
+HpaII
Cntr.
+HpaII
Relative intensity
d
+ McrBC
M
E14
P7
E14
P7
10 Kbp
1 Kbp
E14
P7
Cntr.
+McrBC
Cntr.
+McrBC
Relative intensity
e
+ HpaII
+ McrBC
P7+
+Cre P7-
P7+
+Cre P7-
P7+
+Cre P7-
P7+
+Cre → P7-
Cntr.
+HpaII
+McrBC
Relative intensity
f
H3K9ac
H3K27ac
H4ac
H3K4me3
H3K27me3
E14 P7
E14 P7
E14 P7
E14 P7
E14 P7
H3 modified
1 4.17
1 1.36
1 1.3
1 4.4
1 0.55
Tubulin

Figure 2

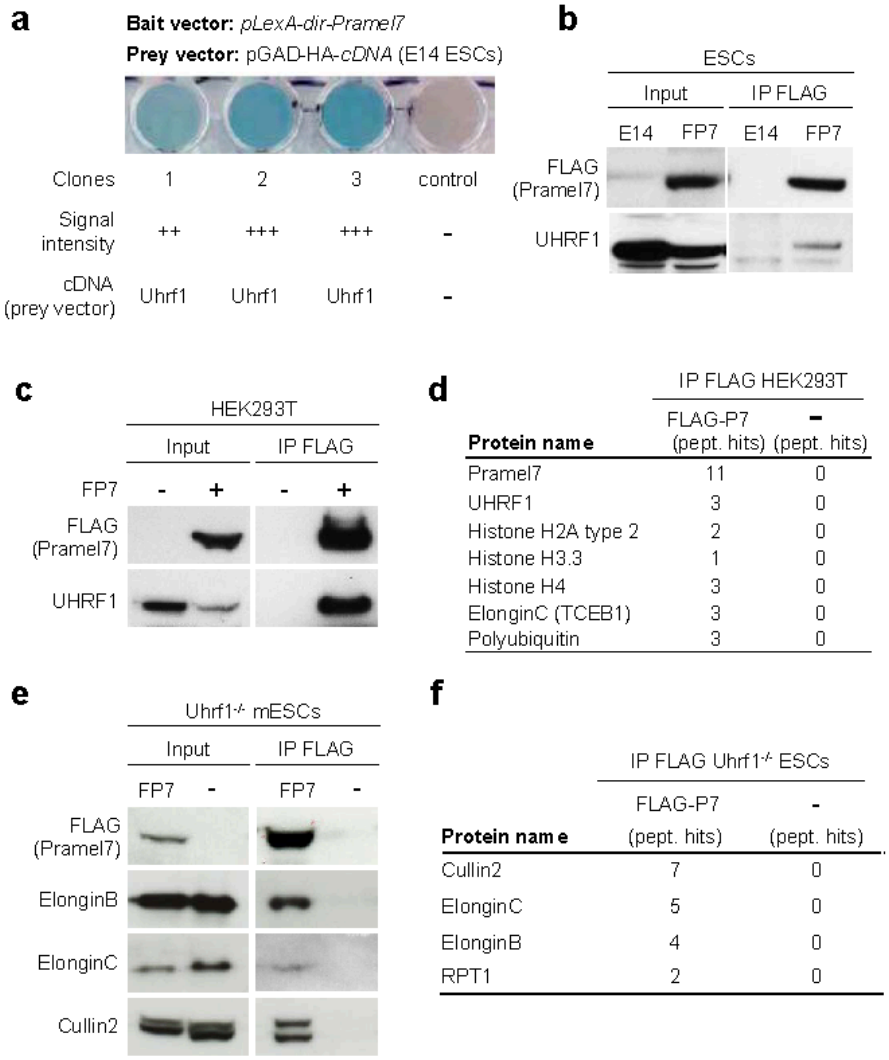
a
Bait vector: pLexA-dir-Pramel7
Prey vector: pGAD-HA-cDNA (E14 ESCs)
Clones 1 2 3 control
Signal intensity ++ +++ +++ -
cDNA (prey vector) Uhrf1 Uhrf1 Uhrf1 -
b
ESCs
Input IP FLAG
E14 FP7 E14 FP7
FLAG (Pramel7)
UHRF1
c
HEK293T
Input IP FLAG
FP7 - + - +
FLAG (Pramel7)
UHRF1
d
IP FLAG HEK293T
Protein name FLAG-P7 (pept. hits) - (pept. hits)
Pramel7 11 0
UHRF1 3 0
Histone H2A type 2 2 0
Histone H3.3 1 0
Histone H4 3 0
ElonginC (TCEB1) 3 0
Polyubiquitin 3 0
e
Uhrf1-/- mESCs
Input IP FLAG
FP7 - FP7 -
FLAG (Pramel7)
ElonginB
ElonginC
Cullin2
f
IP FLAG Uhrf1-/- ESCs
Protein name FLAG-P7 (pept. hits) - (pept. hits)
Cullin2 7 0
ElonginC 5 0
ElonginB 4 0
RPT1 2 0

Figure 3

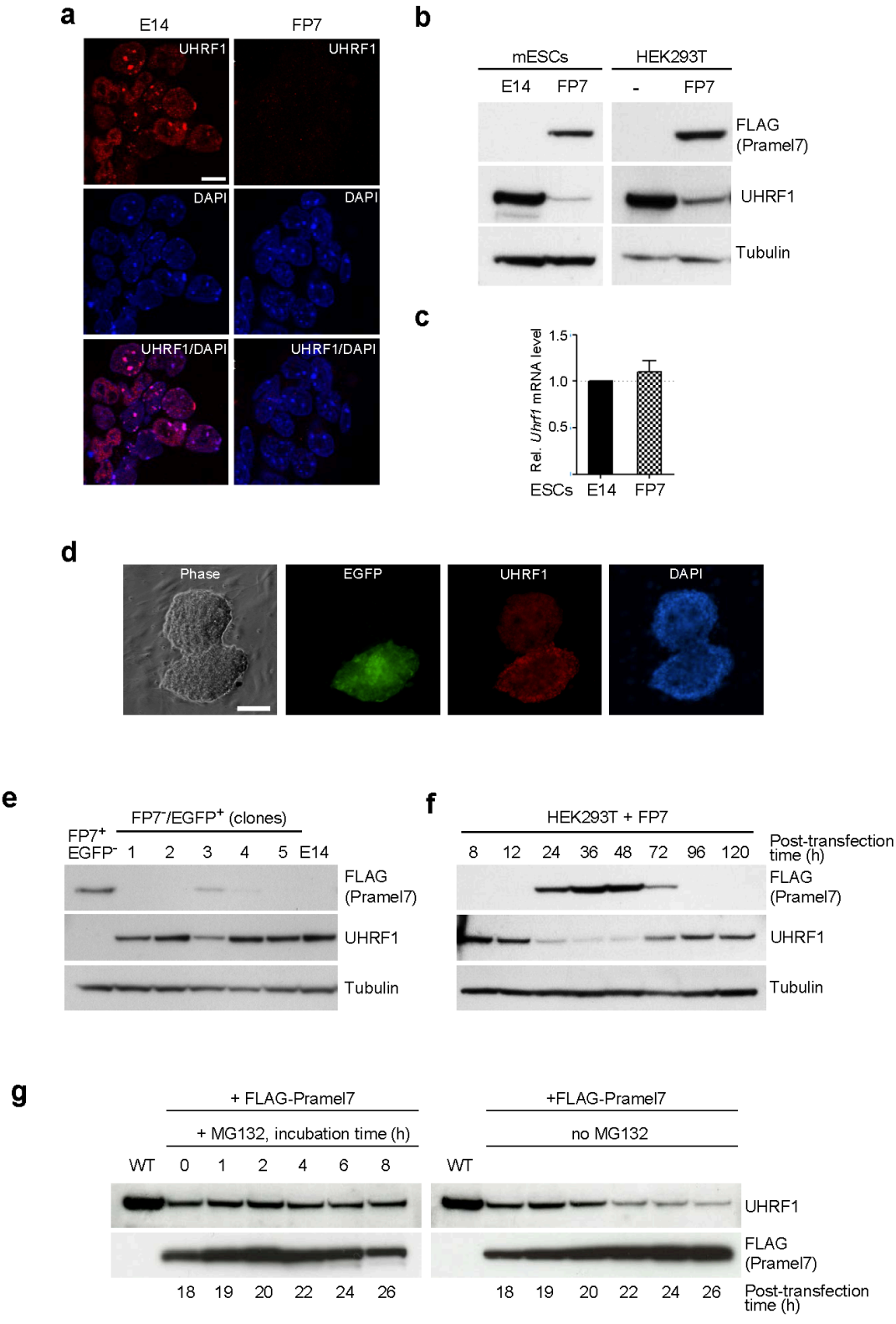
a
E14
FP7
UHRF1
UHRF1
DAPI
DAPI
UHRF1/DAPI
UHRF1/DAPI
b
mESCs
HEK293T
E14
FP7
-
FP7
FLAG
(Pramel7)
UHRF1
Tubulin
c
Rel. Uhrf1 mRNA level
1.5
1.0
0.5
ESCs
E14
FP7
d
Phase
EGFP
UHRF1
DAPI
e
FP7-/EGFP+ (clones)
FP7+
EGFP-
1
2
3
4
5
E14
FLAG
(Pramel7)
UHRF1
Tubulin
f
HEK293T + FP7
8
12
24
36
48
72
96
120
Post-transfection
time (h)
FLAG
(Pramel7)
UHRF1
Tubulin
g
+ FLAG-Pramel7
+ MG132, incubation time (h)
WT
0
1
2
4
6
8
+FLAG-Pramel7
no MG132
WT
UHRF1
FLAG
(Pramel7)
18
19
20
22
24
26
18
19
20
22
24
26
Post-transfection
time (h)

Figure 4

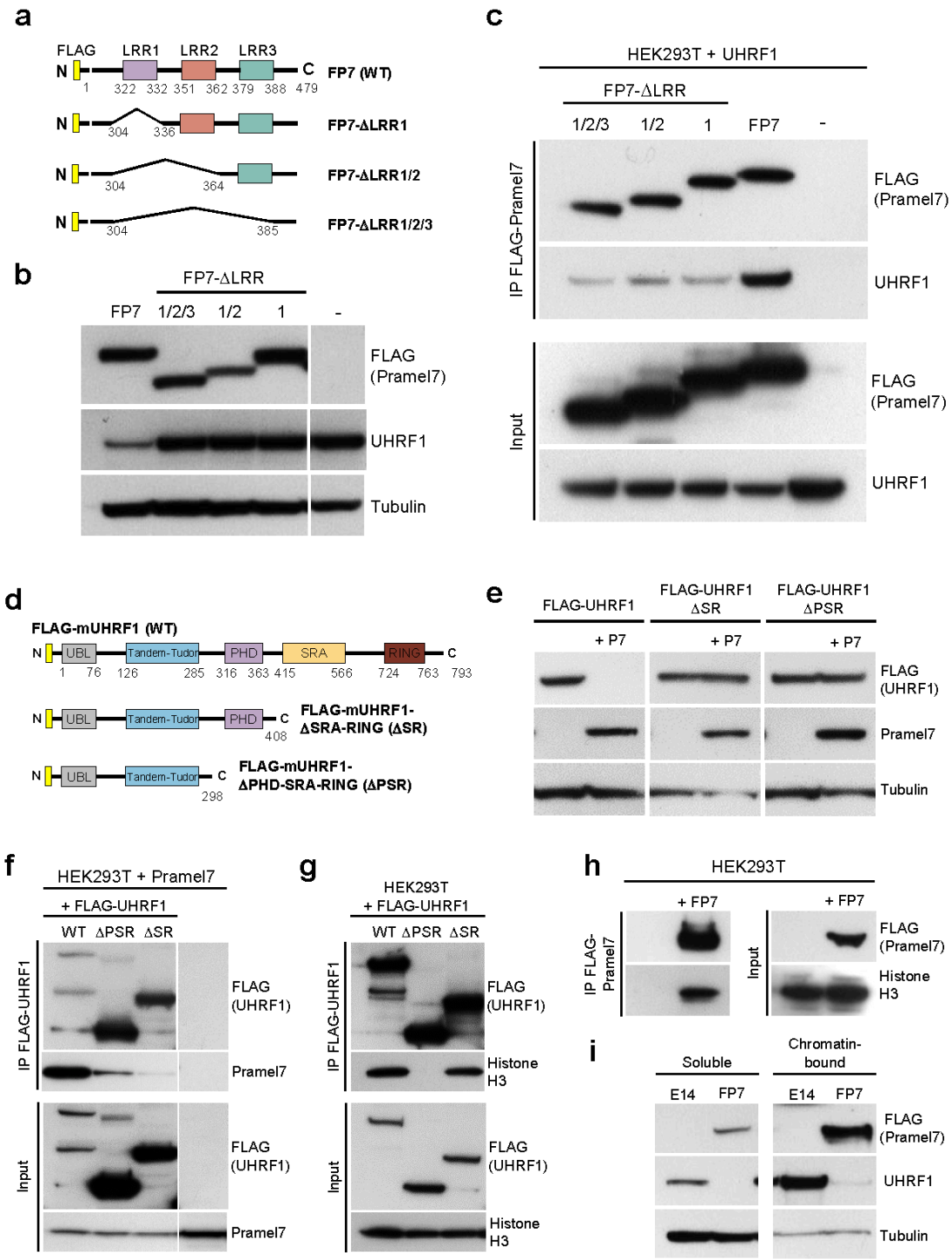
a
FLAG
LRR1
LRR2
LRR3
N
C
1
322 332 351 362 379 388 479
FP7 (WT)
304 336
FP7-ΔLRR1
304 364
FP7-ΔLRR1/2
304 385
FP7-ΔLRR1/2/3
b
FP7-ΔLRR
FP7 1/2/3 1/2 1 -
FLAG (Pramel7)
UHRF1
Tubulin
c
HEK293T + UHRF1
FP7-ΔLRR
1/2/3 1/2 1 FP7 -
IP FLAG-Pramel7
FLAG (Pramel7)
UHRF1
Input
FLAG (Pramel7)
UHRF1
d
FLAG-mUHRF1 (WT)
UBL
Tandem-Tudor
PHD
SRA
RING
1 76 126 285 316 363 415 566 724 763 793
FLAG-mUHRF1-ΔSRA-RING (ΔSR)
408
FLAG-mUHRF1-ΔPHD-SRA-RING (ΔPSR)
298
e
FLAG-UHRF1
FLAG-UHRF1 ΔSR
FLAG-UHRF1 ΔPSR
+ P7
FLAG (UHRF1)
Pramel7
Tubulin
f
HEK293T + Pramel7
+ FLAG-UHRF1
WT ΔPSR ΔSR
IP FLAG-UHRF1
FLAG (UHRF1)
Pramel7
Input
g
HEK293T
+ FLAG-UHRF1
WT ΔPSR ΔSR
IP FLAG-UHRF1
FLAG (UHRF1)
Histone H3
Input
h
HEK293T
+ FP7
IP FLAG-Pramel7
Input
FLAG (Pramel7)
Histone H3
i
Soluble
Chromatin-bound
E14 FP7
FLAG (Pramel7)
UHRF1
Tubulin

Figure 4

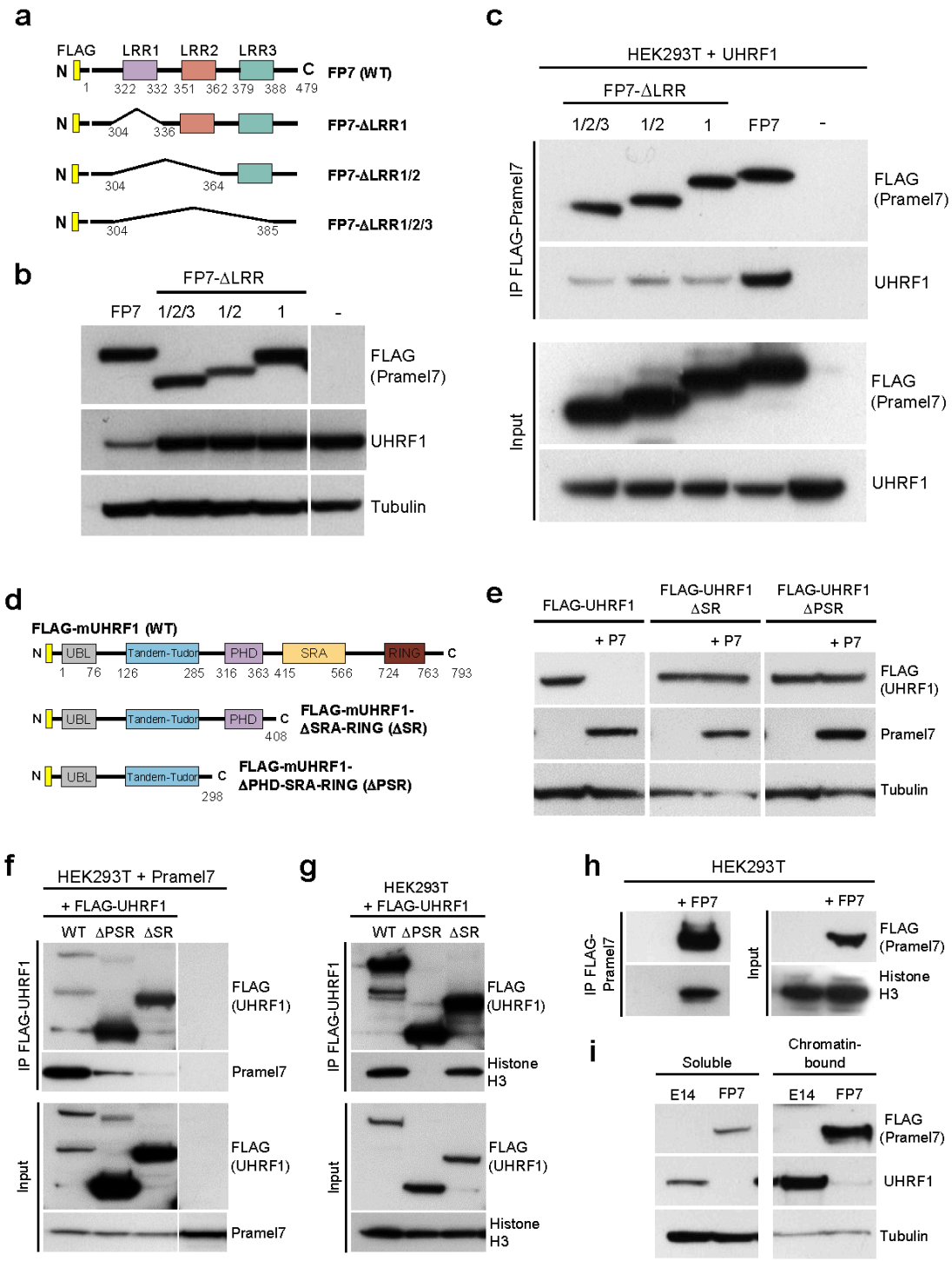
a
FLAG
LRR1
LRR2
LRR3
N
C
1
322 332 351 362 379 388 479
FP7 (WT)
304 336
FP7-ΔLRR1
304 364
FP7-ΔLRR1/2
304 385
FP7-ΔLRR1/2/3
b
FP7-ΔLRR
FP7 1/2/3 1/2 1 -
FLAG (Pramel7)
UHRF1
Tubulin
c
HEK293T + UHRF1
FP7-ΔLRR
1/2/3 1/2 1 FP7 -
IP FLAG-Pramel7
FLAG (Pramel7)
UHRF1
Input
FLAG (Pramel7)
UHRF1
d
FLAG-mUHRF1 (WT)
UBL
Tandem-Tudor
PHD
SRA
RING
1 76 126 285 316 363 415 566 724 763 793
FLAG-mUHRF1-ΔSRA-RING (ΔSR)
408
FLAG-mUHRF1-ΔPHD-SRA-RING (ΔPSR)
298
e
FLAG-UHRF1
FLAG-UHRF1 ΔSR
FLAG-UHRF1 ΔPSR
+ P7
FLAG (UHRF1)
Pramel7
Tubulin
f
HEK293T + Pramel7
+ FLAG-UHRF1
WT ΔPSR ΔSR
IP FLAG-UHRF1
FLAG (UHRF1)
Pramel7
Input
FLAG (UHRF1)
Pramel7
g
HEK293T
+ FLAG-UHRF1
WT ΔPSR ΔSR
IP FLAG-UHRF1
FLAG (UHRF1)
Histone H3
Input
FLAG (UHRF1)
Histone H3
h
HEK293T
+ FP7
+ FP7
IP FLAG-Pramel7
Input
FLAG (Pramel7)
Histone H3
i
Soluble
Chromatin-bound
E14 FP7
E14 FP7
FLAG (Pramel7)
UHRF1
Tubulin

Figure 5

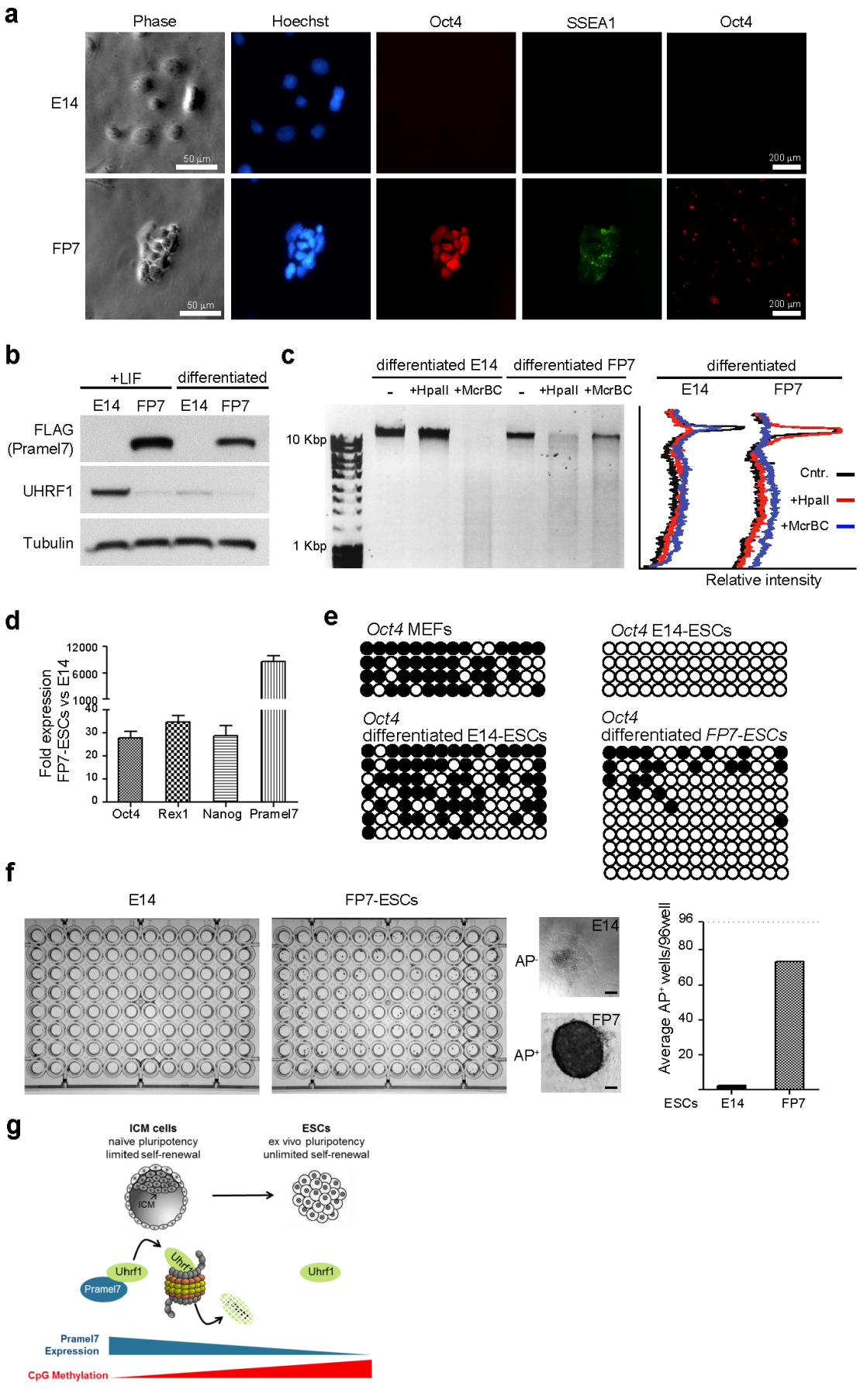
a
Phase
Hoechst
Oct4
SSEA1
Oct4
E14
FP7
50 µm
200 µm
b
+LIF
differentiated
E14
FP7
E14
FP7
FLAG (Pramel7)
UHRF1
Tubulin
c
differentiated E14
differentiated FP7
differentiated
-
+HpaII +McrBC
-
+HpaII +McrBC
E14
FP7
10 Kbp
1 Kbp
Cntr.
+HpaII
+McrBC
Relative intensity
d
Fold expression FP7-ESCs vs E14
12000
6000
1000
40
30
20
10
0
Oct4
Rex1
Nanog
Pramel7
e
Oct4 MEFs
Oct4 E14-ESCs
Oct4 differentiated E14-ESCs
Oct4 differentiated FP7-ESCs
f
E14
FP7-ESCs
AP-
AP+
E14
FP7
Average AP+ wells/96well
96
80
60
40
20
ESCs
E14
FP7
g
ICM cells
naïve pluripotency
limited self-renewal
ESCs
ex vivo pluripotency
unlimited self-renewal
ICM
Uhrf1
Pramel7
Uhrf1
Uhrf1
Pramel7 Expression
CpG Methylation

Supplemental Figure 1

Protein name	FLAG-UHRF1 +P7 (pept. hits)	FLAG-UHRF1 –P7 (pept. hits)	pBS control (pept. hits)
UHRF1	5	12	0
Pramel7	1	0	0
Histone H1.3	5	9	0
Histone H2A type 1-C	6	22	(1)
Macro H2A.1	4	5	0
Histone H2B type 2-E	23	38	0
Histone H2A.Z	2	5	0
Histone 3.1	10	15	(1)
Histone H4	7	17	0
Poly (ADP-ribose) polymerase 1 PARP1 (ARTD1)	9	11	0
SWI/SNF-related matrix-associated actin-dependent regulator of chromatin subfamily A member 5 SMARCA5	2	1	0
X-ray repair cross-complementing protein 5 XRCC5	11	19	0
X-ray repair cross-complementing protein 6 XRCC6	9	19	0
FACT complex subunit SPT16	3	0	0
Chromobox protein homolog 3 CBX3 (HP1γ)	3	0	0
Chromodomain-helicase-DNA-binding protein CHD4	2	0	0
ElonginC (TCEB1)	2	0	0
Polyubiquitin	2	3	(1)
DNA topoisomerase 2-alpha TOP2A	1	0	0

Supplemental Figure 2

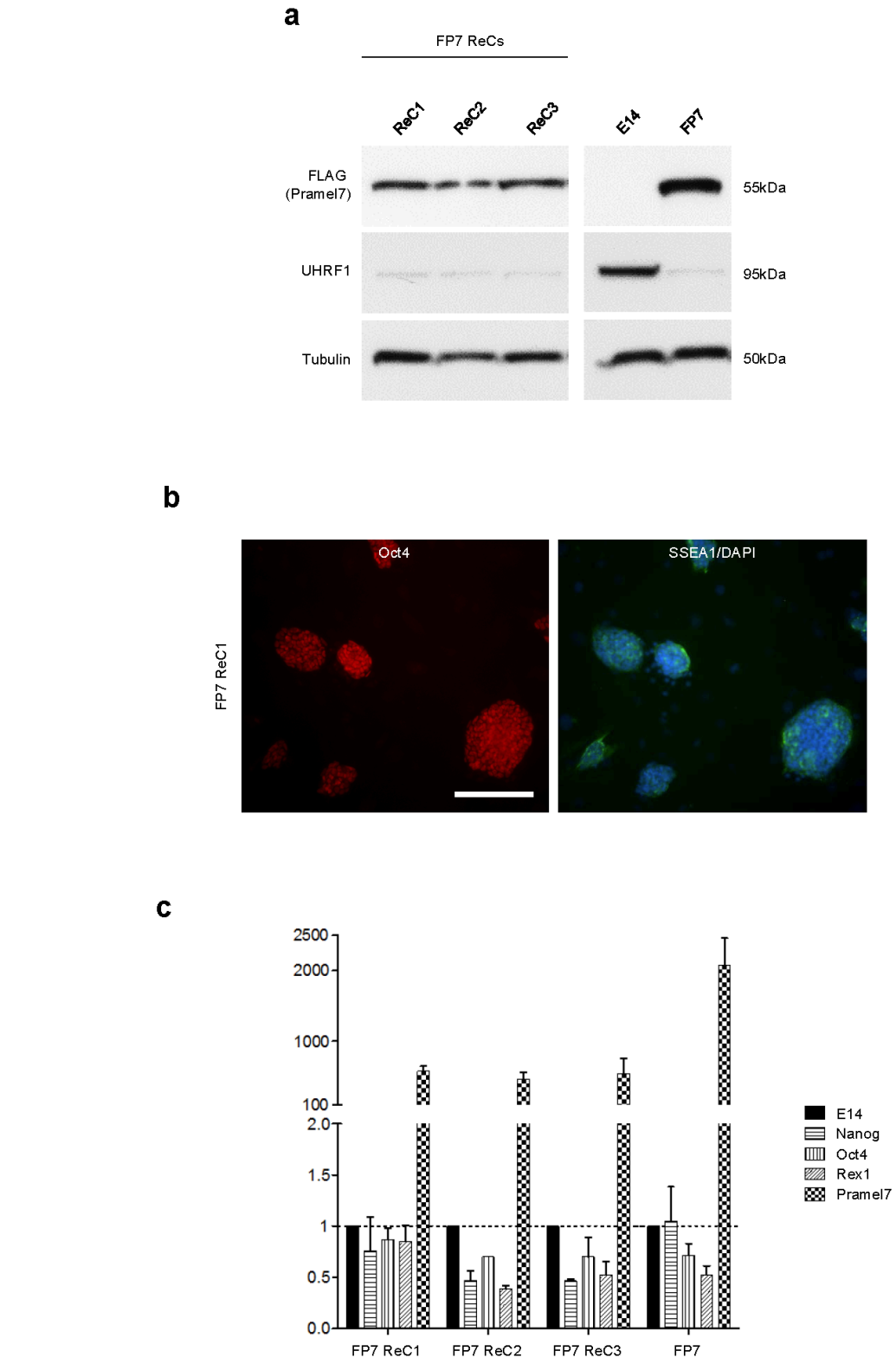

Supplementary Table 1

List of Oct4 Bisulfite primers

Primer	Sequence
bs_Oct4_fw	5'-GTG TAA TGG TTG TTT TGT TTT GGT -3'
bs_Oct4_bw	5'-AAT CCC CAA TAC CTC TAA ACC TAA T -3'
bs_nested Oct4_fw	5'-GGT TTT TTA GAG GAT GGT TGA GTG -3'
bs_nested_ Oct4_bw	5'-TCC AAC CCT ACT AAC CCA TCA CC -3'

Program touchdown PCR for amplification of *Oct4* from bisulfite treated genomic DNA

1. PCR

95°C	2 min	
95°C	40 sec	
60°C → 52.5°C 40 sec	15 cycles	
72°C	30 sec	
95°C	40 sec	
52.5°C	40 sec	25 cycles
72°C	30 sec	
72°C	7 min	

2. Nested PCR

95°C	2 min	
95°C	40 sec	
60°C → 52.5°C 40 sec	15 cycles	
72°C	30 sec	
95°C	40 sec	
52.5°C	40 sec	25 cycles
72°C	30 sec	
72°C	7 min	

Supplementary Table 2

List of real-time PCR primers

Primer	Sequence
Actin_fw	5'-CAT CCA GGC TGT GCT GTC CCT GTA TGC-3'
Actin_bw	5'-CAT CCA GGC TGT GCT GTC CCT GTA TGC-3'
Uhrf1_fw	5'-ACA GTG AAT CAG ACA AGT CGT-3'
Uhrf1_bw	5'-ATT CTT GGC GGG TTT GAC AAT GTC-3'
Pramel7_fw	5'-TCT CTG ATG CGG AGT GCC TA-3'
Pramel7_bw	5'-TTC CCA TCC TGG GGC GAT-3'
Oct4_fw	5'-GGC GTT CGC TTT GGA AAG GTG TTC -3'
Oct4_bw	5'-CTC GAA CCA CAT CCT TCT CT -3'
Nanog_fw	5'-ACA AGG GTC TGC TAC TGA GAT GC-3'
Nanog_bw	5'-GGA GAC TTC TTG CAT CTG CTG G-3'
Rex1_fw	5'-AGA AAG CAG GAT CGC CTC AC-3'
Rex1_bw	5'-AGG GAA CTC GCT TCC AGA AC-3'

3.2 Unpublished Results

3.2.1 PARP1 and UHRF1 bound DNA is heterochromatic and enriched in unmodified Histone 3

The results of Supplementary Figure 4S (3.1.1 Assembly of heterochromatin after replication is a slow process required for DNA methylation) indicated that PARP1 and UHRF1 associate and co-occupy rDNA and alpha satellites. To further characterize the epigenetic environment of PARP1 and UHRF1 bound genes, we performed reChIP experiments and determined which HTMs characterized PARP1 or UHRF1 bound nucleosomes, respectively. To measure and compare the occupancy of defined histones modifications on PARP1 associated nucleosomes, data were normalized to H3 enrichment. Values measured in classical ChIP (single ChIP) indicated the total occupancy of a specific HTMs or histone at a measured sequence. The enrichment of each HTM at PARP1 bound nucleosomes was evaluated by comparing the HTM occupancy of the reChIP (HTMs at PARP1 bound nucleosomes) to the single ChIP values (total levels of HTMs).

First, we assed the relative occupancy of the active HTM H3K4me2 on PARP1 bound nucleosomes. We observed a decreased occupancy of H3K4me2 on PARP1 associated nucleosomes (reChIP) compared to the total amounts determined in the single ChIP (Fig. 7A). Along this line, silent histone mark H3K9me2 levels were enriched on PARP1 bound nucleosomes (Fig. 7B). These results are consistent with previous results showing the association of PARP1 with silent rRNA genes and the role of PARP1 in the inheritance of rDNA heterochromatic structures (Guetg et al., 2012). Moreover, the data indicated that the association of PARP1 with heterochromatic nucleosomes is not only limited to rDNA but also to other repressed regions of the genome such as alpha satellites and IP10 gene. Importantly, we observed an enormous enrichment of unmodified H3 (using an antibody raised against the unmodified histone H3 N-tail, previously shown to only recognize unmodified H3 (Petruk et al., 2012)) in PARP1 bound nucleosomes (Fig. 7C). In the single ChIP, unmodified H3 levels were not detectable, suggesting that histones are modified swiftly after incorporation and unmodified histones are rarely found on chromatin of unsynchronized cells. Taken together our data strongly suggest that PARP1 binds to nucleosomes enriched in silent histone marks and/or to still poorly modified nucleosomes. The enrichment in

unmodified histone H3 might reflect the association of PARP1 with rDNA shortly after the passage of the replication fork, a state that is characterized by the incorporation of new, unmodified histones.

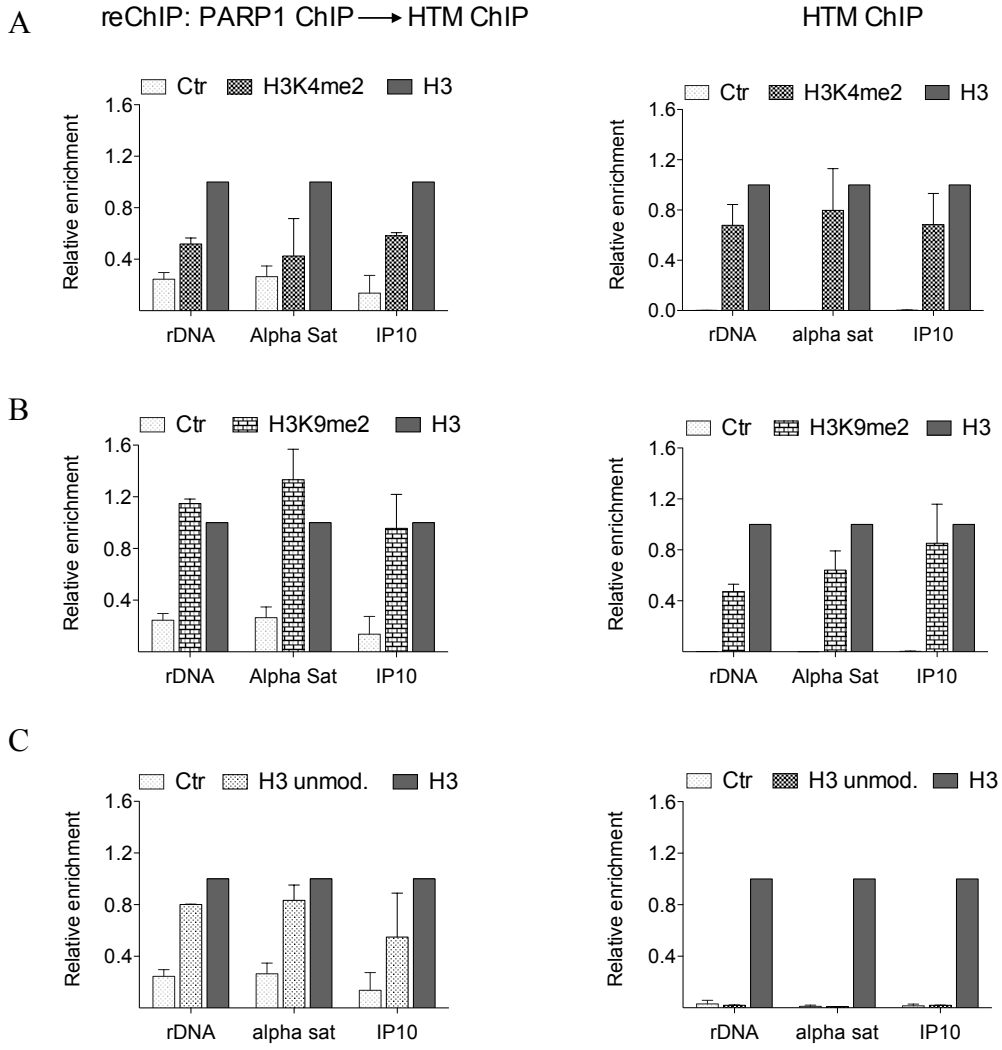

Figure 7. PARP1 binds to H3K9me2 and unmodified H3 rich chromatin. A. Left panel showing the results of the reChIP for H3K4me2 (First ChIP PARP1, Second ChIP H3K4me2). Right panel depicting a single ChIP showing the total ccupancy of H3K4me2 at rDNA, alpha satellites and IP10 chromatin. B. Left panel: Occupancy of H3K9me2 on PARP1 bound nucleosomes. Right panel total occupancy of H3K9me2 at rDNA, alpha satellites and IP10. C. Enriched levels of unmodified H3 at PARP1 bound nucleosomes is seen in the left panel. The single ChIP shown on the right panel shows no unmodified H3 at rDNA, alpha satellites and IP10.
All experiments were carried out in HEK293T cells overexpressing HA-PARP1. Values are presented as bound over input and normalized to H3. Data are mean ± SEM (error bars, independent experiments: n=2).

To gain further insights about the possible crosstalk between PARP1 and UHRF1, we performed a similar reChIP experiment as shown in Figure 8 to characterize the epigenetic signature of UHRF1 bound nucleosomes. We overexpressed HA-UHRF1 in HEK293T cells and performed a first ChIP against the HA-tag, followed by a consecutive ChIP against H3, unmodified H3 and HTMs. As shown in Figure 9 UHRF1 binds to chromatin bearing the same epigenetic signature as PARP1 bound nucleosomes (considering the tested modifications H3K4me2, H3K9me2 and unmodified H3). Comparing the occupancy of the active mark H3K4me2 between the single ChIP and the reChIP, we can conclude that UHRF1 binds to H3K4me2 poor chromatin (Fig. 8A). On the other hand, the silent mark H3K9me2 is enriched on UHRF1 bound nucleosomes (Fig. 8B). Similarly to the results obtained in the PARP1 reChIP experiment, we observed that UHRF1 binds to chromatin, which is highly enriched in unmodified H3 (Fig. 8C). We conclude that UHRF1 as well as PARP1 bind to heterochromatic and nascent rDNA.

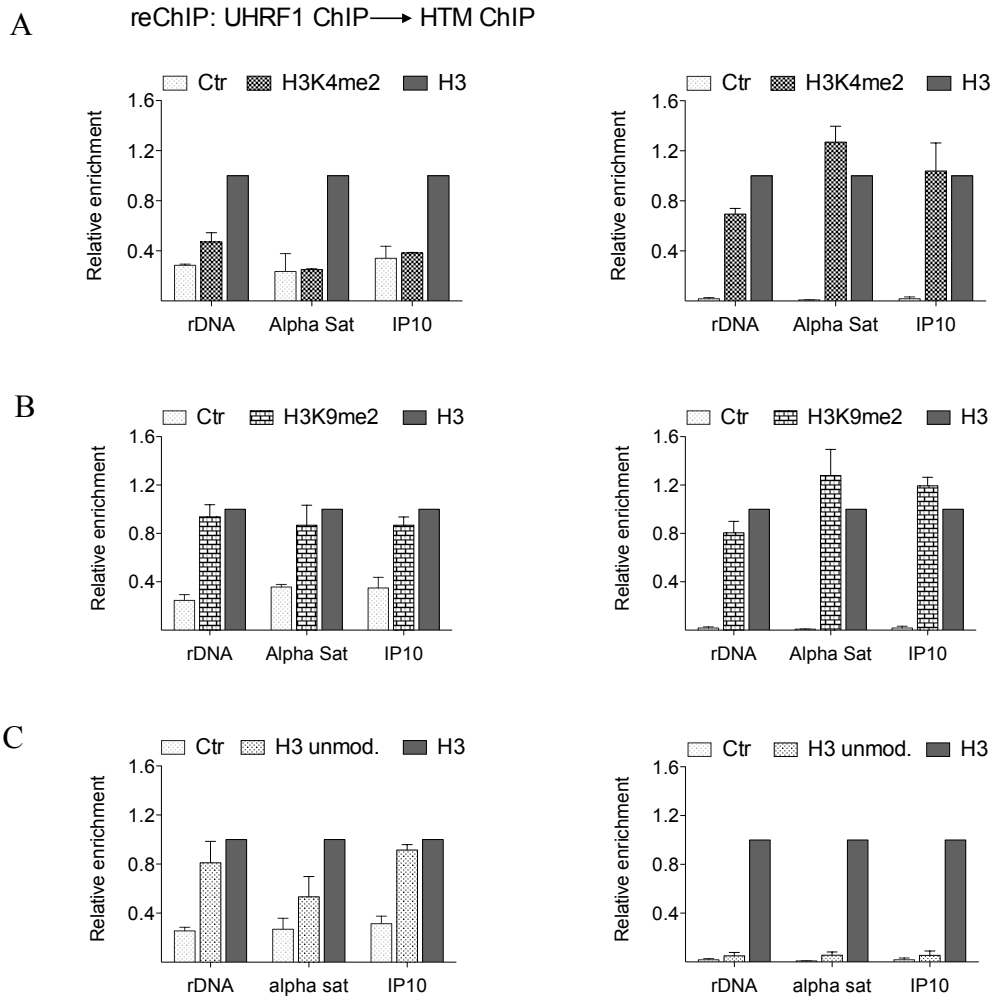

Figure 8. UHRF1 binds to H3K9me2 and unmodified H3 rich chromatin. A. Scheme of nucleosomes used in the indicated reChIP or single ChIP. B. Left panel showing the results of the reChIP for H3K4me2 (First ChIP UHRF1, Second ChIP H3K4me2). Right panel depicting a single ChIP showing the occupancy of H3K4me2 at rDNA, alpha satellites and IP10 chromatin. C. Left panel: Occupancy of H3K9me2 on UHRF1 bound nucleosomes. Right panel total occupancy of H3K9me2 at rDNA, alpha satellites and IP10. D. Enriched levels of unmodified H3 at UHRF1 bound nucleosomes on the left panel. The single ChIP shown on the right panel shows no unmodified H3 at rDNA, alpha satellites and IP10. All experiments were carried out in HEK293T cells overexpressing HA-UHRF1. Values are presented as bound over input and normalized to H3. Data are mean ± SEM (error bars, independent experiments: n=2). Experiments were performed together with Anita Steiner.

4 Discussion

During cell division, the DNA as well as its organization into chromatin has to be duplicated. How complex chromatin structures with their specific epigenetic modifications are restored after the passage of the replication fork remains a fundamental question with implications for eukaryotic development and diseases. The aim of this work was to elucidate the dynamics of restoration of euchromatic and heterochromatic structures after replication. We have established a method to monitor and quantify nucleosome assembly and restoration of epigenetic marks at newly replicated DNA from the passage of the replication fork to mitosis. To exclude a bias based on DNA sequences, we measured chromatin maturation at ribosomal RNA (rRNA) genes, which represent a paradigm of both euchromatin and heterochromatin. We extended this analysis also to other euchromatic and heterochromatic sequences such as the GAPDH gene and alpha satellites. Using this strategy, we determined that the assembly of nucleosomes at heterochromatic repeats is a slow process that lasts until G2/M. This is a specific feature of heterochromatin since nucleosome assembly after replication of euchromatic sequences is a rapid process, as described for bulk chromatin in early works. We showed that the association of histone H3 dimethylated at Lys 9 (H3K9me2) at heterochromatic sequences does not occur immediately after replication and the kinetics of H3K9 methylation incorporation is similar to the one found for the assembly of nucleosomes and histone H3. Remarkably, the restoration of DNA methylation patterns is also a slow process. Furthermore, we discovered that PARP1-mediated ADP-ribosylation on nascent heterochromatin is paramount for the slow acquisition of nucleosomes and for the restoration of DNA methylation. Inhibition of PARP activity caused a rapid assembly of nucleosomes at nascent heterochromatin as observed at euchromatin and impairs DNA methylation without altering the association of the DNA methylation machinery. Based on these results we concluded that ADP-ribosylation might facilitate methylation on DNA by temporarily keeping an open chromatin conformation at nascent heterochromatin (**Figure 9**). Our work unravelled a post-replicative temporal coordination between nucleosome deposition and DNA methylation and suggests that a delayed post-replicative nucleosome assembly at heterochromatin might serve to facilitate restoration of DNA methylation patterns.

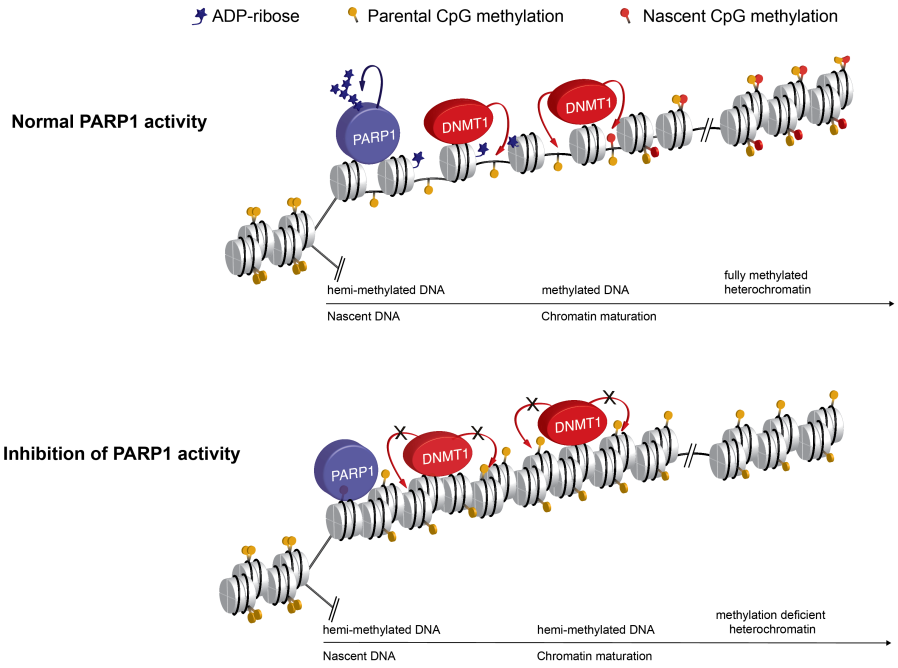

Figure 9. Model showing the slow deposition of nucleosomes after replication of heterochromatic DNA. The restrained assembly of nucleosomes mediated by PARP1-ADP-ribosylation allows the completion of methylation at DNA, which would be otherwise inefficiently modified when assembled into chromatin. Inhibition of PARP1 induced rapid assembly of nucleosomes and impairs methylation, without affecting the association of the DNA methylation machinery (here represented only with DNMT1).

4.1 Establishment of heterochromatic states does not occur immediately after the passage of the replication fork

Rapid assembly of nucleosomes after DNA replication appears as an undisputed concept in the chromatin field. This model is based on pioneering work (Hildebrand et al., BBRC 1976; Seale, Nature 1975) using nucleases to probe chromatin assembly after replication, which defined a time window of approximately 15-20 min for new DNA to be packaged into a structure similar to bulk chromatin. However, this model has never been re-investigated, even though in the last 30 years our knowledge on chromatin greatly increased, particularly for the molecular characterization of the different chromatin states like euchromatin and heterochromatin. These original studies were performed on total replicating DNA and, consequently, they are not informative on the kinetics of nucleosome assembly at different chromatin domains. Moreover, until recently the post-replicative re-establishment of heterochromatin has been considered to occur rapidly after the passage of the replication fork. Indeed,

several chromatin and epigenetic factors (i.e CAF-1, HDACs, HMTs, DNMT1, SNF2H, UHRF1) have been shown to localize to replication foci during S-phase and associate with PCNA (Probst et al., 2009). PCNA forms a heterotrimeric ring around the DNA helix at the replication fork, however even its trivalent nature cannot possibly manage to bind all the potential binding partners (i.e epigenetic regulators) at the same time in a coordinated fashion.

Our results propose that the assembly of nucleosome and chromatin maturation at heterochromatin after replication is a slow process. We showed that the incorporation of nucleosomes, histone H3 and H3K9me2 last until G2/M – several hours after DNA synthesis. The fact that this observation has been missed until now was probably due to the limitations of earlier studies analyzing bulk chromatin and not specific sequences or specific chromatin structures (Hildebrand et al., BBRC 1976; Seale, Nature 1975). This is also true for recent studies describing the restoration of histone modifications using a proteomic approach that does not distinguish early from mid-late S phase and the distinct chromatin structures (Alabert et al., 2015; Xu et al., 2012; Zee et al., 2012). Important information emerging from these recent proteomic analyses shows that the majority of lysine modifications on new histones are acquired after the S phase. Although in our experimental set-up we cannot distinguish parental from new histones, the slow acquisition of H3K9 methylation at nascent heterochromatin is consistent with these results.

The quantification of chromatin formation on specific sequences performed in our study determined that some sequences assemble nucleosomes slower than others, unraveling a further level of regulation for the inheritance of chromatin and epigenetic states.

4.2 PARP1-activity creates a indispensable window of opportunity for DNMT1 to methylate nascent DNA

Much evidence exists to support a paradoxical dual contribution of PARP1 in transcription and chromatin regulation. Although PARP1 has been generally associated with the regulation of transcriptional active states, PARP1 has also been implicated in the regulation of heterochromatic regions such as the inactive X chromosome, telomeres, pericentric heterochromatin and silent rRNA genes (Beneke

et al., 2008; Dantzer and Santoro, 2013; Guetg et al., 2012; Kanai et al., 2003). However, the mechanistic insights of PARP1-mediated regulation remain yet to be elucidated. In this work, we showed that PARP1-mediated ADP-ribosylation orchestrates the slow assembly of nucleosomes at nascent heterochromatin. Inhibition of PARP activity caused a rapid deposition of nucleosomes as well as histone H3 at nascent heterochromatin as observed at euchromatin. Previous work determined that the association of PARP1 and ADP-ribosylation of histones at heterochromatic rRNA genes is limited within the first 2 hours after replication (Guetg et al., 2012).

The ability of ADP-ribosylation to affect chromatin structures has been well documented in the last three decades. PARylation of native polynucleosomes by PARP1 was shown to promote a decondensation of the chromatin and 40 ADP-ribose residues covalently attached to PARP1 apparently suffice to fully disrupt a chromatosome (Althaus, 1992; Poirier et al., 1982; Realini and Althaus, 1992). The affinity of histones for poly(ADP-ribose), especially on automodified PARP1, led to propose a 'histone shuttle' mechanism for chromatin relaxation/recondensation involving poly(ADP-ribose) (Realini and Althaus, 1992). The possibility that automodified PARP1 can act as a scaffold for the transient and local sequestration of histones in order to facilitate a transient decondensation of chromatin is an attractive model, not only for its role in replication at heterochromatin described in our work, but also for other processes such as repair and transcription.

Until now, the prevailing view for the maintenance of DNA methylation is that DNMT1 restores DNA methylation patterns swiftly after replication. This model is mainly based on the association of DNMT1 with PCNA and sites of DNA replication (Chuang et al., 1997; Leonhardt et al., 1992). Experimental evidence showed that the catalytic efficiency of DNMT1 is significantly compromised on nucleosome substrate compared to naked DNA (Okuwaki and Verreault, 2004; Robertson et al., 2004), a result that is consistent with the low DNA methylation content measured on nucleosomes in vivo (Felle et al., 2011). The inaccessibility of nucleosomal DNA for methylation was also proposed for the *de novo* methylation directed by DNMT3A and DNM3B, which is occluded from nucleosomal DNA (Baubec et al., 2015). Together with DNMT1 localization to replication foci these findings suggest that DNMT1 has to act close to replication fork before DNA is repackaged into a tight, unfavourable nucleosomal conformation. However, the assumption linking DNMT1 and DNA replication tightly together stands on shaky grounds, due to a difference of 3-4 orders

of magnitude in the estimated kinetics of DNA replication in vivo (0.035s per nucleotide) and DNA methylation by DNMT1 *in vitro* (70-450s per methyl group transfer) (Jackson and Pombo, 1998; Pradhan et al., 1999). How DNMT1 would catch up with the overwhelming speed of the replication fork has not been understood to date. Furthermore, the ability of DNMT1 to bind PCNA is neither absolutely required nor sufficient for DNA methylation maintenance (Pradhan et al., 1999; Schermelleh et al., 2007; Spada et al., 2007). A major limitation in the field of DNA methylation has been the lack of a quantitative method to measure the incorporation of methyl groups at hemimethylated nascent DNA. In this work, we have developed a method based on sequential immunoprecipitation of nascent methylated DNA strands (MeDIP) followed by the isolation of nascent DNA (anti-BrdU IP). This method allowed us to assess quantitative measurements on the incorporation of methyl-groups at rRNA sequences after replication. Our results determined that DNA methylation on heterochromatic rDNA is restored slowly and is not completed until G2/M. These data reflect the observed different kinetics of DNA replication and DNA methylation by showing *in vivo* that these two processes are not necessarily coordinated and that methylating a cytosine might take far longer that to incorporate it.

We have further shown that PARP1-activity regulates DNA methylation maintenance, as nascent DNA is not efficiently methylated in absence of PARP1 activity. Remarkably, inhibition of PARP activity impairs DNA methylation without altering the expression and the association of two crucial factor of the DNA methylation machinery, DNMT1 and UHRF1. Despite several reports suggesting a regulatory role for PARP1 in DNMT1 stability and expression (directly or through UHRF1) (De Vos et al., 2014; Reale et al., 2005), we did not detect any differences in DNMT1 and UHRF1 levels or recruitment with or without PARP1 activity or PARP1 itself. Based on these results, we postulate that the PARP1-mediated slow nucleosome assembly creates a window of opportunity for DNMT1 to efficiently methylate DNA. The ADP-ribosylated, nucleosome-poor nascent heterochromatin might allow the DNMT1 to methylate the nascent strand and faithfully maintain DNA methylation at its given speed. In absence of PARP1 activity, the nucleosomes are rapidly assembled after DNA synthesis, denying DNMT1 to methylate its hemimethylated substrate.

4.3 Genomic and epigenomic instability in cancer

Hypomethylation at repetitive sequences is a hallmark of cancer genomes (Ehrlich, 2009). Accordingly, aberrant overexpression of pericentromeric satellite repeats has been reported in several epithelial cancers including pancreas, lung, kidney, colon and prostate (Eymery et al., 2009; Hall et al., 2012; Ting et al., 2011). Furthermore, decondensation of pericentromeric heterochromatin and transcription activation has also been observed in several genetic disorders (Ehrlich et al., 2008; Shumaker et al., 2006). In addition, loss of constitutive heterochromatin favors DNA breaks and genomic rearrangements, events that are often observed in cancer (Saksouk et al., 2015). How hypomethylation of cancer genomes is initiated is not understood. According to our results, even a mildly inhibitory effect on DNMT activity by nucleosomes assembled on newly synthesized DNA would result in substantial losses in DNA methylation over the course of many cell divisions. The post-replicative temporal coordination of DNA methylation and nucleosome assembly at heterochromatin might represent an important process to consider in future studies aimed to understand alterations in epigenome and genome integrity during tumor progression.

The use of PARP inhibitor in cancer therapy has been recently received much attention: the synthetic lethal interactions between *PARP1* and *BRCA1/2* were confirmed with PARP inhibitors *in vitro*, in mouse models, and in a landmark phase I clinical trial (Dedes et al., 2011). To fully realize the potential of PARP inhibitors, it is necessary to better understand PARP biology. It will be particularrly crucial to examine potential long-term effects of PARP inhibition as these clinical trials mature. Our results, elucidating a PARP1-dependent mechanism to faithfully propagate DNA methylation at heterochromatic repeats, may contribute to better understand, prevent or fight diseases and cancer.

Bibliography

Alabert, C., Barth, T.K., Reveron-Gomez, N., Sidoli, S., Schmidt, A., Jensen, O.N., Imhof, A., and Groth, A. (2015). Two distinct modes for propagation of histone PTMs across the cell cycle. Genes Dev *29*, 585-590.

Alabert, C., Bukowski-Wills, J.C., Lee, S.B., Kustatscher, G., Nakamura, K., de Lima Alves, F., Menard, P., Mejlvang, J., Rappsilber, J., and Groth, A. (2014). Nascent chromatin capture proteomics determines chromatin dynamics during DNA replication and identifies unknown fork components. Nat Cell Biol *16*, 281-293.

Alabert, C., and Groth, A. (2012). Chromatin replication and epigenome maintenance. Nat Rev Mol Cell Biol *13*, 153-167.

Althaus, F.R. (1992). Poly ADP-ribosylation: a histone shuttle mechanism in DNA excision repair. J Cell Sci *102 (Pt 4)*, 663-670.

Alvarez-Gonzalez, R., and Jacobson, M.K. (1987). Characterization of polymers of adenosine diphosphate ribose generated in vitro and in vivo. Biochemistry *26*, 3218-3224.

Aubin, R.J., Frechette, A., de Murcia, G., Mandel, P., Lord, A., Grondin, G., and Poirier, G.G. (1983). Correlation between endogenous nucleosomal hyper(ADP-ribosyl)ation of histone H1 and the induction of chromatin relaxation. Embo J *2*, 1685-1693.

Bannister, A.J., Zegerman, P., Partridge, J.F., Miska, E.A., Thomas, J.O., Allshire, R.C., and Kouzarides, T. (2001). Selective recognition of methylated lysine 9 on histone H3 by the HP1 chromo domain. Nature *410*, 120-124.

Baranzini, S.E., Mudge, J., van Velkinburgh, J.C., Khankhanian, P., Khrebtukova, I., Miller, N.A., Zhang, L., Farmer, A.D., Bell, C.J., Kim, R.W.*, et al.* (2010). Genome, epigenome and RNA sequences of monozygotic twins discordant for multiple sclerosis. Nature *464*, 1351-1356.

Baubec, T., Colombo, D.F., Wirbelauer, C., Schmidt, J., Burger, L., Krebs, A.R., Akalin, A., and Schubeler, D. (2015). Genomic profiling of DNA methyltransferases reveals a role for DNMT3B in genic methylation. Nature *520*, 243-247.

Beneke, S., Cohausz, O., Malanga, M., Boukamp, P., Althaus, F., and Burkle, A. (2008). Rapid regulation of telomere length is mediated by poly(ADP-ribose) polymerase-1. Nucleic Acids Res *36*, 6309-6317.

Bernard, P., Maure, J.F., Partridge, J.F., Genier, S., Javerzat, J.P., and Allshire, R.C. (2001). Requirement of heterochromatin for cohesion at centromeres. Science *294*, 2539-2542.

Bernstein, E., and Hake, S.B. (2006). The nucleosome: a little variation goes a long way. Biochemistry and Cell Biology-Biochimie Et Biologie Cellulaire *84*, 505-517.

Bestor, T.H. (2000). The DNA methyltransferases of mammals. Hum Mol Genet *9*, 2395-2402.

Brown, K.D., and Robertson, K.D. (2007). DNMT1 knockout delivers a strong blow to genome stability and cell viability. Nat Genet *39*, 289-290.

Cao, R., Wang, L., Wang, H., Xia, L., Erdjument-Bromage, H., Tempst, P., Jones, R.S., and Zhang, Y. (2002). Role of histone H3 lysine 27 methylation in Polycomb-group silencing. Science *298*, 1039-1043.

Carone, D.M., and Lawrence, J.B. (2013). Heterochromatin instability in cancer: from the Barr body to satellites and the nuclear periphery. Semin Cancer Biol *23*, 99-108.

Chuang, L.S., Ian, H.I., Koh, T.W., Ng, H.H., Xu, G., and Li, B.F. (1997). Human DNA-(cytosine-5) methyltransferase-PCNA complex as a target for p21WAF1. Science *277*, 1996-2000.

Conconi, A., Widmer, R.M., Koller, T., and Sogo, J.M. (1989). Two different chromatin structures coexist in ribosomal RNA genes throughout the cell cycle. Cell *57*, 753-761.

Cosgrove, M.S., and Wolberger, C. (2005). How does the histone code work? Biochem Cell Biol *83*, 468-476.

d'Adda di Fagagna, F., Hande, M.P., Tong, W.M., Lansdorp, P.M., Wang, Z.Q., and Jackson, S.P. (1999). Functions of poly(ADP-ribose) polymerase in controlling telomere length and chromosomal stability. Nat Genet *23*, 76-80.

D'Amours, D., Desnoyers, S., D'Silva, I., and Poirier, G.G. (1999). Poly(ADP-ribosyl)ation reactions in the regulation of nuclear functions. Biochem J *342 (Pt 2)*, 249-268.

Dantzer, F., and Santoro, R. (2013). The expanding role of PARPs in the establishment and maintenance of heterochromatin. Febs J.

Daujat, S., Weiss, T., Mohn, F., Lange, U.C., Ziegler-Birling, C., Zeissler, U., Lappe, M., Schubeler, D., Torres-Padilla, M.E., and Schneider, R. (2009). H3K64 trimethylation marks heterochromatin and is dynamically remodeled during developmental reprogramming. Nat Struct Mol Biol *16*, 777-781.

De Vos, M., El Ramy, R., Quenet, D., Wolf, P., Spada, F., Magroun, N., Babbio, F., Schreiber, V., Leonhardt, H., Bonapace, I.M.*, et al.* (2014). Poly(ADP-ribose) polymerase 1 (PARP1) associates with E3 ubiquitin-protein ligase UHRF1 and modulates UHRF1 biological functions. J Biol Chem *289*, 16223-16238.

Dedes, K.J., Wilkerson, P.M., Wetterskog, D., Weigelt, B., Ashworth, A., and Reis-Filho, J.S. (2011). Synthetic lethality of PARP inhibition in cancers lacking BRCA1 and BRCA2 mutations. Cell Cycle *10*, 1192-1199.

Dillon, N., and Festenstein, R. (2002). Unravelling heterochromatin: competition between positive and negative factors regulates accessibility. Trends Genet *18*, 252-258.

Ehrlich, M. (2009). DNA hypomethylation in cancer cells. Epigenomics *1*, 239-259.

Ehrlich, M., Sanchez, C., Shao, C., Nishiyama, R., Kehrl, J., Kuick, R., Kubota, T., and Hanash, S.M. (2008). ICF, an immunodeficiency syndrome: DNA methyltransferase 3B involvement, chromosome anomalies, and gene dysregulation. Autoimmunity *41*, 253-271.

Eymery, A., Horard, B., El Atifi-Borel, M., Fourel, G., Berger, F., Vitte, A.L., Van den Broeck, A., Brambilla, E., Fournier, A., Callanan, M.*, et al.* (2009). A transcriptomic analysis of human centromeric and pericentric sequences in normal and tumor cells. Nucleic Acids Res *37*, 6340-6354.

Felle, M., Hoffmeister, H., Rothammer, J., Fuchs, A., Exler, J.H., and Langst, G. (2011).

Nucleosomes protect DNA from DNA methylation in vivo and in vitro. Nucleic Acids Res *39*, 6956-6969.

Fuks, F., Hurd, P.J., Deplus, R., and Kouzarides, T. (2003). The DNA methyltransferases associate with HP1 and the SUV39H1 histone methyltransferase. Nucleic Acids Res *31*, 2305-2312.

Goren, A., and Cedar, H. (2003). Replicating by the clock. Nat Rev Mol Cell Biol *4*, 25-32.

Guetg, C., Lienemann, P., Sirri, V., Grummt, I., Hernandez-Verdun, D., Hottiger, M.O., Fussenegger, M., and Santoro, R. (2010). The NoRC complex mediates the heterochromatin formation and stability of silent rRNA genes and centromeric repeats. EMBO J *29*, 2135-2146.

Guetg, C., Scheifele, F., Rosenthal, F., Hottiger, M.O., and Santoro, R. (2012). Inheritance of Silent rDNA Chromatin Is Mediated by PARP1 via Noncoding RNA. Mol Cell *45*, 790-800.

Hall, L.E., Mitchell, S.E., and O'Neill, R.J. (2012). Pericentric and centromeric transcription: a perfect balance required. Chromosome Res *20*, 535-546.

Han, L., Su, B., Li, W.H., and Zhao, Z. (2008). CpG island density and its correlations with genomic features in mammalian genomes. Genome Biol *9*, R79.

Hand, R. (1978). Eucaryotic DNA: organization of the genome for replication. Cell *15*, 317-325.

Hassa, P.O., Haenni, S.S., Elser, M., and Hottiger, M.O. (2006). Nuclear ADP-ribosylation reactions in mammalian cells: where are we today and where are we going? Microbiol Mol Biol Rev *70*, 789-829.

Hassa, P.O., and Hottiger, M.O. (2008). The diverse biological roles of mammalian PARPS, a small but powerful family of poly-ADP-ribose polymerases. Front Biosci *13*, 3046-3082.

Henderson, A.S., Warburton, D., and Atwood, K.C. (1972). Location of ribosomal DNA in the human chromosome complement. Proc Natl Acad Sci U S A *69*, 3394-3398.

Hermann, A., Goyal, R., and Jeltsch, A. (2004). The Dnmt1 DNA-(cytosine-C5)-methyltransferase methylates DNA processively with high preference for hemimethylated target sites. The Journal of biological chemistry *279*, 48350-48359.

Hildebrand, C.E., and Walters, R.A. (1976). Rapid assembly of newly synthesized DNA into chromatin subunits prior to joining to small DNA replication intermediates. Biochem Biophys Res Commun *73*, 157-163.

Hottiger, M.O., Hassa, P.O., Luscher, B., Schuler, H., and Koch-Nolte, F. (2010). Toward a unified nomenclature for mammalian ADP-ribosyltransferases. Trends Biochem Sci *35*, 208-219.

Imai, S., and Guarente, L. (2014). NAD+ and sirtuins in aging and disease. Trends Cell Biol *24*, 464-471.

Jackson, D.A., and Pombo, A. (1998). Replicon clusters are stable units of chromosome structure: evidence that nuclear organization contributes to the efficient activation and propagation of S phase in human cells. J Cell Biol *140*, 1285-1295.

Jenuwein, T., and Allis, C.D. (2001). Translating the histone code. Science *293*, 1074-1080.

Kanai, M., Tong, W.M., Sugihara, E., Wang, Z.Q., Fukasawa, K., and Miwa, M. (2003). Involvement of poly(ADP-Ribose) polymerase 1 and poly(ADP-Ribosyl)ation in regulation of centrosome function. Mol Cell Biol *23*, 2451-2462.

Karagianni, P., Amazit, L., Qin, J., and Wong, J. (2008). ICBP90, a novel methyl K9 H3 binding protein linking protein ubiquitination with heterochromatin formation. Mol Cell Biol *28*, 705-717.

Kawaichi, M., Ueda, K., and Hayaishi, O. (1980). Initiation of poly(ADP-ribosyl) histone synthesis by poly(ADP-ribose) synthetase. J Biol Chem *255*, 816-819.

Keshet, I., Lieman-Hurwitz, J., and Cedar, H. (1986). DNA methylation affects the formation of active chromatin. Cell *44*, 535-543.

Kim, J.K., Esteve, P.O., Jacobsen, S.E., and Pradhan, S. (2009). UHRF1 binds G9a and participates in p21 transcriptional regulation in mammalian cells. Nucleic Acids Res *37*,

493-505.

Kim, M.Y., Mauro, S., Gevry, N., Lis, J.T., and Kraus, W.L. (2004). NAD+-dependent modulation of chromatin structure and transcription by nucleosome binding properties of PARP-1. Cell *119*, 803-814.

Kornberg, R.D. (1974). Chromatin structure: a repeating unit of histones and DNA. Science *184*, 868-871.

Kouzarides, T. (2007). Chromatin modifications and their function. Cell *128*, 693-705.

Krishnakumar, R., Gamble, M.J., Frizzell, K.M., Berrocal, J.G., Kininis, M., and Kraus, W.L. (2008). Reciprocal binding of PARP-1 and histone H1 at promoters specifies transcriptional outcomes. Science *319*, 819-821.

Krishnakumar, R., and Kraus, W.L. (2010). The PARP side of the nucleus: molecular actions, physiological outcomes, and clinical targets. Mol Cell *39*, 8-24.

Lachner, M., O'Carroll, D., Rea, S., Mechtler, K., and Jenuwein, T. (2001). Methylation of histone H3 lysine 9 creates a binding site for HP1 proteins. Nature *410*, 116-120.

Lachner, M., O'Sullivan, R.J., and Jenuwein, T. (2003). An epigenetic road map for histone lysine methylation. J Cell Sci *116*, 2117-2124.

Lanzuolo, C., Lo Sardo, F., and Orlando, V. (2012). Concerted epigenetic signatures inheritance at PcG targets through replication. Cell Cycle *11*, 1296-1300.

Laurent, L., Wong, E., Li, G., Huynh, T., Tsirigos, A., Ong, C.T., Low, H.M., Kin Sung, K.W., Rigoutsos, I., Loring, J.*, et al.* (2010). Dynamic changes in the human methylome during differentiation. Genome Res *20*, 320-331.

Lehnertz, B., Ueda, Y., Derijck, A.A., Braunschweig, U., Perez-Burgos, L., Kubicek, S., Chen, T., Li, E., Jenuwein, T., and Peters, A.H. (2003). Suv39h-mediated histone H3 lysine 9 methylation directs DNA methylation to major satellite repeats at pericentric heterochromatin. Curr Biol *13*, 1192-1200.

Leonhardt, H., Page, A.W., Weier, H.U., and Bestor, T.H. (1992). A targeting sequence directs DNA methyltransferase to sites of DNA replication in mammalian nuclei. Cell *71*,

865-873.

Li, E., and Zhang, Y. (2014). DNA methylation in mammals. Cold Spring Harb Perspect Biol *6*, a019133.

Li, J., Santoro, R., Koberna, K., and Grummt, I. (2005). The chromatin remodeling complex NoRC controls replication timing of rRNA genes. EMBO J *24*, 120-127.

Liu, X., Gao, Q., Li, P., Zhao, Q., Zhang, J., Li, J., Koseki, H., and Wong, J. (2013). UHRF1 targets DNMT1 for DNA methylation through cooperative binding of hemi-methylated DNA and methylated H3K9. Nat Commun *4*, 1563.

Margueron, R., and Reinberg, D. (2010). Chromatin structure and the inheritance of epigenetic information. Nat Rev Genet *11*, 285-296.

Martin, C., and Zhang, Y. (2005). The diverse functions of histone lysine methylation. Nature reviews Molecular cell biology *6*, 838-849.

Marx, V. (2012). Epigenetics: Reading the second genomic code. Nature *491*, 143-147.

Mayer, C., Neubert, M., and Grummt, I. (2008). The structure of NoRC-associated RNA is crucial for targeting the chromatin remodelling complex NoRC to the nucleolus. EMBO Rep *9*, 774-780.

Mayer, C., Schmitz, K.M., Li, J., Grummt, I., and Santoro, R. (2006). Intergenic transcripts regulate the epigenetic state of rRNA genes. Mol Cell *22*, 351-361.

McKnight, S.L., and Miller, O.L., Jr. (1976). Ultrastructural patterns of RNA synthesis during early embryogenesis of Drosophila melanogaster. Cell *8*, 305-319.

McStay, B., and Grummt, I. (2008). The epigenetics of rRNA genes: from molecular to chromosome biology. Annu Rev Cell Dev Biol *24*, 131-157.

Meister, P., and Taddei, A. (2013). Building silent compartments at the nuclear periphery: a recurrent theme. Curr Opin Genet Dev *23*, 96-103.

Muramatsu, D., Singh, P.B., Kimura, H., Tachibana, M., and Shinkai, Y. (2013). Pericentric heterochromatin generated by HP1 protein interaction-defective histone methyltransferase Suv39h1. J Biol Chem *288*, 25285-25296.

Muthurajan, U.M., Hepler, M.R., Hieb, A.R., Clark, N.J., Kramer, M., Yao, T., and Luger, K. (2014). Automodification switches PARP-1 function from chromatin architectural protein to histone chaperone. Proc Natl Acad Sci U S A *111*, 12752-12757.

Nusinow, D.A., Hernandez-Munoz, I., Fazzio, T.G., Shah, G.M., Kraus, W.L., and Panning, B. (2007). Poly(ADP-ribose) polymerase 1 is inhibited by a histone H2A variant, MacroH2A, and contributes to silencing of the inactive X chromosome. J Biol Chem *282*, 12851-12859.

Okano, M., Bell, D.W., Haber, D.A., and Li, E. (1999). DNA methyltransferases Dnmt3a and Dnmt3b are essential for de novo methylation and mammalian development. Cell *99*, 247-257.

Okuwaki, M., and Verreault, A. (2004). Maintenance DNA methylation of nucleosome core particles. J Biol Chem *279*, 2904-2912.

Peng, J.C., and Karpen, G.H. (2007). H3K9 methylation and RNA interference regulate nucleolar organization and repeated DNA stability. Nat Cell Biol *9*, 25-35.

Pesavento, J.J., Yang, H., Kelleher, N.L., and Mizzen, C.A. (2008). Certain and progressive methylation of histone H4 at lysine 20 during the cell cycle. Mol Cell Biol *28*, 468-486.

Petruk, S., Sedkov, Y., Johnston, D.M., Hodgson, J.W., Black, K.L., Kovermann, S.K., Beck, S., Canaani, E., Brock, H.W., and Mazo, A. (2012). TrxG and PcG proteins but not methylated histones remain associated with DNA through replication. Cell *150*, 922-933.

Pluta, A.F., Mackay, A.M., Ainsztein, A.M., Goldberg, I.G., and Earnshaw, W.C. (1995). The centromere: hub of chromosomal activities. Science *270*, 1591-1594.

Poirier, G.G., de Murcia, G., Jongstra-Bilen, J., Niedergang, C., and Mandel, P. (1982). Poly(ADP-ribosyl)ation of polynucleosomes causes relaxation of chromatin structure. Proc Natl Acad Sci U S A *79*, 3423-3427.

Pradhan, S., Bacolla, A., Wells, R.D., and Roberts, R.J. (1999). Recombinant human DNA (cytosine-5) methyltransferase. I. Expression, purification, and comparison of de novo and maintenance methylation. The Journal of biological chemistry *274*, 33002-33010.

Probst, A.V., Dunleavy, E., and Almouzni, G. (2009). Epigenetic inheritance during the cell cycle. Nat Rev Mol Cell Biol *10*, 192-206.

Qin, W., Leonhardt, H., and Spada, F. (2011). Usp7 and Uhrf1 control ubiquitination and stability of the maintenance DNA methyltransferase Dnmt1. J Cell Biochem *112*, 439-444.

Reale, A., Matteis, G.D., Galleazzi, G., Zampieri, M., and Caiafa, P. (2005). Modulation of DNMT1 activity by ADP-ribose polymers. Oncogene *24*, 13-19.

Realini, C.A., and Althaus, F.R. (1992). Histone shuttling by poly(ADP-ribosylation). J Biol Chem *267*, 18858-18865.

Robertson, A.K., Geiman, T.M., Sankpal, U.T., Hager, G.L., and Robertson, K.D. (2004). Effects of chromatin structure on the enzymatic and DNA binding functions of DNA methyltransferases DNMT1 and Dnmt3a in vitro. Biochem Biophys Res Commun *322*, 110-118.

Rouleau, M., Aubin, R.A., and Poirier, G.G. (2004). Poly(ADP-ribosyl)ated chromatin domains: access granted. J Cell Sci *117*, 815-825.

Rowbotham, S.P., Barki, L., Neves-Costa, A., Santos, F., Dean, W., Hawkes, N., Choudhary, P., Will, W.R., Webster, J., Oxley, D.*, et al.* (2011). Maintenance of silent chromatin through replication requires SWI/SNF-like chromatin remodeler SMARCAD1. Mol Cell *42*, 285-296.

Ruf, A., Mennissier de Murcia, J., de Murcia, G., and Schulz, G.E. (1996). Structure of the catalytic fragment of poly(AD-ribose) polymerase from chicken. Proc Natl Acad Sci U S A *93*, 7481-7485.

Saksouk, N., Simboeck, E., and Dejardin, J. (2015). Constitutive heterochromatin formation and transcription in mammals. Epigenetics & chromatin *8*, 3.

Santoro, R. (2005). The silence of the ribosomal RNA genes. Cell Mol Life Sci *62*, 2067-2079.

Santoro, R. (2011). The nucleolus. The epigenetics of the nucleolus: structure and function of active and silent ribosomal RNA genes In The Nucleolus, M.O.J. Olson, ed. (Springer),

pp. 57-82.

Santoro, R., and Grummt, I. (2005). Epigenetic mechanism of rRNA gene silencing: temporal order of NoRC-mediated histone modification, chromatin remodeling, and DNA methylation. Mol Cell Biol *25*, 2539-2546.

Santoro, R., Li, J., and Grummt, I. (2002). The nucleolar remodeling complex NoRC mediates heterochromatin formation and silencing of ribosomal gene transcription. Nat Genet *32*, 393-396.

Santoro, R., Schmitz, K.M., Sandoval, J., and Grummt, I. (2010). Intergenic transcripts originating from a subclass of ribosomal DNA repeats silence ribosomal RNA genes in trans. EMBO Rep *11*, 52-58.

Sarma, K., and Reinberg, D. (2005). Histone variants meet their match. Nat Rev Mol Cell Biol *6*, 139-149.

Savic, N., Bar, D., Leone, S., Frommel, S.C., Weber, F.A., Vollenweider, E., Ferrari, E., Ziegler, U., Kaech, A., Shakhova, O.*, et al.* (2014). lncRNA maturation to initiate heterochromatin formation in the nucleolus is required for exit from pluripotency in ESCs. Cell Stem Cell *15*, 720-734.

Scharf, A.N., Barth, T.K., and Imhof, A. (2009). Establishment of histone modifications after chromatin assembly. Nucleic Acids Res *37*, 5032-5040.

Schermelleh, L., Haemmer, A., Spada, F., Rosing, N., Meilinger, D., Rothbauer, U., Cardoso, M.C., and Leonhardt, H. (2007). Dynamics of Dnmt1 interaction with the replication machinery and its role in postreplicative maintenance of DNA methylation. Nucleic Acids Res *35*, 4301-4312.

Schotta, G., Lachner, M., Sarma, K., Ebert, A., Sengupta, R., Reuter, G., Reinberg, D., and Jenuwein, T. (2004). A silencing pathway to induce H3-K9 and H4-K20 trimethylation at constitutive heterochromatin. Genes Dev *18*, 1251-1262.

Seale, R.L. (1975). Assembly of DNA and protein during replication in HeLa cells. Nature *255*, 247-249.

Sharif, J., Muto, M., Takebayashi, S., Suetake, I., Iwamatsu, A., Endo, T.A., Shinga, J.,

Mizutani-Koseki, Y., Toyoda, T., Okamura, K.*, et al.* (2007). The SRA protein Np95 mediates epigenetic inheritance by recruiting Dnmt1 to methylated DNA. Nature *450*, 908-912.

Shumaker, D.K., Dechat, T., Kohlmaier, A., Adam, S.A., Bozovsky, M.R., Erdos, M.R., Eriksson, M., Goldman, A.E., Khuon, S., Collins, F.S.*, et al.* (2006). Mutant nuclear lamin A leads to progressive alterations of epigenetic control in premature aging. Proc Natl Acad Sci U S A *103*, 8703-8708.

Smith, S., and Stillman, B. (1989). Purification and characterization of CAF-I, a human cell factor required for chromatin assembly during DNA replication in vitro. Cell *58*, 15-25.

Sobel, R.E., Cook, R.G., Perry, C.A., Annunziato, A.T., and Allis, C.D. (1995). Conservation of deposition-related acetylation sites in newly synthesized histones H3 and H4. Proceedings of the National Academy of Sciences of the United States of America *92*, 1237-1241.

Sogo, J.M., Ness, P.J., Widmer, R.M., Parish, R.W., and Koller, T. (1984). Psoralen-crosslinking of DNA as a probe for the structure of active nucleolar chromatin. J Mol Biol *178*, 897-919.

Sogo, J.M., Stahl, H., Koller, T., and Knippers, R. (1986). Structure of replicating simian virus 40 minichromosomes. The replication fork, core histone segregation and terminal structures. J Mol Biol *189*, 189-204.

Spada, F., Haemmer, A., Kuch, D., Rothbauer, U., Schermelleh, L., Kremmer, E., Carell, T., Langst, G., and Leonhardt, H. (2007). DNMT1 but not its interaction with the replication machinery is required for maintenance of DNA methylation in human cells. J Cell Biol *176*, 565-571.

Strahl, B.D., and Allis, C.D. (2000). The language of covalent histone modifications. Nature *403*, 41-45.

Sweet, S.M., Li, M., Thomas, P.M., Durbin, K.R., and Kelleher, N.L. (2010). Kinetics of re-establishing H3K79 methylation marks in global human chromatin. J Biol Chem *285*, 32778-32786.

Thoma, F., Koller, T., and Klug, A. (1979). Involvement of histone H1 in the organization of the nucleosome and of the salt-dependent superstructures of chromatin. J Cell Biol *83*, 403-427.

Ting, D.T., Lipson, D., Paul, S., Brannigan, B.W., Akhavanfard, S., Coffman, E.J., Contino, G., Deshpande, V., Iafrate, A.J., Letovsky, S.*, et al.* (2011). Aberrant overexpression of satellite repeats in pancreatic and other epithelial cancers. Science *331*, 593-596.

Tran, V., Feng, L., and Chen, X. (2013). Asymmetric distribution of histones during Drosophila male germline stem cell asymmetric divisions. Chromosome Res *21*, 255-269.

Tulin, A., and Spradling, A. (2003). Chromatin loosening by poly(ADP)-ribose polymerase (PARP) at Drosophila puff loci. Science *299*, 560-562.

Volkel, P., and Angrand, P.O. (2007). The control of histone lysine methylation in epigenetic regulation. Biochimie *89*, 1-20.

Xu, M., Wang, W., Chen, S., and Zhu, B. (2012). A model for mitotic inheritance of histone lysine methylation. EMBO Rep *13*, 60-67.

Yang, X.J. (2004). Lysine acetylation and the bromodomain: a new partnership for signaling. BioEssays : news and reviews in molecular, cellular and developmental biology *26*, 1076-1087.

Yokochi, T., and Robertson, K.D. (2002). Preferential methylation of unmethylated DNA by Mammalian de novo DNA methyltransferase Dnmt3a. J Biol Chem *277*, 11735-11745.

Zampieri, M., Guastafierro, T., Calabrese, R., Ciccarone, F., Bacalini, M.G., Reale, A., Perilli, M., Passananti, C., and Caiafa, P. (2012). ADP-ribose polymers localized on Ctcf-Parp1-Dnmt1 complex prevent methylation of Ctcf target sites. Biochem J *441*, 645-652.

Zampieri, M., Passananti, C., Calabrese, R., Perilli, M., Corbi, N., De Cave, F., Guastafierro, T., Bacalini, M.G., Reale, A., Amicosante, G.*, et al.* (2009). Parp1 localizes within the Dnmt1 promoter and protects its unmethylated state by its enzymatic activity. PLoS One *4*, e4717.

Zee, B.M., Britton, L.M., Wolle, D., Haberman, D.M., and Garcia, B.A. (2012). Origins

and formation of histone methylation across the human cell cycle. Mol Cell Biol *32*, 2503-2514.

Zhang, L.F., Huynh, K.D., and Lee, J.T. (2007). Perinucleolar targeting of the inactive X during S phase: evidence for a role in the maintenance of silencing. Cell *129*, 693-706.

Zhou, Y., Santoro, R., and Grummt, I. (2002). The chromatin remodeling complex NoRC targets HDAC1 to the ribosomal gene promoter and represses RNA polymerase I transcription. Embo J *21*, 4632-4640.

Curriculum Vitae

PERSONAL INFORMATION

Surname	**Vollenweider**
Name	**Eva**
Date of Birth	**February 13, 1988**
Hometown	**Zurich, Switzerland**

EDUCATION

2012 – present	Doctoral Thesis in Molecular Biology (Dr. sc. nat./Ph.D.)
	University of Zurich
2006 – 20011	Bachelor and Master studies in Genetics (MSc University of Zurich)
	University of Zurich, Switzerland
	University of Technology Sydney, Australia
	Diploma Thesis: "Intracellular Trafficking and Secretion of Wingless"
2002 – 2006	High School – Matura Typus D
	Kantonsschule Stadelhofen, Zurich, Switzerland

REWARDS

Forschungskredit 2013, the University of Zurich

PUBLICATION LIST

Eva Vollenweider, Anita Steiner & Raffaella Santoro (2015). Assembly of heterochromatin after replication is a slow process required for DNA methylation. (Manuscript submitted)

Natasa Savic, Dominik Bär, Sergio Leone, Sandra C. Frommel, Fabienne A. Weber, Eva Vollenweider, Elena Ferrari, Urs Ziegler, Andres Kaech, Olga Shakhova, Paolo Cinelli & Raffaella Santoro (2014). lncRNA maturation to initiate heterochromatin formation in the nucleolus is required for exit from pluripotency in ESCs. Cell Stem Cell *15*, 720-734

Urs Graf, Elisa Casanova, Eva Vollenweider, Sarah Wyck, Fabienne A. Weber, Sameera S. Patel, Jiwen Li, Jafar Sharif, Guido A. Wanner, Haruhiko Koseki, Jiemin Wong, Raffaella Santoro and Paolo Cinelli. (2015). Pramel7 is implicated in naïve pluripotency through

proteasomal-epigenetic combined pathways. (Under revision in Molecular Cell)

Acknowledgements

First, I would like to thank my supervisor, Dr. Raffaella Santoro for her excellent scientific guidance, constant support and supervision of my work during my PhD. Her passion for science and research was a great motivation and a major encouragement to me.

I am grateful to Prof. Dr. Dr. Michael O. Hottiger for helpful discussions related to my project and for being the chairman of my doctoral thesis committee. At this point I also want to express my gratitude to the remaining members of my Thesis Committee, Dr. Maria-Elena Torres Padilla, Prof. Claus Azzalin and Prof. Konrad Basler for agreeing to review my work, their academic support and constructive discussions.

I would like to thank Anita Steiner for her experimental help during her master thesis work and the fun we had during her time in our lab. Big thanks to all the current and former lab members: Claudio, Sandra, Natasa, Sergio, Damian, Dominik, Nina, Karolina and Rodrigo. Many thanks go to all the other present and former members of the IVBMB and CABMM institutes for the lovely and helpful atmosphere. I greatly enjoyed working in this environment where I could always find someone for a quick laugh on the corridor. Special thanks go to Gregor, Stephan, Natasa, Flo, Friedlo and Anneli for making my PhD life in- and outside the lab a time to remember dearly.

Thanks to all my friends and family, especially Dani, Michèle and my cousins, for the laughter, support and the horses we can steal. A special thanks goes to my parents and siblings Philip, Lexi and Isabel for always being there and the love we all share.